

# **The Role of the Hedgehog Receptor Patched in LysM<sup>+</sup> Cells in Mice**

## **Dissertation**

for the award of the degree  
"Doctor of Natural Sciences" (Dr. rer. nat.)  
Division of Mathematics and Natural Sciences  
of the Georg-August-Universität Göttingen

**submitted by**

**Penelope Pelczar**

from Manila, Philippines

**Göttingen 2013**

**Members of the thesis Committee:**

**Prof. Dr. Heidi Hahn (Reviewer)**

Dept. of Human Genetics  
Georg-August-Universität Göttingen

**Prof. Dr. Matthias Dobbelsstein (Reviewer)**

Dept. of Molecular Oncology  
Georg-August-Universität Göttingen

**Prof. Dr. Holger Reichardt**

Dept. of Cellular and Molecular Immunology  
Georg-August-Universität Göttingen

Date of the oral examination: February 28, 2013

## **Affidavit**

I hereby declare that the PhD thesis entitled "The Role of the Hedgehog Receptor Patched in LysM<sup>+</sup> Cells in Mice" has been written independently and with no other sources and aids than quoted.

---

**Penelope Pelczar**

January, 2013

Göttingen



1	Summary .....	1
2	Introduction.....	3
2.1	Key components of the Hedgehog signaling pathway.....	3
2.2	Models of Hedgehog pathway activity in cancer.....	5
2.2.1	Role of Hh signaling in gastrointestinal stromal tumors (GIST).....	7
2.3	The role of Hedgehog signaling in immune cells .....	9
2.3.1	Hematopoiesis.....	9
2.3.2	The innate immune system .....	9
2.3.3	Hh signaling in immune cells .....	11
2.3.3.1.	Hh signaling and the lymphoid lineage .....	12
2.3.3.2.	Hh signaling and the myeloid lineage .....	13
2.4	Patched knockout mice: A model to study the function of Hh signaling in cancer and immunity.....	14
2.5	LysMcre mice: a tool for highly efficient cre-mediated deletion of loxP-flanked target genes in myeloid cells.....	15
3	Aim of the Study.....	17
4	Materials and Methods.....	18
4.1	Technical equipment.....	18
4.2	Consumable materials.....	19
4.3	Reagents and Chemicals .....	20
4.4	Kits and ready-to-use reaction systems.....	21
4.5	Buffers and solutions .....	22
4.6	Media .....	24
4.6.1	Media for bacterial culture.....	24
4.6.2	Agar plates .....	24
4.6.3	Media and reagents for cultivation of eukaryotic cell lines.....	25
4.7	Biological materials .....	25
4.7.1	Bacterial strains and growth.....	25
4.7.2	Eukaryotic cell lines.....	25
4.7.3	Mouse lines .....	26
4.8	Synthetic Oligonucleotides .....	27
4.9	Antibodies .....	30
4.10	Molecular biology methods .....	32
4.10.1	Nucleic acid isolation.....	32
4.10.2	Photometric quantification of nucleic acids.....	33
4.10.3	Polymerase chain reaction (PCR) .....	33
4.10.4	Agarose gel electrophoresis .....	35

4.11 Cell biology methods .....	35
4.11.1 Isolation of bone marrow cells and preparation of murine bone marrow-derived macrophages (BMDM).....	35
4.11.2 Isolation of splenocytes.....	36
4.11.3 Isolation of CD11b <sup>+</sup> and CD11c <sup>+</sup> cells .....	36
4.11.4 Isolation of Thy1.2 <sup>+</sup> cells .....	37
4.11.5 Analysis of blood and bone-marrow-derived cells .....	37
4.11.6 Stimulation of BMDM with LPS or BLP .....	38
4.11.7 Cell viability and cell proliferation assay .....	38
4.11.8 Flow cytometric analysis .....	38
4.11.9 Enzyme-linked immunosorbent assay (ELISA) .....	39
4.11.10 Cellular transformation assay .....	39
4.12 Protein chemistry and immunohistochemistry methods .....	39
4.12.1 Protein isolation and quantification .....	39
4.12.2 Western blot .....	40
4.12.3 Hematoxylin-Eosin (HE) Staining.....	40
4.12.4 Electron microscopy .....	41
4.12.5 In situ hybridization .....	41
4.12.6 LacZ staining .....	42
4.12.7 Immunohistochemistry (IHC) .....	42
4.12.8 Assessment of skin thickness and nevi area .....	43
4.13 Animal Experiments .....	43
4.13.1 Breeding of mice.....	43
4.13.2 Tail biopsy and genotyping of mice.....	44
4.13.3 Perfusion of mice .....	44
4.13.4 Isolation of tumors .....	44
4.13.5 Adoptive transfer of BM.....	44
4.13.6 Tumor xenografts.....	45
4.13.7 Imatinib treatment of mice.....	45
4.13.8 Transplantation of syngeneic melanoma cells .....	45
4.13.9 Transplantation of syngeneic ovarian carcinoma cells and bioimaging .....	46
4.13.10 Two-stage chemical carcinogenesis DMBA/TPA protocol.....	46
4.14 Softwares.....	47
4.15 Databases .....	47
4.16 Statistical Analysis.....	47
5 Results.....	48
5.1 Generation and phenotype of Ptch <sup>flox/flox</sup> LysMcre <sup>+/-</sup> mice .....	48

5.2	$Ptch^{flox/flox}LysMcre^{+/-}$ mice develop GIST-like tumors .....	52
5.2.1	Histological characteristics of the tumors of $Ptch^{flox/flox}LysMcre^{+/-}$ mice .....	52
5.2.2	Molecular characteristics of gastrointestinal tumors of $Ptch^{flox/flox}LysMcre^{+/-}$ mice .....	54
5.2.3	Activation of Hh signaling in gastrointestinal tumors of $Ptch^{flox/flox}LysMcre^{+/-}$ mice .....	57
5.3	Differentiation of the tumors of $Ptch^{flox/flox}LysMcre^{+/-}$ mice from LMS .....	59
5.3.1	Comparison of gene expression profiles between human GIST, human and murine LMS and tumors of $Ptch^{flox/flox}LysMcre^{+/-}$ mice .....	59
5.3.2	Gastrointestinal tumors of $Ptch^{flox/flox}LysMcre^{+/-}$ mice are responsive to imatinib .....	64
5.4	GIST-like tumors of $Ptch^{flox/flox}LysMcre^{+/-}$ mice are derived from $LysM^{+}$ cells of the GI tract .....	66
5.4.1	$LysM^{+}$ cells of the GI tract can express $Pdgfra$ but not $Kit$ .....	68
5.5	HH signaling cooperates with PDGFRA signaling, but not with KIT signaling, in cellular transformation .....	70
5.6	Functional analysis of immune cells of $Ptch^{flox/flox}LysMcre^{+/-}$ mice.....	73
5.6.1	Analysis of $Ptch$ -deficient BMDM .....	75
5.6.2	Effects of $Ptch$ -deficient $LysM^{+}$ cells on tumor surveillance.....	82
6	Discussion .....	92
6.1	GIST-like tumors in $Ptch$ mutant mice .....	92
6.1.1	Differentiation of the tumors from $Ptch^{flox/flox}LysMcre^{+/-}$ mice from LMS .....	93
6.1.2	GIST-like tumors of $Ptch^{flox/flox}LysMcre^{+/-}$ mice express $Pdgfra$ , but not $Kit$ .....	94
6.1.3	GIST-like tumors of $Ptch^{flox/flox}LysMcre^{+/-}$ mice are derived from $LysM^{+}$ cells of the intestine.....	95
6.1.4	GIST-like tumors of $Ptch^{flox/flox}LysMcre^{+/-}$ mice are derived from $Kit$ negative cells of the intestine .....	96
6.1.5	GIST-like tumors of $Ptch^{flox/flox}LysMcre^{+/-}$ mice may occur due to cooperation of active Hh and $Pdgfra$ signaling in $LysM^{+}$ cells.....	97
6.1.6	Implications for GIST therapy .....	98
6.2	Functional role of $Ptch$ in the innate immune system.....	99
6.2.1	Role of $Ptch$ in inflammatory responses after stimulation with TLR agonists .....	99
6.2.2	The role of $Ptch$ in tumor immune surveillance .....	101
6.3	Outlook on the future studies on the role $Ptch$ in macrophages and other cells derived from the myeloid lineage .....	108
7	References.....	110
9	Abbreviations.....	123
10	Acknowledgement .....	127
11	Curriculum vitae .....	128





## 1 Summary

Cancer development is frequently linked to signaling pathways that are required for normal embryonic patterning. One of the pathways important in patterning and growth of the embryo is the Hedgehog (Hh) signaling cascade. Activation or inappropriate maintenance of this pathway in the adult organism is frequently caused by mutations in the Hh receptor Patched (Ptc) or overexpression of Hh and can result in the development of a variety of tumors. Whereas the pathway's function in tissues such as skin, brain, lung, muscle, bladder, breast and prostate is well studied, the knowledge about its role and tumorigenic potential in cells composing the immune system is very limited. The original goal of this thesis was to elucidate the function of Ptc in macrophages. For this purpose *Ptc*<sup>flx/flx</sup> mice were crossed with *LysMcre* mice. The latter mice express a cre recombinase specifically in lysozyme M (LysM) positive cells that are mainly macrophages, granulocytes and dendritic cells (DC), which are derived from the myeloid lineage.

Surprisingly, the *Ptc* mutation in LysM positive cells resulted in multiple tumors arising from the wall of the stomach or the intestine. In the tumors Hh signaling was activated. Furthermore the histology, localization, responsiveness to imatinib, and molecular analysis were suggestive of Gastrointestinal Stromal Tumors (GIST). Because human GIST are considered to arise from KIT- or PDGFRA-expressing cells of the smooth muscle layer of the GI tract, this observation was inconsistent with the *Ptc* mutation in the myeloid lineage. To resolve this discrepancy, a lineage tracing experiment was performed. The data showed that the tumors indeed arose from LysM-expressing cells. In addition, these cells were Kit-negative and sometimes expressed *Pdgfra*. Similar relationships of Kit and *Pdgfra* expression were found in the GIST-like tumors, which were all negative for Kit, but highly expressed *Pdgfra*. Since HH- and PDGFRA, but not KIT-signaling pathways cooperated in oncogenic transformation, the data suggest that the GIST-like tumors in *Ptc* mutant mice developed due to the cooperativity between Hh and *Pdgfra* pathways from Kit-negative cells in the intestine.

In addition, the function of *Ptc*-deficient macrophages was analyzed. First, the response to inflammatory stimuli was investigated. For this purpose, bone-marrow derived macrophages (BMDM) were isolated from *Ptc*<sup>flx/flx</sup>*LysMcre*<sup>+/-</sup> animals and were challenged with lipopolysaccharide (LPS) or bacterial lipoprotein (BLP). The preliminary analyses showed

that *Ptch* was important for *IL-6* expression and macrophage proliferation after BLP stimulation.

Second, in order to study the role of *Ptch*-deficient macrophages (and other myeloid cells) in tumor immune surveillance, tumors (other than GIST) were induced in *Ptch<sup>flox/flox</sup>LysMcre<sup>+/-</sup>* mice. In a first approach, syngeneic melanoma cells were injected i.p. or i.v. into *Ptch<sup>flox/flox</sup>LysMcre<sup>+/-</sup>* and respective control mice. The analysis revealed that the *Ptch*-deficiency had no impact on primary or metastatic tumor growth. Similar observations were made after i.p. injection of the slow-growing ovarian carcinoma cell line ID8-LUC and monitoring of tumor growth by chemoluminescence. Finally, *Ptch<sup>flox/flox</sup>LysMcre<sup>+/-</sup>* and control mice were subjected to the two-stage chemical carcinogenesis DMBA/TPA protocol, which results in the development of papilloma and melanoma-like nevi. Whereas papilloma growth was not affected by the *Ptch* mutation, the nevi growth was significantly enhanced in *Ptch<sup>flox/flox</sup>LysMcre<sup>+/-</sup>* animals which were associated with a stronger infiltration with skin macrophages. Taken together, these results suggest that *Ptch*-deficiency in LysM-expressing cells such as macrophages modulates inflammatory responses and may promote growth of melanoma.

## 2 Introduction

### 2.1 Key components of the Hedgehog signaling pathway

Many components of the Hh signaling cascade were initially described by the two Nobel laureates, Nüsslein-Volhard and Wieschaus, in 1980. In their systematic search for embryonic patterning in mutant *Drosophila melanogaster*, Nüsslein-Volhard and Wieschaus identified 15 loci which, when mutated, altered the segmental pattern of the larva <sup>1</sup>. For example, they observed mutant larvae that failed to develop the naked posterior part of each segment and showed duplication of the anterior denticle band. Since the mutant larvae were almost entirely covered with denticles leading to a 'hedgehog-like' appearance, the responsible gene was named *Hedgehog* (*Hh*). Besides the *Hh* gene, they also identified other genes, which later turned out to be key components of the Hh signaling pathway <sup>1</sup>. These genes included the *Drosophila Hh* receptor *Patched* (*Ptch*), the kinase *fused* (*fu*), and the downstream transcription factor *ci* (reviewed in <sup>2</sup>).

In mammals three Hh homologs have been identified. These are Sonic (Shh), Desert (Dhh), and Indian hedgehog (Ihh). In addition, one *smo* (*Smo*), two *ptc* (*Ptch1* and *Ptch2*) and three *ci* homologues (*Gli1*, *Gli2* and *Gli3*) have been discovered. The expression and function of *Ptch1* (referred to as *Ptch* from here on) is similar to that of *D. melanogaster ptc*. The expression of *Ptch2* is more restricted than *Ptch*, and it may have distinct functional properties. The post-translational regulation of *ci* and the Gli proteins is similar (reviewed in <sup>3</sup>).

All three Hh homologs play a role in developmental patterning. In vertebrates, Shh has been shown to regulate patterning of the developing limb bud, the axial mesoderm, and the neural tube <sup>4,5</sup>. Moreover, disruption of Shh in mice results in midline defects such as cyclopia and absence of the spinal column and most of the ribs <sup>6</sup>. Ihh has been reported to play a major role in chondrocyte maturation and skeletal development <sup>7</sup>, while Dhh has been shown to regulate both early and late stages of spermatogenesis <sup>8</sup>.

Figure 1 shows a simplified model of the Hh signaling pathway in vertebrates. In the absence of the Hh ligand, the signaling pathway is maintained inactive by the 12-transmembrane-domain receptor protein Ptch. Normally Ptch is concentrated at the base of the primary cilium, a single antenna-like structure that protrudes from the cell surface of many adherent

cell types and functions as a signal transduction compartment<sup>9</sup>. Ptch blocks the activity of the 7-transmembrane-domain protein Smo, which is a positive regulator of the Hh signaling pathway<sup>10</sup>. The exact mechanism of Smo inhibition by Ptch is not well understood, but is probably caused by sterols, which can be secreted by Ptch<sup>11</sup>. Hh signaling activation occurs when the secreted Hh ligand binds to Ptch. The interaction of Hh with Ptch removes Ptch from the primary cilium, thus allowing Smo to translocate to the primary cilia. There it transduces downstream signals to activate the Gli family of transcription factors by promoting the dissociation of the Suppressor of fused (Sufu) from the Sufu/Gli complex. This ultimately regulates the expression of Hh downstream target genes<sup>9</sup>.

There are three members of the Gli family in vertebrates, which are Gli1, Gli2 and Gli3. Gli3 exists in two forms: these are the full-length Gli3 form, capable of activating transcription in some systems (GliA), and a shorter (due to a truncated amino-terminal fragment) form that mediates the major role of Gli3 as a transcriptional repressor (GliR). In contrast to Gli3, Gli2 is mainly a transcriptional activator<sup>12</sup>. Activation of Gli2 and Gli3 leads to the transcription of *Gli1*, which further amplifies the initial Hh signal at the transcriptional level. Thus, the mRNA level of *Gli1* is considered a reliable indicator of the pathway's activity. Another Hh target is *Ptch* itself, which thus regulates the Hh expression in a negative feedback<sup>5</sup>.

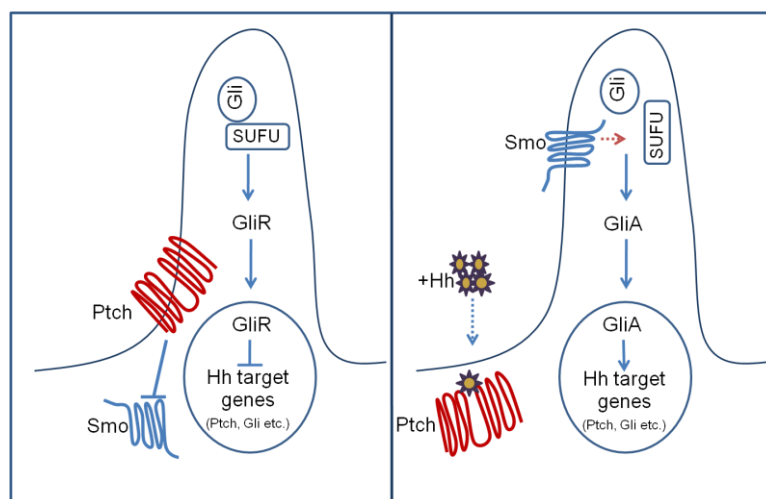


**Figure 1. Simplified scheme of the Hh signaling pathway.** The figure shows the interactions between the major components of the pathway. In unstimulated cells (left), the activity of the transmembrane protein Smo is suppressed by the Hh receptor Ptch (by blocking its translocation into the cilium). This keeps Gli attached to Sufu and in its repressive (GliR) form. In the presence of Hh ligands (right), the binding of Hh to Ptch suspends the inhibition of Smo, thereby allowing Smo to translocate to the cilium. This results in stabilization of the Gli activator (GliA) forms, which are released from the Sufu/Gli complex and translocated to the nucleus where they induce the transcription of Hh target genes. Adapted from<sup>13, 14</sup>.

The Hh pathway regulates the development of numerous tissues and organs<sup>15</sup>. In the embryo, gradients of Hh are generated and, possibly in combination with other signaling factors, regulate apoptosis, proliferation, and differentiation of cells. This signaling is controlled in an area-specific and time-dependent manner<sup>16</sup>.

Hh signaling also remains active, albeit limited, throughout adult life. In adults it plays a key role in the maintenance and expansion of stem cell populations through modulation of their self-renewal capacity. This is important in the maintenance of tissue homeostasis, repair and regeneration<sup>17</sup>.

In summary, precise control of the onset, strength, and termination of Hh signaling is a critical requirement for proper pattern formation, morphogenesis, cell proliferation, survival, and differentiation (reviewed in<sup>18</sup>).

## **2.2 Models of Hedgehog pathway activity in cancer**

Cancer remains one of the leading causes of mortality and morbidity throughout the world<sup>19</sup>. Although the different types of cancer may have a different cellular origin, all cancers share the same fundamental features characterized by the acquisition of the following hallmarks that determine tumor development, progression, and metastasis<sup>20</sup>: self sufficiency of growth, unlimited replicative potential, activation of anti-apoptotic programmes, insensitivity to anti-growth factors, sustained angiogenesis, tissue invasion and metastasis. All these hallmarks determine tumor development, progression, and metastasis and can be directly or indirectly regulated by signaling cascades initiated by extracellular cues and signaling molecules<sup>20</sup>. One of these signaling cascades is the Hh signaling pathway.

Abnormal Hh signaling in cancer can be categorized as Hh ligand-dependent or ligand-independent. The ligand-dependent mode of aberrant Hh signaling is subdivided into additional mechanisms. These are a) ligand-dependent autocrine signaling, which means that Hh is both produced and responded to by the same tumor cell, and b) ligand-dependent paracrine signaling which means that Hh produced by the tumor cells and signals to the stroma or c) “reverse paracrine” signaling, whereby Hh is secreted from stromal cells to receiving cells in a tumor (for review see ref<sup>21</sup>). Examples of ligand-dependent tumors include tumors of the digestive tract (including those of the esophagus, stomach, biliary tract and pancreas)<sup>22</sup>, of the lung<sup>23</sup>, breast<sup>24</sup> and brain<sup>25</sup> and hematological malignancies

including multiple myeloma, chronic myeloid leukemia, acute lymphocytic leukemia, and lymphomas<sup>26, 27, 28, 29</sup> (reviewed in<sup>21</sup>).

In contrast, ligand-independent mechanisms of Hh-activity in cancer are mutation-driven. This was initially shown in humans suffering from Gorlin syndrome (also known as basal cell nevus syndrome)<sup>30</sup>. Patients with Gorlin syndrome show somatic mutations of *PTCH*<sup>30</sup> which lead to constitutively active HH signaling in the absence of the HH ligand. Affected individuals develop multiple basal cell carcinomas (BCC) as well as medulloblastomas (MB) and other tumors including rhabdomyosarcomas (RMS)<sup>31</sup>. In recent years it became obvious that more than 85% of cases of sporadic BCC are also due to inactivating *PTCH* mutations, whereas a smaller portion can be caused by activating mutations in *SMO*. Furthermore, inactivating *PTCH* or *SUFU* mutations have been detected in approximately 25% of sporadic MB, which is pediatric cancer of the cerebellum<sup>32, 33</sup>. Similarly, RMS, which is a tumor of the skeletal muscle in children, has been associated with loss of heterozygosity of the *PTCH* and *SUFU* loci<sup>34</sup>.

The discovery of small molecule antagonists of SMO inhibitors such as cyclopamine has opened up exciting new prospects for molecularly targeted therapies of human cancers associated with Hh signaling. This potential has been tested in many mouse models and cell lines. For example, cyclopamine is effective in inhibiting the Hh signaling pathway and the proliferation of several tumors including those derived from BCC<sup>35</sup>, MB<sup>36, 37</sup> prostate<sup>38, 39</sup> breast<sup>24</sup> and pancreas<sup>40</sup> both *in vitro* and *in vivo*. Furthermore, oral cyclopamine has shown efficacy in endogenously developing tumors in mice. Thus, cyclopamine can block the growth of UV-induced BCC in *Ptch*<sup>+/-</sup> mice by 50%<sup>35</sup>. Furthermore, cyclopamine treatment in this mouse model prevents formation of BCC, implying a potential use of cyclopamine for BCC prevention. In addition, cyclopamine administration reduced BCC, but not squamous cell carcinomas (SCC) or fibrosarcomas that do not show activation of Hh signaling, highlighting the specificity of cyclopamine for the Hh pathway<sup>35</sup>. Similarly, intraperitoneal injection of cyclopamine is effective in reducing MB development in *Ptch*<sup>+/-</sup> *p53*<sup>-/-</sup> mice<sup>41</sup>. In recent years other more potent synthetic SMO inhibitors, such as vismodegib (GDC-0449) from Curis/Genentech, have been developed. Vismodegib is an orally available small-molecule inhibitor of HH signaling, which was recently approved by the U.S. Food and Drug Administration for the treatment of locally advanced or metastatic BCC<sup>42</sup>. Unfortunately,

although the toxicity of vismodegib is generally not severe, the chronic nature of side effects frequently leads to discontinuation of therapy in almost half of the patients <sup>42</sup>.

### **2.2.1 Role of Hh signaling in gastrointestinal stromal tumors (GIST)**

Hh signaling is involved in many types of tumors (see above). However, its role in the pathogenesis of gastrointestinal stromal tumors (GIST) remains obscure. Because GIST is a major subject of this thesis, I will give a short introduction to this tumor entity here:

GIST are the most common mesenchymal tumors of the gastrointestinal tract <sup>43, 44</sup>. GIST are most frequently found in the stomach or small intestine, but can arise anywhere in the gastrointestinal tract and are occasionally found in the omentum, peritoneum and mesentery <sup>43</sup>. Until recently, most GIST were classified as smooth muscle tumors. Based on histological data and immunoreactivity these tumors, which show almost no smooth muscle differentiation, they have been reclassified as GIST <sup>45</sup>.

Data about Hh signaling in GIST are rare. However, a recent immunohistochemical analysis showed that HH, GLI1, and PTCH are overexpressed in a fraction of human GIST <sup>46</sup>. Furthermore, the PTCH locus is lost in 30% - 50% of these tumors <sup>45, 47</sup>. Together with the observation that HH expression correlates with the grade of GIST risk category and size <sup>46</sup>, these findings suggest that HH signaling may play a role in the biology of this tumor entity.

In contrast, constitutive activation of either the KIT or PDGFRA receptor tyrosine kinase (RTK) by oncogenic mutations plays a central pathogenetic role in GIST. Indeed, identification of these mutations eventually led to the acceptance of GIST as a separate tumor entity from its nearest histological relative, leiomyosarcomas (LMS) <sup>48, 49, 50</sup>. Based on their sequence homology and similar conformational structure, KIT and PDGFRA belong to the same class (III) of RTK. Whereas PDGFRA is stimulated by its ligands PDGFA, PDGFB and PDGFC (but not PDGFD) <sup>51</sup>, the only known ligand for KIT is the stem cell factor, SCF. The KIT ligand is constitutively produced by some endothelial and stromal cells in the bone marrow, spleen, lymph nodes, and thymus of adults (reviewed in <sup>52</sup>). The KIT receptor plays a critical role in the normal development and function of the interstitial cells of Cajal (ICC). Thus, KIT is expressed by ICC <sup>53</sup>. In addition, inactivating mutations in *Kit* result in the lack of the network of ICC that are associated with Auerbach's nerve plexus and

that show intestinal pacemaker activity in mice <sup>54</sup>. Because GIST are located in the muscularis propria in association with the myenteric plexus and because GIST frequently express KIT, these tumors are thought to originate from ICC <sup>55</sup>.

In GIST, the majority of the activating KIT mutations (70–75%) have been found in the juxtamembrane domain in a hotspot region at the 5' end of exon 11 involving codons 550–560 <sup>56</sup>. By analogy with other RTK, the juxtamembrane domain may function as a negative regulator of the KIT kinase. Disruption of the conformational integrity of this domain may impair its negative regulatory function. Thus, the oncogenic potential of the juxtamembrane domain mutations is attributed to the loss of this inhibitory function. A second, less common hotspot in the juxtamembrane domain is located at the 3' end of exon 11 <sup>56</sup>. Activating KIT mutations in the hotspot regions do not appear to be associated with a specific clinicopathologic phenotype, but the presence of deletions rather than substitutions predicts a more aggressive tumor behavior. Exon 9 mutations occur in 10–15% of GIST patients with KIT mutation and comprise a distinct subset of GIST that are often located in the small bowel and show more aggressive behavior <sup>56</sup>. In contrast to the more common KIT mutations in exons 9 and 11, mutations have been rarely described in the KIT kinase domain (exons 13 and 17) <sup>57</sup> (also reviewed in <sup>52</sup>).

Approximately 15% of GIST show no activation of KIT. Half of these cases show activating mutations in PDGFRA within exons 12, 14, or 18 <sup>50, 58</sup>. The most common PDGFRA mutation (63%) is the D842V substitution in exon 18 <sup>59</sup>. Many PDGFRA mutant GIST express PDGFRA, show a preference for gastric location, epithelioid morphology and a variable or absent KIT expression by immunohistochemistry (IHC). In addition, these tumors are relatively benign <sup>58</sup>. In approximately 10% of GIST patients, mutations in neither KIT nor PDGFRA have been identified. In particular, most GIST in children are wild type (wt; not mutated) for both genes <sup>60</sup>.

At present, it is unclear if PDGFRA-positive GIST arise from ICC in which KIT expression has been turned down, or from different cells. In support of the latter possibility, KIT-negative but PDGFRA-positive fibroblast-like cells have been found in association with ICC and nerve bundles <sup>61-63</sup>. On the other hand, Bardsley and colleagues reported PDGFRA-expressing ICC precursors with low KIT levels, which differentiate into KIT-positive ICC



cells and form tumors in nude mice <sup>64</sup>. However, unlike GIST, these tumors are resistant to imatinib, a drug that targets the kinase-activity of both KIT and PDGFRA <sup>65</sup>, and their significance to in situ (i.e. gastro-intestinal) GIST formation is unclear.

## 2.3 The role of Hedgehog signaling in immune cells

### 2.3.1 Hematopoiesis

The establishment and maintenance of the hematopoietic system relies on self-renewing hematopoietic stem cells (HSC) that normally reside in small numbers in the bone marrow niche of adult mammals. HSC divide to form more HSC (self-generation) or to form cells committed to the generation of either myeloid cells (common myeloid progenitors, CMP) or lymphoid cells (common lymphoid progenitors, CLP). CMP are large blast cells that give rise to the more restricted i) granulocyte-macrophage progenitors (GMP) able to generate monocytes, macrophages, and granulocytes (neutrophil, eosinophil and basophil) and ii) megakaryocyte-erythroid progenitors (MEP) committed to the formation of erythroid and megakaryocytic progeny (reviewed in <sup>66</sup>). CLP give rise to NK cells, T and B cells (Figure 2).

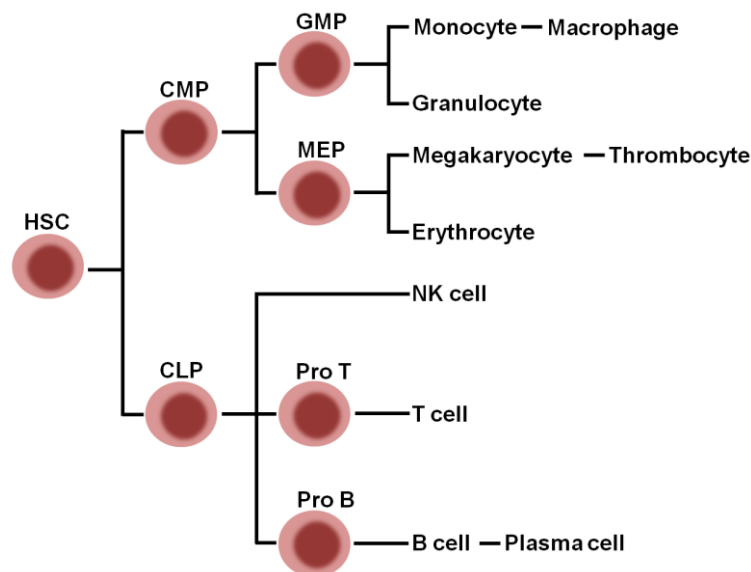


**Figure 2 HSC and derived haematopoietic cell lineages.** HSC: hematopoietic stem cells; CMP: common myeloid progenitor; CLP: common lymphoid progenitor; GMP:granulocyte-monocyte progenitor; MEP: megakaryocyte-erythrocyte progenitor. Figure adapted from <sup>67</sup>.

### 2.3.2 The innate immune system

The innate immune system comprises the first line of host defense during infection and therefore plays a crucial role in the early recognition and subsequent triggering of a pro-inflammatory response to invading pathogens. The adaptive immune system, on the other

hand, is responsible for elimination of pathogens in the late phase of infection and in the generation of immunological memory. Whereas the adaptive immune response is characterized by specificity developed by clonal gene rearrangements from a broad repertoire of antigen-specific receptors on lymphocytes, the innate immune response can be mediated by phagocytic cells such as granulocytes, macrophages, and DC, and has been regarded as relatively non-specific<sup>68</sup>. Most cells eliciting innate immune responses are myeloid-derived cells<sup>69</sup>

The innate immune response relies on a large family of pattern recognition receptors such as Toll-like receptors (TLR). TLR can trigger intracellular signaling cascades ultimately culminating in the expression of a variety of pro-inflammatory molecules, which together orchestrate the early host response to infection, and also are a prerequisite for the subsequent activation and shaping of adaptive immunity. In order to avoid a pathologic immune response, this system is tightly regulated by a number of endogenous molecules that limit the magnitude and duration of the inflammatory response<sup>68</sup>. Generally, TLR can regulate leukocyte recruitment to sites of infection by activating several cell type subsets, including tissue stromal cells, tissue-resident innate cells (most notably DC and macrophages), and circulating leukocytes. During acute inflammation, the cellular infiltrate consists of monocytes, DC, neutrophils, and NK cells. Among these, neutrophils and NK cells are critical innate effector cells protecting the host by killing pathogenic microbes and infected cells, respectively<sup>68</sup>.

The link between inflammation and cancerous tumors has long been recognized. Experimental, clinical and epidemiological studies have revealed that inflammation contributes to tumor progression and even predisposes to different types of cancer. Macrophages are usually the most abundant immune population present in the tumor microenvironment<sup>70, 71</sup>. These macrophages have a distinct capability to express different cytokines, chemokines and growth factors in response to different microenvironmental signals, which typically manifest themselves in pathological conditions such as infections and cancer. The balance between the phenotypic roles played by the macrophages in cancer is critical to its promotion or suppression. In response to cytokines and microbial products, mononuclear phagocytes express specialized specific genes resulting in characteristic functional properties. These cells are then referred to as polarized M1 or M2 macrophages.

The “classically” activated M1 macrophages are induced by IFN- $\gamma$  alone or by microbial stimuli (i.e. LPS and BLP). By releasing high levels of cytokines such as TNF $\alpha$ , IL-6 and IL12<sup>72</sup>, M1 macrophages have cytotoxic ability toward tumor cells as well as toward cells that have ingested intracellular microorganisms. M1 macrophages are generally considered as potent effector cells, which defend the body against the attack of pathogens and tumor cells.

On the other hand, the “alternatively” activated M2 macrophages function as suppressors of inflammatory responses<sup>70</sup>. Tumor-associated macrophages share many characteristics with M2 macrophages in that they express the Triggering receptor expressed on myeloid cells-2 (Trem2)<sup>73</sup>, Resistin-like molecule  $\alpha$  (Rlm $\alpha$  or Fizz1)<sup>74</sup> and Arginase 1 (Arg1)<sup>75</sup>. Many experiments indicate that, in the tumor microenvironment, tumor-associated macrophages have several protumoral functions which are more similar to M2 macrophages, including expression of growth factors and matrix proteases, promotion of angiogenesis and suppression of adaptive immunity<sup>70</sup>.

### 2.3.3 Hh signaling in immune cells

There have been several studies on the role of Hh signaling in embryonic development and tissue patterning. However, the knowledge about its role in hematopoiesis and in the immune system is sparse. Bhardwaj and colleagues provided evidence that Hh proteins play a functional role in the development of human blood cells. They showed that *SHH*, *PTCH*, *SMO* and *GLI1-3* are expressed in CD34<sup>+</sup>CD38<sup>-</sup>LIN<sup>-</sup> stem cells isolated from human blood and also in cells comprising the haematopoietic microenvironment such as BM stromal cells. *SHH* and its receptors *PTCH* and *SMO* were also detected on committed cell subsets such as CD33<sup>+</sup> (myeloid), CD19<sup>+</sup> (B) and CD3<sup>+</sup> (T) cell populations. Since the downstream transcriptional regulators of the HH pathway, *GLI1-3* were not expressed in lineage restricted hematopoietic cells, the authors concluded that HH signaling is not essential to hematopoietic cell maturation. However, the authors found that blocking of endogenously produced HH or addition of exogenous soluble HH controlled the proliferation of uncommitted human hematopoietic cells. This showed that HH signals are critical to the proliferative regulation of hematopoietic progenitor cells and that HH is capable of regulating primitive blood cells and inducing human stem cell expansion<sup>76</sup>. Moreover, HH pathway activation is involved in the self-renewal capacity of HSC<sup>26</sup>.

### 2.3.3.1. Hh signaling and the lymphoid lineage

*SHH* and its receptor *PTCH* are also expressed on resting and activated human peripheral CD4<sup>+</sup> cells. Therefore it has been hypothesized that HH signaling may control the effector function of mature T lymphocytes. Indeed, *in vitro* experiments showed that the addition of exogenous SHH increased the production of IL-2, IFN- $\gamma$ , and IL-10 in activated CD4<sup>+</sup> T cells<sup>77</sup>. Furthermore, addition of Shh significantly enhanced proliferation of anti-CD3/28 Ab-activated CD4<sup>+</sup> T cells by promoting the entry of the cells into the S-G(2) proliferative phase of the cell cycle and not by anti-apoptotic effect<sup>78</sup>. Finally, endogenously produced Shh may also play a physiological role in the clonal expansion of murine T cells<sup>79</sup>. On the other hand, depletion of *Ptch* in mature T cells (which likewise should result in activation of Hh signaling) did not result in a definite defect of T cell function (Kai Michel et. al, manuscript in review).

Shh is not expressed by B cells in the germinal centers (GC), which are sites within lymph nodes where mature B lymphocytes rapidly proliferate and differentiate and produce their antibodies during a normal immune response to an infection. However, the follicular DC surrounding the B cells in GC strongly express Shh, which may transduce the signal to the neighboring B cells. Indeed, all B cells in GC express the Hh receptors *Ptch* and *Smo* and thus are capable of binding Hh proteins at their cell surface. Therefore, a fraction of these cells is probably capable of transducing the Hh signal into the cell. Indeed, inhibition of the Hh pathway by the addition of cyclopamine or anti-Shh mAb reduces the survival, and consequently the proliferation and immunoglobulin secretion of B cells in GC. Inversely, addition of Shh rescues B cells from apoptosis due to Fas ligation in GC<sup>80</sup>.

An interaction of B cells with HH produced by stromal cells is also evident in B cell malignancies<sup>81</sup>. Thus, infiltrating lymphoma cells in the spleen and BM of transgenic E $\mu$ -Myc mice expressed Gli1, Gli2 and Smo, whereas the surrounding DC, the mesenchymal stem cells as well as splenic stromal cells expressed Hh ligands, which function as survival factors for the tumor cells. This effect of stromal HH was the same on lymphoma and plasmacytoma cells isolated from humans with these malignancies. Furthermore, a blockage of Hh signaling *in vivo* inhibited expansion of mouse lymphoma cells and reduced the tumor mass in mice with fully developed disease. Therefore, stromally induced Hh signaling may provide an important survival signal for B cell malignancies<sup>81</sup>.

Hh signaling also seems to be involved in T and B cell lineage commitment. The first hint came from the study by El Andaloussi and colleagues. Using pre-T cell-specific, mature T cell-specific and ubiquitous deletion of *Smo* in mice, the authors reported that Hh is an essential positive regulator of T cell progenitor differentiation. Furthermore, their data localized Hh function to a stage preceding pre-T cell receptor signaling<sup>82</sup>. By inducibly abrogating *Ptch* expression in mice, our group then demonstrated that Hh signaling in stromal cells is mandatory for the specification of both B and T cell lineages at the CLP stage in the BM<sup>83</sup>. This was revealed by ubiquitous *Ptch* inactivation in the adult animal. *Ptch* mutant mice showed thymic atrophy and a defective T and B cell development, which was probably due to the loss of *Ptch* function in the stromal cell compartment.

### 2.3.3.2. Hh signaling and the myeloid lineage

The data about the role of HH signaling in cell subsets derived from the myeloid lineage is sparse. Detmer and colleagues demonstrated that HH signaling might be one of the mechanisms in the regulation of proliferation and differentiation of erythroid progenitor cells *in vitro*<sup>84,85</sup>. In addition, there is evidence that HH signaling may influence processes involved in myeloid leukemia, because HH signaling was activated in Bcr-Abl-positive leukemic stem cells via upregulation of *SMO*. In addition, *in vitro*, inhibition of HH signaling using cyclopamine induced apoptosis in Bcr-Abl-positive cells<sup>26</sup>. *Vice versa*, mouse experiment showed that loss of *Smo* and pharmacological inhibition of Hh signaling using cyclopamine impaired the induction and the propagation, respectively, of Bcr-Abl-associated chronic myelogenous leukemia (CML) by causing depletion of CML stem cells<sup>86</sup>. Finally, the chemotherapy-resistant phenotype of myeloid leukemia cells was recently correlated with activation of HH signaling, whereas in chemosensitive cells such activation was less pronounced<sup>87</sup>. These data indicated that Hh pathway activity is required for maintenance of normal and CML stem cells<sup>86</sup> and also plays a role in response of leukemic cell lines to chemotherapy.

In contrast, our group did not observe CML or other blood-related malignancy when *Ptch* was conditionally inactivated in mice<sup>83</sup>. In addition, the *Ptch* mutation had no effect on the differentiation of multipotent clonogenic myeloid progenitors into granulocytes, erythrocytes, megakaryocytes or macrophages. This difference to the above-mentioned data may have been caused by an incomplete loss of *Ptch* (both in the BM stroma and myeloid lineage) after conditional mutagenesis.

It is known that human CD33<sup>+</sup> (myeloid) cells express components of the HH pathway such as *PTCH* and *SMO* but lack the expression of *GLI1-3*<sup>76</sup>. About 80% of macrophages in human aortic atherosclerotic lesion also express PTCH. Furthermore, monocytes express *IHH* and *DHH* but not *SHH* or *GLI1-2*. Both SHH and IHH induce migration of human monocytes *ex vivo* in a concentration-dependent fashion<sup>88</sup>. Furthermore, Pereira et. al showed that macrophages in liver of patients infected with schistosoma can produce IHH and SHH and adopt a M2 phenotype. The authors also showed that exposure of murine macrophages to schistosoma egg antigen not only resulted in increased expression of *Gli* and *Ptch*, but also in increased expression of the M2 markers *Arg1* and *Fizz1*. The schistosoma egg antigen-induced expression of the M2 markers and of *Gli* and *Ptch* was inhibited after treatment of cells with the Smo inhibitor GDC-0449<sup>89</sup>. In contrast, exposure of murine macrophages with LPS did not lead to any significant change in *Ihh*, *Gli1* or *Ptch* expression. Together, these data suggest a role of Hh signaling in the function of more mature cell subsets derived from the myeloid lineage, i.e. macrophage, granulocytes or DC.

#### **2.4 Patched knockout mice: A model to study the function of Hh signaling in cancer and immunity**

Experiments in various mouse models have enormously improved our knowledge about Hh signaling not only in cancer but also in the immune system (see above). These models include transgenic *Smo* and *Sufu* or *Ptch* knockout mice (reviewed in<sup>90</sup>). In the present work, we applied a conditional mouse model of *Ptch*-deficiency (*Ptch*<sup>flox</sup>) to investigate the role of Hh signaling in LysM positive cells.

The conditional knockout *Ptch*<sup>flox/flox</sup> mouse model was generated by flanking exons 8 and 9 of the *Ptch* gene by loxP sequences<sup>83</sup>. The respective loxP sites are localized in introns 7 and 9. The loxP sites are recognized by the cre recombinase enzyme resulting in site-specific DNA recombination and the deletion of the loxP-flanked gene sequence in targeted tissues. The conditional *Ptch* knockout mouse has several benefits over the conventional knockout type. Thus, the homozygous *Ptch* deletion in conventional knockout mice results in embryonic lethality at d9.5 – d10.5 and impedes the investigation of effects of a biallelic *Ptch* knockout in the adult. In conditional knockout mice, the *Ptch* gene can be deleted in a time- and tissue-specific manner. In addition, the gene can be deleted mono- or biallelically both in the embryo and the adult organism. Tissue-specific gene deletions are usually carried out by

crossing mice with a floxed allele to mice expressing the cre recombinase under a tissue-specific promotor.

As reported by our group, *Ptch*<sup>flx/flx</sup> mice are born at the expected Mendelian ratio and are viable and fertile. Neither the loxP sites nor the neomycin resistance cassette in intron 9 disturb the normal splicing of the *Ptch* mRNA derived from the *Ptch*<sup>flx</sup> allele. The excision of exons 8 and 9 can be carried out very effectively, thereby generating the *Ptch*<sup>del</sup> allele<sup>91, 92, 83</sup>. This results in an aberrant *Ptch* transcript with exon 7 spliced into exon 10. This leads to a frameshift and a premature stop codon. Similar to homozygous mutants observed in conventional *Ptch* knockout mice on the same genetic background, homozygous *Ptch*<sup>del/del</sup> mutants die before embryonic day 10 in utero while *Ptch*<sup>del/+</sup> mice survive.

Our group has recently crossed *Ptch*<sup>flx/flx</sup> mice with the *Rosa26CreERT2* (*ERT2*) strain. *ERT2* is a knock-in mouse expressing a tamoxifen-inducible cre recombinase under control of the endogenous *Rosa26* promoter, which is ubiquitously active. Therefore, *Ptch* can be ubiquitously inactivated in the resulting *Ptch*<sup>flx/flx</sup>*ERT2*<sup>+/-</sup> offspring by injection of tamoxifen. This mouse model has been extensively used by our group to study the function of *Ptch* in the specification of B and T cell lineages<sup>83, 93</sup> and in the pathogenesis of RMS and BCC<sup>92, 94, 91</sup>.

## 2.5 *LysMcre* mice: a tool for highly efficient cre-mediated deletion of loxP-flanked target genes in myeloid cells

The antimicrobial, cationic protein Lys was identified as a major constitutive secretory product of mouse and human macrophages in culture<sup>95</sup>. In humans, LYS is strongly expressed in tissue monocytes and macrophages in several tissues like the spleen, lungs, kidneys, stomach and small intestine. Other organs like parts of the brain, pancreas and skin as well as muscle tissues are negative for LYS<sup>96</sup>.

In contrast to humans, who has one *LYS* gene<sup>97</sup>, the murine genome encodes for two *Lys* genes. These are the *LysM* gene specific for myeloid cells and the *LysP* gene expressed in Paneth cells<sup>98</sup>. The two murine genes evolve from a gene duplication event and thus share a high degree of homology<sup>99, 98</sup>. In mice, the highest *LysM* expression levels is found in lung and bone marrow, while weaker expression is detected in small intestine, spleen, and thymus. The levels of *LysM* are very low in the myeloblast and in immature macrophages, but are

very high in mature macrophages<sup>100</sup>. In addition to its constitutive expression in macrophages, up-regulation of *LysM* transcription is a marker of macrophage activation in murine tissues<sup>101</sup>. It has been shown that ablation of the *LysM* gene in mice leads to an increased inflammatory response to bacterial infections due to impaired function of granulocytes and macrophages<sup>102</sup>. Other than that, the mice show no overt defects in the hematopoietic system<sup>103</sup>.

In *LysMcre* mice, the *cre* recombinase gene is inserted into the first exon of the *LysM* gene. When crossed with a reporter mouse containing a lox-P site-flanked cassette, excision was detected in myelomonocytic cells including macrophages and granulocytes. In contrast, no significant deletion was observed in tail DNA or purified T and B cells<sup>104</sup>. Similarly, another study by Miyamoto and colleagues showed that virtually all myelomonocytic cells (granulocytes and monocytes) are *LysM*<sup>+</sup>. However, the authors also showed that *LysM* is not only expressed in myeloid progenitor cells but also in lymphoid progenitor cells, although at very low level. Thus, they found that 1–5% of CLP and Pro T cells expressed minimal levels of *LysM*<sup>67</sup>. In the myeloid pathway, 62% of CMP expressed significant levels of *LysM* while GMP expressed a 5-fold increase of *LysM* compared to CMP. A lineage tracing experiment further showed that besides macrophages (85.9 ± 4.0%,) also B cells (9.3 ± 3.9%,) and T cells (7.8 ± 3.9%) are derived from a *LysM*<sup>+</sup> precursor cell. Indeed, a consecutive analysis of HSC revealed that 20% of HSC express *LysM*. These results demonstrate that *LysM* expression does not only mark myeloid cells but probably other cells.



### **3 Aim of the Study**

The primary aim of the study was to analyze and understand the function of the Hh receptor *Ptch* in macrophages. For this purpose *Ptch* was conditionally mutated in *LysM* positive cells in *Ptch<sup>flox/flox</sup>LysMcre<sup>+/-</sup>* mice. According to the literature, this should result in the *Ptch* deletion mainly in macrophages, DC and granulocytes. Surprisingly, when *Ptch* was inactivated in *LysM*-expressing cells, the animals developed tumors of the gastrointestinal tract. To characterize the tumors, in situ hybridization, immunohistochemistry, immunoblot, quantitative RT-PCR analyses, cell transformation assays and lineage tracing experiments using *R26R-LacZ* reporter mice were performed.

Additional experiments were performed to get insight into the function of *Ptch* in myeloid cells. For this purpose the cytokine production, viability and proliferation of BMDM derived from *Ptch<sup>flox/flox</sup>LysMcre<sup>+/-</sup>* mice with/without stimulation with LPS or BLP was analyzed. Finally, in order to test the influence of the *Ptch*-deficient cells on the immune surveillance of tumors, *Ptch<sup>flox/flox</sup>LysMcre<sup>+/-</sup>* mice were either subjected to the two-stage chemical carcinogenesis DMBA/TPA protocol or were transplanted with syngeneic melanoma and ovarian carcinoma cells.

## 4 Materials and Methods

### 4.1 Technical equipment

**Table 1. List of laboratory equipment.**

Equipment	Supplier
-80°C Freezer(MDF-U71V)	Sanyo Electric Co., Ltd., Japan
Agarose gel electrophoresis chamber	Peqlab Biotechnologie GmbH, Erlangen
Agilent 2100 Bioanalyzer	Agilent Technologies, Waldbronn
Autoclave	W. Krannich GmbH & Co. K.G., Göttingen
Incubators	Kendro Laboratory Products GmbH, Hanau
Crosslinker (Crosslinker CL-1)	Herolab GmbH, Wiesloch
Digital Photo camera (PowerShot G2)	Canon Inc., Japan
Single channel pipettes	Eppendorf, Hamburg
Developing machine(Curix 60)	AGFA Deutschland Vertriebsgesellschaft mbH & Co, Köln
Weighing scale (Sartorius Basic plus)	Sartorius AG, Göttingen
Film cassette	Sigma-Aldrich Chemie GmbH, Steinheim
Gas burner (Gasprofi 2 scs)	WLD-TEC GmbH, Göttingen
Automated tissue processor (TP 1020)	Leica Mikrosysteme Vertrieb GmbH, Bensheim
Heat block (Thermomixer)	Eppendorf, Hamburg
Heating and stirring plate (MR 3000/3001)	Heidolph Instruments, Schwabach
Homogenizer (Micra D-1)	ART-moderne Labortechnik e.K., Müllheim
Hybridization oven (HB-1000 Hybridizer)	UVP, Inc., Upland, USA
Inverse microscope with fluorescence filter (Axiovert 25, Filter Set 43, 01, 09)	Carl Zeiss Jena GmbH, Jena
Cryostat (Modell CM 1900-1-1)	Leica Microsysteme Vertrieb GmbH, Bensheim
MilliQ-water purifier	MembraPure GmbH, Bodenheim
Mini centrifuge	Carl Roth GmbH, Karlsruhe
Multipette	Eppendorf, Hamburg
Paraffin dispenser, embedding machine (Dispenser PAG 12)	Medite Medizintechnik GmbH, Burgdorf
PCR machine	Eppendorf, Hamburg
PCR-machine (PrimusHT)	MWG AG Biotech, Ebersberg
PCR-machine (Robocycler Gradient 96 Combo)	Stratagene, Amsterdam Zuidoost, Netherlands
pH-Meter (inoLab pH Level 1)	WTW GmbH, Vienna, Austria
Photometer (Biophotometer 6131, Thermodrucker DPU-414)	Eppendorf, Hamburg, Germany
Pipette controller(Accu-jet)	Brand GmbH & Co. KG, Wertheim, Germany
Microtome (HN 40)	Leica Microsysteme Vertrieb GmbH, Bensheim, Germany
Shaker	New Brunswick Scientific GmbH, Nürtingen, Germany
Shaking water bath (1083)	GFL GmbH, Burgwedel, Germany
Sequencing machine (ABI 3100)	Applied Biosystems, Darmstadt, Germany
Stereo microscope (Stemi 2000)	Carl Zeiss Jena GmbH, Jena, Germany
Clean bench (Euroflow Class IIA)	Clean Air Techniek bv, Woerden, Netherlands
Power source for electrophoresis	Peqlab Biotechnologie GmbH, Erlangen, Germany
Liquid nitrogen tank	L'air liquide S.A., Paris, France

TaqMan (ABI Prism 7900HT)	Applied Biosystems, Darmstadt, Germany
UV-printer(Digital Monochrome Printer P91D)	Mitsubishi, Ratingen, Germany
UV-Transilluminator/Software	Intas, Göttingen, Germany
Vacuum pump	Schütt Labortechnik, Göttingen, Germany
Vortexer (Vortex-Genie 2)	Scientific Industries, Inc., Bohemia, USA
Cell counter	Omnilab-Krannich, Göttingen, Germany
Centrifuges (Biofuge pico, fresco, primo, Multifuge 3L-R)	Kendro Laboratory Products GmbH, Hanau, Germany
12 Channel-pipette	Eppendorf, Hamburg, Germany

## 4.2 Consumable materials

**Table 2. List of consumable materials.**

Consumer Goods	Supplier
1.5 ml microcentrifuge tubes	Ochs GmbH, Bovenden/Lenglern, Germany
13 ml tubes	Nunc GmbH & Co.KG, Wiesbaden, Germany
15 ml conical tubes	Greiner Bio-One GmbH, Frickenhausen, Germany
2.0 ml microcentrifuge tubes	Sarstedt AG & Co., Nürnberg, Germany
50 ml conical tubes	Sarstedt AG & Co., Nürnberg, Germany
Tissue Culture Plate (6-Well)	Sarstedt AG & Co., Nürnberg, Germany
Cleaning plate 96-well (MAHVN45)	Amersham Biosciences Europe GmbH, Freiburg, Germany
Blotting-Paper (GB 33 B003)	Heinemann Labortechnik GmbH, Duderstadt, Germany
Cover glass	Menzel GmbH & Co.KG, Braunschweig, Germany
Disposable pipette tips (Combitips plus)	Eppendorf, Hamburg, Germany
ECL-Film (Hyperfilm ECL)	Amersham Biosciences Europe GmbH, Freiburg, Germany
Disposable syringes (BD Plastipak)	BD GmbH, Heidelberg, Germany
Filter paper	Schleicher & Schüll, Dassel
Glasswares	Schott AG, Mainz, Germany
Disposable needles (Sterican Ø 0,45 x 12 mm)	B. Braun Medical AG, Emmenbrücke, Germany
Cryopreservation solution (Cryo.s)	Greiner Bio-One GmbH, Frickenhausen, Germany
Cuvettes (UVette)	Eppendorf, Hamburg, Germany
96 Well Assay Plate (for luminescence measurement)	Costar, Corning Incorporated, New York, USA
Nitrocellulose membrane (Hybond-XL)	Amersham Biosciences Europe GmbH, Freiburg, Germany
Microscope slides (SuperFrost Plus)	Menzel GmbH & Co.KG, Braunschweig, Germany
2 well culture slides (Culture Slides)	BD Falcon, Heidelberg, Germany
Pasteur pipettes	Brand GmbH & Co.KG, Wertheim, Germany
PCR-reaction tube and lid (ThermoFast 96, non-skirted, natural domed cap strips, natural)	Sarstedt AG & Co., Nürnberg, Germany
Petri dish	Ochs GmbH, Bovenden/Lenglern, Germany
Pipette tips, with filter (10 µl, 100 µl, 200 µl, 1000 µl)	G. Kisker GbR, Steinfurt, Germany
Pipette tips, without filter (10 µl, 200 µl)	Ochs GmbH, Bovenden/Lenglern, Germany
Pipettenspitzen, ungestopft (1000 µl)	Sarstedt AG & Co., Nürnberg, Germany

Serological pipettes (5 ml, 10 ml, 25 ml)	Sarstedt AG & Co., Nürnberg, Germany
Scalpel	Aesculap AG & Co.KG, Tuttlingen, Germany
Sterile filter	Omnilab-Krannich, Göttingen, Germany
96-Well Optical Reaction Plate, 384-well Optical Reaction Plate, Optical Adhesive Covers	Applied Biosystems, Darmstadt, Germany
Cell culture plates, 100 mm, 35 mm (NuncIon Surface)	Nunc GmbH & Co.KG, Wiesbaden, Germany

### 4.3 Reagents and Chemicals

The chemicals not listed below were obtained from Sigma-Aldrich Chemie GmbH, Steinheim, Germany.

**Table 3. List of chemical and reagents.**

Chemicals and Reagents	Supplier
1 kb DNA, 50 bp und 100 bp DNA Ladder	Invitrogen GmbH, Karlsruhe, Germany
Acetic anhydride	Carl Roth GmbH & Co. KG, Karlsruhe, Germany
Agarose	Invitrogen GmbH, Karlsruhe, Germany
BLP (Pam <sub>3</sub> CSK <sub>4</sub> )	InvivoGen San Diego, USA
BM Purple	Roche Diagnostics GmbH, Mannheim, Germany
Boric acid	ICN Biomedicals Inc., Aurora, USA
Citric acid (monohydrate)	Carl Roth GmbH & Co. KG, Karlsruhe, Germany
Cryoblock embedding medium	Medite Medizintechnik GmbH, Burgdorf, Germany
Deoxyribonucleotidtriphosphate (dNTP)	Roche Diagnostics GmbH, Mannheim, Germany
Diethyldicarbonate (DEPC)	Carl Roth GmbH & Co. KG, Karlsruhe, Germany
Dig RNA Labelling Mix, 10x conc.	Roche Diagnostics GmbH, Mannheim, Germany
Dulbecco's Modified Eagle Medium (DMEM)	PAN Biotech GmbH, Aidenbach, Germany
Eosin Y	Carl Roth GmbH & Co. KG, Karlsruhe, Germany
Ethylenediaminetetraacetic acid (EDTA)	ICN Biochemicals Inc., Aurora, USA
Fetal Calf Serum (or Fetal Bovine Serum)	Gibco, Invitrogen GmbH, Karlsruhe, Germany
Formamide, 99% DNase, RNase free	Acros Organics, Geel, Belgium
Glycer gel mounting medium	Dako GmbH, Hamburg, Germany
Horse serum (heat inactivated)	Gibco, Invitrogen GmbH, Karlsruhe, Germany
Hydrogen peroxide, 30%	Merck KGaA, Darmstadt, Germany
I-Block (for antibody blocking buffer)	Tropix, Bedford, USA
Imatinib (Glivec)	Novartis International AG, Basel, Switzerland
Immuno Mount	Shandon Thermo Electron Corporation, Waltham, USA
Insulin	Sigma-Aldrich Chemie GmbH, Steinheim, Germany
Lipopolysaccharide (LPS, from <i>E. coli</i> , serotype O55:B5)	Enzo Life Sciences GmbH, Lörrach, Germany
Ketanest S (25 mg/ml)	Pfizer Pharma GmbH, Karlsruhe, Germany

Mayer's Hemalaun solution	Merck KgaA, Darmstadt, Germany
Mounting medium (Vectrashield Mounting Medium with DAPI)	Vector Laboratories, Inc., Burlingame, USA
Oligo(dT)-Nucleotide (50 ng/μl)	Roche Diagnostics GmbH, Mannheim, Germany
Paraformaldehyde	Carl Roth GmbH & Co. KG, Karlsruhe, Germany
PBS tablets; ready to use solution	GIBCO Invitrogen GmbH, Karlsruhe, Germany
PDGF-BB (recombinant, human)	R&D Systems, Wiesbaden-Nordenstadt, Germany
Penicillin (10000 U/ml)/Streptomycin (10 mg/ml)	PAN Biotech GmbH, Aidenbach, Germany
Pertex mounting medium	Medite Medizintechnik GmbH, Burgdorf, Germany
Polyinosinic-polycytidylic acid (Poly I:C)	Enzo Life Sciences GmbH, Lörrach, Germany
Rapid-hyb Buffer	Amersham Biosciences Europe GmbH, Freiburg, Germany
Ringer-Lactate	B. Braun Melsungen AG, Melsungen, Germany
RNase-DNase free water	Invitrogen GmbH, Karlsruhe, Germany
Rompun (2%)	Bayer AG, Leverkusen, Germany
RPMI 1640 Medium	PAN Biotech GmbH, Aidenbach, Germany
Sephadexg-50 fine	Amersham Biosciences Europe GmbH, Freiburg, Germany
Sodiumdodecylsulfate (SDS)	Carl Roth GmbH & Co. KG, Karlsruhe, Germany
TrypLE Express	Gibco, Invitrogen GmbH, Karlsruhe
TRIzol	Invitrogen GmbH, Karlsruhe, Germany
Tween-20	Scharlau Chemie S.A., Barcelona, Spain
water (Ampuwa)	Fresenius Kabi Deutschland GmbH, Bad Homburg, Germany
WST-1 reagent	Roche Diagnostics GmbH, Mannheim, Germany
X-Gal	Carl Roth GmbH & Co. KG, Karlsruhe, Germany
Xylene	J. T. Baker B.V., Deventer, Netherlands

#### 4.4 Kits and ready-to-use reaction systems

All kits and ready-to-use reagents were used according to manufacturer's instructions.

**Table 4. List of ready-to use kits and reaction systems.**

Ready-to-use Kits and Reaction Systems	Supplier
Pierce ® BCA Protein Assay Kit	Thermo Fisher Scientific, Rockford, USA
CD11b Microbeads	Miltenyi Biotec, Cologne, Germany
Cell Proliferation ELISA, BrdU (chemiluminescence)	Roche Diagnostics GmbH, Mannheim, Germany
Dako REAL TM EnVision TM Detection System	Dako Denmark A/S, Glostrup, Denmark
Enhanced chemoluminescence (ECL) Kit	Amersham Biosciences Europe GmbH, Freiburg, Germany
PureLink HiPure Plasmid Midiprep Kit	Invitrogen GmbH, Karlsruhe, Germany
QuantiTect SYBR Green PCR	Qiagen GmbH, Hilden, Germany
RotiFect	Carl Roth GmbH & Co. KG, Karlsruhe,

SYBR Green

Germany  
Invitrogen Invitrogen GmbH, Karlsruhe,  
Germany

## 4.5 Buffers and solutions

Unless otherwise mentioned, all solutions were prepared using double distilled water (Sartorius AG, Goettingen).

**Table 5. List of buffers and solutions.**

AEC chromogen pH 5.2	30 mM Acetic acid 70 mM Sodium acetate trihydrate 16 mM 3-Amino-9 Ethylcarbazole (dissolved in dimethyl formamide)
Boric acid pH 5.1	0.2 M Boric acid pH 5.1
Citrate buffer pH 3.0	10 mM Sodium citrate pH 3.0
Citrate buffer pH 6.0	10 mM Sodium citrate pH 6.0
Cresol	0.1% (w/v) Cresol Saturated sucrose solution
Denaturing buffer	1.5 M NaCl 0.5 M NaOH
Deoxyribonucleotide Triphosphate (dNTP-Mix)	10 mM dATP 10 mM dTTP 10 mM dGTP 10 mM dCTP
Eosin, 1%	1% (w/V) Eosin y (water soluble) 80% (v/v) Ethanol
Glutaraldehyde/1xPBS	0.2% (v/v) Glutaraldehyde 1x PBS
High-Stringency buffer	0.1% (w/v) Sodium dodecyl sulfate (SDS) 0.2 x standard sodium citrate solution (SSC). pH 7.0
Hybridization buffer	40% (v/v) Formamide 10% (w/v) Dextran sulfate 4x SSC pH 6.4 1x Denhards
LacZ-staining buffer	5 mM $K_3Fe(CN)_6$ 5 mM $K_4Fe(CN)_6$ 2 mM $MgCl_2$ 0.02% (v/v) NP-40 0.01% (w/v) Natrium Deoxycholate 500 µg/ml X-Gal 1x PBS
LacZ-buffer	2 mM $MgCl_2$ 0.02% (v/v) NP-40 0.01% (w/v) Sodium Deoxycholate

	1x PBS
Running buffer	50% (v/v) Glycerol 0.02% (w/v) Xylenecyanol 0.02% (w/v) Bromphenol blue 0.02% (w/v) SDS 100 mM EDTA
MBSTL buffer pH 7,5	0.15 M NaCl 0.1 M Maleic acid 2 mM Levamisole 0.1% Tween-20
New Fuchsine chromogen	0.6% (v/v) N,N-Dimethyl formamide 0.05% (w/v) Levamisole 0.03% (w/v) Naphtol As-Bi Phosphate 0.02% (w/v) NaN <sub>3</sub> 0.01% (w/v) New Fuchsine 1x TBS pH 8.8 (Tris-buffered saline solution)
Neutralizing buffer	2.55 M Potassium acetate pH 5.5
Low stingency buffer	0.1% SDS 2x SSC pH 7.0
NT-buffer	0.15 M NaCl 0.1 M Tris/HCl pH 7.5
NTM-Puffer	0.1 M NaCl 0.1 M Tris/HCl pH 9.5 50 mM MgCl <sub>2</sub>
NTMLT-buffer	0.1 M NaCl 0.1 M Tris/HCl pH 9.5 50 mM MgCl <sub>2</sub> 2 mM Levamisole 0.1% Tween-20
Paraformaldehyde	4% (w/v) Paraformaldehyde 1x PBS
Phosphate buffered saline solution, 10x, pH 7,4 (PBS, stock solution)	1.4 M NaCl 27 mM KCl 15 mM KH <sub>2</sub> PO <sub>4</sub> 65 mM Na <sub>2</sub> HPO <sub>4</sub>
Proteinase K-buffer	50 mM Tris/HCl pH 8.0 5 mM EDTA 40 µg/ml Proteinase K
Resuspension buffer	50 mM Tris/HCl pH 8.0 10 mM EDTA 100 µg/µl RNase A (Ribonuclease A; Qiagen GmbH, Hilden)
Standard sodium citrate solution (SSC), 20x pH 7.0	0.3 M Sodium citrate 3 M NaCl

STE-buffer	50 mM Tris/HCl pH 8.0 100 mM NaCl 1 mM EDTA 1% (w/v) SDS
STE- <i>in situ</i> -buffer	10 mM Tris/HCl pH 8.0 5 mM EDTA pH 8.0 0.5 M NaCl
Stop-buffer	10 mM Tris/HCl pH 8 1 mM EDTA
Tris-EDTA buffer pH 9,0 (TE)	10 mM Tris 1 mM EDTA
Tris-Boric acid-EDTA Solution, 10x (TBE; stock solution)	890 mM Tris/HCl pH 8.0 730 mM Borsäure 12.5 mM EDTA
Tris-buffered saline solution, 10x (TBS; stock solution)	0.5 M Tris/HCl pH 7.4 1.5 M NaCl
X-Gal stock solution	40 mg/ml X-Gal 100% N,N-Dimethylsulfoxide (DMSO)

## 4.6 Media

### 4.6.1 Media for bacterial culture

Lysogeny broth medium (LB medium; 1% (w/v) Bacto-tryptone, 0.5% (w/v) yeast extract, 1% (w/v) NaCl (pH 7.0) was prepared with double-distilled water, autoclaved and stored at 4°C. By adding 50 µg/ml ampicillin (Carl Roth GmbH, Karlsruhe, Germany) or 25 µg/ml kanamycin (Carl Roth GmbH, Karlsruhe, Germany) was carried out immediately prior to use of the medium, the selection on respective resistance-mediating genes.

### 4.6.2 Agar plates

LB agar plates were prepared using LB medium with 1.5% (w/v) agar. The solution was autoclaved and cooled to 55°C. Appropriate antibiotics were added to the warm LB agar. Then, the agar was poured into 10 cm Petri dishes. When solidified, the agar plates were stored in sterile plastic bags at 4°C.



### 4.6.3 Media and reagents for cultivation of eukaryotic cell lines

**Table 6. List of supplementary materials used for cell culture.**

Supplementary materials	Supplier
Dulbecco's Modified Eagle Medium (DMEM)	PAN Biotech GmbH, Aidenbach, Germany
Fetal Calf Serum (or Fetal Bovine Serum)	Gibco, Invitrogen GmbH, Karlsruhe, Germany
Horse serum (heat inactivated)	Gibco, Invitrogen GmbH, Karlsruhe, Germany
Insulin	Sigma-Aldrich Chemie GmbH, Steinheim, Germany
Penicillin (10000 U/ml)/Streptomycin (10 mg/ml)	PAN Biotech GmbH, Aidenbach, Germany
RPMI 1640 Medium	PAN Biotech GmbH, Aidenbach, Germany
Sodium selenite	Sigma-Aldrich Chemie GmbH, Steinheim, Germany
Transferrin	Sigma-Aldrich Chemie GmbH, Steinheim, Germany
TrypLE Express	Gibco, Invitrogen GmbH, Karlsruhe

## 4.7 Biological materials

### 4.7.1 Bacterial strains and growth

The transformation and amplification of plasmid DNA was done in chemical-competent host strain *E. coli* DH5  $\alpha$  (Invitrogen GmbH, Karlsruhe, Germany). Fifty  $\mu$ l of competent cells were thawed on ice. One hundred ng of pure plasmid was added and incubated for 20 min, on ice. Cells were heat shocked by putting them at 42°C for 45 sec to allow the plasmid to enter the cell. Cells were then placed again on ice for 2 min and then filled with 500  $\mu$ l SOC medium and incubated for 1 h at 37°C with gentle shaking. About 10-250  $\mu$ l of transformed cells were plated on agar plates with appropriate antibiotics. Agar plates were incubated overnight in an incubator at 37°C.

### 4.7.2 Eukaryotic cell lines

The media and supplements used to grow eukaryotic cell lines are specified in Table 6. Eukaryotic cells were generally grown in Dulbecco's Modified Eagle Medium (DMEM) or RPMI 1640 medium supplemented with 10% FBS and 1% antibiotics. All cell lines were cultured in an incubator with constant 37°C, 5% CO<sub>2</sub> and 95% humidity. Media was refreshed every 3 to 4 days. When reaching 80% to 90% confluence, the cells were passaged. The cell lines and the respective culture conditions are given in Table 7.

**Table 7. List of the eukaryotic cell lines, media and supplement used in this study.**

Cell line	Media	Supplement given
B16F10 (murine melanoma cells)	RPMI 1640	10% FBS
GIST-T1 (human GIST cells)	RPMI 1640	100 U/ml penicillin/(100 µg/ml)Streptomycin 10% FBS
NIH/3T3 (murine embryonic fibroblast)	DMEM	100 U/ml Penicillin/(100 µg/ml)Streptomycin 10% FBS
L929 (murine fibroblast)	RPMI 1640	100 U/ml Penicillin/(100 µg/ml)Streptomycin 10% FBS
ID8-Luciferase (ID8-LUC) (murine ovarian carcinoma with infected with luciferase reporter construct)	DMEM	4% FBS 5 µg/ml insulin 5 µg/ml transferrin 5 ng/ml sodium selenite
BMDM (murine bone marrow-derived macrophages)	DMEM	Pluznik medium for differentiation: 10% FBS 30% L929-CM 5% horse serum 0,002% β-Mercaptoethanol
	DMEM	BMDM-culture medium: 15% L929-CM 10% FBS

### 4.7.3 Mouse lines

All experiments using animals were performed in compliance with all legal and ethical requirements. *Ptch*<sup>flx/flx</sup> mice were crossed to *LysMcre*<sup>+/-</sup> mice. The resulting *Ptch*<sup>flx/+</sup>*LysMcre*<sup>+/</sup> were backcrossed to *Ptch*<sup>flx/flx</sup> mice resulting in *Ptch*<sup>flx/flx</sup>*LysMcre*<sup>+/-</sup>. *Ptch*<sup>flx/flx</sup> mice have *loxP* sites in *Ptch* introns 7 and 9<sup>83</sup>. *LysMcre* mice express cre recombinase under the control of the endogenous *LysM*-promoter (see introduction). This cre driver targets mouse cells of the myeloid lineage, due to their expression of *LysM*<sup>104</sup>. *R26R-LacZ* and mice carry a cre-inducible *LacZ* under the control of the endogenous, ubiquitously-active *Rosa26* promoter<sup>105, 106</sup>. *Ptch*<sup>flx/flx</sup> mice were on a mixed C57BL/6 x Balb/c and all other mice on a C57BL/6 background. *Ptch*<sup>flx/flx</sup>*LysMcre*<sup>+/-</sup> mice were crossed to *R26R-LacZ* animals resulting in *Ptch*<sup>flx/flx</sup>*LysMcre*<sup>+/-</sup>*R26R-LacZ*<sup>+/-</sup> mice. In the latter mice all *LysM*-expressing cells are marked by the permanent expression of *LacZ*.

**Table 8. Mouse lines used.**

Mouse line	Genetic background	Genetic modification
<i>Ptch</i> <sup>lox</sup>	mixed C57BL/6 x Balb/c or C57BL/6	Floxed exons 8 and 9 of the murine <i>Ptch</i> gene; useful for conditional <i>Ptch</i> gene deletion <sup>83</sup>
<i>ROSA26-R</i>	C57BL/6	Integration of the beta-galactosidase gene in the ROSA26 locus <sup>105</sup>
<i>LysMcre</i>	C57BL/6	Targeted insertion of <i>cre</i> cDNA into the endogenous <i>LysM</i> locus <sup>104</sup>
<i>Rag-2</i> <sup>-/-</sup> $\gamma$ <i>c</i> <sup>-/-</sup>	C57BL/6	<i>Rag2</i> coding region is deleted; Lacks mature T and B lymphocytes due to an inability to initiate V(D)J rearrangement <sup>107</sup>

#### 4.8 Synthetic Oligonucleotides

Synthetic DNA oligonucleotides were obtained from Qiagen GmbH, Hilden, Germany. The stock concentration of 100  $\mu$ M was adjusted with DNase and RNase-free water. For PCR (see section 4.10.3) the working concentration was 10  $\mu$ M.

**Table 9. Gene-specific DNA-oligonucleotides (primers) for mouse genotyping.**

Genotyping		
Primer Name	Primer Sequence (5'-3' orientation)	Application
mLys1	CTTGGGCTGCCAGAATTTCTC	Genotyping of <i>LysMcre</i> mice
mLys2	TTACAGTCGGCCAGGCTGAC	
Cre8	CCCAGAAATGCCAGATTACG	
Rosa1	AAAGTCGCTCTGAGTTGTTAT	Genotyping of Rosa26R- <i>LacZ</i> knock-in mice
Rosa2	GCGAAGAGTTTGTCTCAACC	
Rosa3	GGAGCGGGAGAAATGGATATG	
p910F.4	GCGAAGAGTTTGTCTCAACC	Genotyping of <i>Ptch</i> <sup>lox</sup> mice
p1011R.2	GGAGCGGGAGAAATGGATATG	
Neo-F	CGTGATATTGCTGAAGAGCTTGG	
Neo-R	GCATCAGAGCAGCCGATTGTCTG	
Exon 7-F	AGGAAGTATATGCATTGGCAGGAG	
mPTCwt_R.2	ACACAACAGGGTGGAGACCAC T	
mPTCN <sub>x</sub> _f	TGGTAATTCTGGGCTCCCGT	
mPTCN <sub>x</sub> _r	CCGGTAGAATTAGCTTGAAGTTCCT	

**Table 10. List of primers used for semi-quantitative PCR in this study.**

Semi-Quantitative RT-PCR		
Primer Name	Primer Sequence (5'-3' orientation)	Application
mCD21F.1	CTGTGAGAGTGATTTCCCTCTGGA	murine <i>CD21</i> expression analysis
mCD21R.2	GCAAATAGCCAGGTTACAACTGTA	
mCD23F.1	ATTTCAAAGGGAAGTGCATGCA	murine <i>CD23</i> expression analysis
mCD23R.1	ACTAGTCGCCCTTGCAGGTCA	
mCD35F.1	TTGTAATCAAGGATACCGCCTCATT	murine <i>CD35</i> expression analysis
mCD35R.1	AGAAATCTCCATTGGGAATGCCT	
Krt 7 F1	GCCTGGAGGTGGAAGTGCAGAAC	murine <i>Krt7</i> expression analysis
Krt 7 F2	CAGCTCGAGACACTGCAGCTGGAT	
Gapdh-F	ATCTTCTTGTGCAGTGCCAG	murine <i>Gapdh</i> expression analysis
Gapdh-R	ATGGCATGGACTGTGGTCAT	

**Table 11. List of primers used for quantitative RT-PCR.**

Quantitative RT-PCR		
Primer Name	Primer Sequence (5'-3' orientation)	Application
mHand2F.1	TGGCCAAGGACGACCAGAA	murine <i>Hand2</i> expression analysis
mHand2R.1	TTCAAGATCTCATTCAGCTCTTCTTC	
mFoxf1F.1	AACAGCCTCTGTCCCCTTGC	murine <i>FoxF1</i> expression analysis
mFoxf1R.1	CGAGGGATGCCTTGCAGTTCT	
mPTC10	TACAGTCCGGGACAGCATACC	murine <i>Ptch</i> expression analysis
mPTC11R	GTACCCATGGCCAAGTTCGGCTTT	
mGli1-tq-f	TACATGCTGGTGGTGCACATG	murine <i>Gli1</i> expression analysis
mGli1-tq-r	ACCGAAGGTGCGTCTTGAGG	
Gli2-RT-PCR-F	GGTCATCTACGAGACCAACTGC	murine <i>Gli2</i> expression analysis
Gli2-RT-PCR-R	GTGTCTTCAGGTTCTCCAGGC	
Gli3F2	GAAGGAACAACCCTAGTCAAGGAGGA	murine <i>Gli3</i> expression analysis

Quantitative RT-PCR

Primer Name	Primer Sequence (5'-3' orientation)	Application
<i>Gli3</i> -sybrgree R	CCAGCGGCACACGAACTCCTTCT	
mPdga F	GCAAGACCAGGACGGTCATTTAC	murine <i>Pdga</i> expression analysis
mPdga R	GGCTTCTTCCTGACATACTC	
mPdgb F	GGCTGCTGCAATAACCGCAATG	murine <i>Pdgb</i> expression analysis
mPdgb R	CCTGGATGTCCCAGGACTTCTAG	
mPdgc F	GTACCTAGAGCCAGATCGATGG	murine <i>Pdgc</i> expression analysis
mPdgc R	CTCTTCCCGTATGGACACTGAG	
18S-fwd	CGCAAATTACCCACTCCCG	murine <i>18s</i> expression analysis
18S-rev2	TTCCAATTACAGGGCCTCGAA	
hGLI2 F	TGGCCGCTTCAGATGACAGATGTTG	human <i>GLI2</i> expression analysis
hGLI2 R	CGTTAGCCGAATGTCAGCCGTGAAG	
<i>PTCH</i> F	TGGGATTAAGCAGCGAAC	human <i>PTCH</i> expression analysis
<i>PTCH</i> R	TCTCCAATCTTCTGGCGAGT	
HAND2 F	CCTTTGAGGCATCTGCTCC	human <i>HAND2</i> expression analysis
HAND2 R	GCACACGGGAGTGTCTC	
FOXF1 F	CGTATCTGCACCAGAACAGC	human <i>FOXF1</i> expression analysis
FOXF1 R	GACAACTCCTTTCGGTCACA	

**Table 12 List of primers used for quantification of recombination efficiency<sup>108</sup>.**

<b>Probe based qRT-PCR</b>			
mPTCN <sub>x</sub> _f	TGGTAATTCTGGGCTCCCGT	exon 9/ intron 9-10	quantification of <i>Ptch</i> <sup>del</sup> <i>alleles</i>
mPTCdelN <sub>x</sub> _f	TTCATTGAACCTTGGGGAACATT	intron 7-8	
mPTCN <sub>x</sub> _r	CCGGTAGAATTAGCTTGAAGTTCCT	targeting vector	
mPTCN <sub>x</sub> _S2	YYE <sup>6</sup> ~ TTGGTTTGTAAATTTACTTTG ACGGTACCTCGA ~ BHQ2a~Q <sup>7</sup> (in combination with primers mPTCN <sub>x</sub> _f / mPTCN <sub>x</sub> _r; see above)	intron 9-10	
mPTCdelN <sub>x</sub> _S1	FAM <sup>8</sup> ~ CACACCAGACCAGCTTGCAAA GAGATC ~ BHQ1 <sup>7</sup> (in combination with primers mPTCdelN <sub>x</sub> _f mPTCN <sub>x</sub> _r; see above)	intron 7-8	
Pelo-F1	CGGTCTGAGTGCTGGTAGGGA	3' UTR	quantification of <i>Pelota</i>
Pelo-R	TCTGCACCTTAGCGTGAAGCC	3' UTR	
Pelo-Sonde2	FAM <sup>8</sup> ~ GAG CGA GCA AAG CCA GGC AGA GTT ~ BHQ1 <sup>7</sup>	3' UTR	

#### 4.9 Antibodies

For western blotting see 4.12.

**Table 13. List of antibodies used for western blot and the appropriate dilutions.**

<b>Primary antibodies for Western Blot</b>	<b>Dilution ***</b>
pAb rabbit anti- p-cKit (Tyr 719) Cell Signaling, 3319	1:1000
pAb rabbit anti- p-Pdgfra (Tyr 754) Santa Cruz Biotechnologies, SC12911	1:500
pAb rabbit anti- Pdgfra (C-20) Santa Cruz Biotechnologies, SC 338	1:500
mAb mouse anti-β actin (C4) Santa Cruz Biotechnologies, SC 47778	1:5000
mAb rabbit anti- Actin Cell signaling 4970S	1:5000
mAb mouse anti p-p44/42 (Thr202/Tyr204) Cell Signaling, 9106	1:1000

pAb rabbit anti p44/42 Cell Signaling, 9102	1:1000
mAb mouse anti p-c-JUN (KM-1) Santa Cruz Biotechnologies, SC-822	1:200
mAb rabbit anti c-JUN (60A8) Cell Signaling, 9165	1:500
<b>secondary antibodies for Western Blot</b>	<b>dilution</b>
pAb mouse anti- rabbit/HRP** Sigma AO545	1:5000
pAb sheep anti- mouse/HRP** Amersham NA931	1:10000

\*:antibody binding was visualized using DAB+ (En vision+ system-HRP, Dako) or aminoethylcarbazol as chromogen; \*\*: signals were visualized using the ECL plus detection system (GE Healthcare); \*\*\*: diluted 0.02% casein in TBS.

**Table 14. Primary and secondary antibodies and the antigen retrieval methods used for immunohistochemistry.**

<b>primary antibodies for IHC</b>	<b>dilution (diluting buffer)</b>	<b>antigen retrieval</b>
pAb rabbit anti-Pdgfra (C-20) Santa Cruz Biotechnologies, SC 338	1:1000 (TBS)	boric acid pH 5.2; 30 min, 60°C
mAb rabbit anti- Pdgfrβ (C82A3) Cell Signaling 4564	1:1000 (TBS)	citric acid pH 6; heat mediated
pAb rabbit anti- Desmin Dianova 13732	1:1000 (TBS)	citric acid pH 6; heat mediated
mAb rat anti- cKit Cedarlane CL8936AP	1:200 (TBS)	none
mAb rat anti-F4/80 Serotec MCA497GA; Clone CI:A3-1	1:100 (0.02% casein in TBS)	none
mAb mouse anti-Ki-67 BD Pharmingen	1:50 (TBS)	citric acid pH 6; heat mediated
mAb mouse anti-SMA Beckman Coulter PN IM1144 clone 1A4	1:50 (TBS)	none
mAb rat anti-MHC II (purified anti-mouse I-A/I-E) BioLegend, #107602	1: 100 (0.02% casein in TBS)	boric acid pH 5.2; 30 min, 60°C
pAb rat anti-CD3 Serotec; Clone CD3-12, MCA1477	1: 100 (TBS)	citric acid pH 6; heat mediated
<b>secondary antibodies for IHC</b>	<b>dilution</b>	
En vision+ anti- rabbit/mouse/HRP* Dako K5007	undiluted	
rabbit anti rat/biotinylated Dako E0468 and Streptavidin/HRP* Dako P0397	1:100 (0.02% casein in TBS) 1:1000 (TBS)	
<b>primary antibodies for immunofluorescence</b>	<b>dilution</b>	
mAb rat anti- cKit Cedarlane CL8936AP	1:200 (TBS)	
mAb rabbit anti- PDGFRα Cell signaling 3174	1:100 (TBS)	
pAb goat anti- GFP Rockland 600-101-215	1:400 (TBS)	

secondary antibodies for immunofluorescence	dilution
Rhodamin red conj. anti- rat Jackson Laboratories 712-295-153	1:200 (TBS)
488 (green) anti- rat Invitrogen A-21208	1:1000 (TBS)
488 (green) anti- rabbit Invitrogen A-21206	1:1000 (TBS)
568 (red) anti- goat Invitrogen A-11057	1:1000 (TBS)

**Table 15. Primary antibodies and used for flow cytometric analysis.**

primary antibodies for immunofluorescence	dilution*
mAb rabbit anti-B220 PE-Cy7 BD Bioscience	1:50
mAb rat anti-CD19 FITC BD Bioscience	1:50
mAb rat anti-CD3-Cy5 BD Bioscience	1:50
mAb rat anti-TCR $\beta$ -FITC BD Bioscience	1:50
mAb rat anti-CD11b-FITC BD Bioscience	1:50
mAb rat -Gr1- PE BD Bioscience	1:50
mAb rat -IL4R $\alpha$ BD Bioscience	1:50

\* All antibodies were diluted in PBS.

## 4.10 Molecular biology methods

### 4.10.1 Nucleic acid isolation

#### 4.10.1.1 Genomic DNA isolation

Genomic DNA (gDNA) was isolated from tissue which was incubated overnight at 55°C in 400  $\mu$ l of STE buffer containing 0.5 mg/ml Proteinase K. Undigested tissue was separated by centrifugation for 10 min at 13000 rpm. Nucleic acid in the supernatant was precipitated in 99% ethanol and pelleted by centrifugation (25 min, 13000 rpm). The pellet was washed with 70% ethanol, dried and diluted in 125  $\mu$ l ddH<sub>2</sub>O for 10 min at 42°C (with shaking).

#### 4.10.1.2 Total RNA isolation

RNA was extracted from tissue and cell samples using TRIzol reagent (Invitrogen), following the manufacturer's instructions. Briefly, cells were rinsed with PBS and detached in 1 ml TRIzol by pipetting. To avoid RNA degradation the following steps were performed on ice, unless stated otherwise. Samples were vortexed for 2 min and then incubated for 5



min at room temperature (RT). Subsequently, 200 µl chloroform were added followed by vortexing for 15 sec and an incubation step for 3 min at RT. Afterwards, the mixture was centrifuged for 10 min at 6000 g and 4°C. The upper phase was transferred into a new 1.5 ml E-cup containing 1 ml isopropyl alcohol, inverted and precipitated overnight at -20°C. Subsequently, the mixture was centrifuged for 30 min at 10000 g and 4°C. The supernatant was discarded and the remaining pellet was washed with 1 ml 70% ethanol (-20°C) by centrifugation for 10 min at 10000 g and 4°C. Afterwards, supernatant was removed and the pellet was air-dried at RT. Subsequently, pellet was dissolved in 20 µl RNase-free H<sub>2</sub>O for 5-10 min at 56°C.

The DNA and RNA concentration were measured using a photometer (see quantification method below).

#### **4.10.2 Photometric quantification of nucleic acids**

One µl of DNA or RNA sample was diluted (100x) in RNase- and DNase-free water. The concentration of nucleic acids was measured using a photometer at a wavelength of 260 nm to quantify the DNA/RNA and at a wavelength of 280 nm to determine the purity of the sample. DNA or RNA concentrations can be estimated by measuring the optical density at 260 nm (OD<sub>260</sub>), using the relationship that an OD<sub>260</sub> of 1.0 equates 50 µg/ml or 40 µg/ml pure DNA or RNA, respectively. The concentration thus can be calculated according to the following formula: concentration (µg/ml) = OD<sub>260</sub> × dilution factor × 50 (for DNA) or 40 µg/ml (for RNA). The purity of the sample was assessed by OD reading at 280 nm (OD<sub>280</sub>) for the amount of protein in the sample. Pure preparations of DNA and RNA have OD<sub>260</sub>/OD<sub>280</sub> values of 1.8 to 2.0, respectively.

#### **4.10.3 Polymerase chain reaction (PCR)**

##### **4.10.3.1 Reverse Transcription (cDNA synthesis)**

Two µg of RNA were reverse transcribed in a final volume of 20 µl. 250 ng hexamers were incubated with RNA for 10 min at 70°C. Next, 1st strand buffer (Invitrogen), 10 mM DTT (Invitrogen) and 0.5 mM dNTPs were added and incubated at 25°C for 10 min and then at 42°C for 2 min. Subsequently, 50 or 100 U SuperScript II Reverse Transcriptase (Invitrogen) was added and the mixture was incubated for 1 h at 42°C. The reaction was stopped at 70°C for 10 min. Under the assumption that the reverse transcription was 50% efficient, the amount of cDNA was estimated 50 ng/µl cDNA

#### **4.10.3.2 PCR for gDNA and cDNA semi-quantification**

The amplification of DNA was done in reaction volumes of 10 or 20 µl per assay and was performed with the following reagents and final concentrations:

10 - 100 ng	DNA template
0.5 µM	sequence-specific forward DNA oligonucleotide (forward primer)
0.5 µM	sequence-specific reverse DNA oligonucleotide (reverse primer)
0.2 mM	dNTP-Mix
1% (v/v)	N.N.-Dimethylsulfoxide (DMSO)
10% (v/v)	Cresol
1x	Polymerase-buffer
0.1 U	Polymerase

The primers used for genotyping or semi-quantitative PCR are listed in Table 9 and Table 10, respectively. The PCR conditions varied depending on the assay but always included: 1) initiation step of 5 to 10 min at 95°C; 2) denaturation step of 30 to 60 sec at 95°C; 3) annealing step of 30 sec to 2 min at 55° to 68°C, depending on the DNA oligonucleotide 4) elongation step at of 1 to 2 min at 68° or 72°C. Steps 2) to 4) were repeated between 25 to 35 cycles. The reaction was terminated by a final elongation step for 10 min at 72°C. The reaction was analyzed by agarose gel electrophoresis.

#### **4.10.3.3 Quantitative RT-PCR**

Gene expression was analyzed by SYBR-green-based qRT-PCR assays. All primer pairs used for amplification were intron-spanning and they are shown in (Table 12). The reaction contained 2.5 ng template-cDNA, 0.4 µM sequence-specific forward-DNA-oligonucleotides, 0.4 µM sequence-specific reverse-DNA-oligonucleotides and 1x SYBR Green in a total of a 10 µl reaction mixture. For quantification of the expression of murine genes data were calculated using the standard curve method. Each gene that was measured had a corresponding standard curve with cDNA created as a template. To prepare the standard curve for each gene, 1:5 serial dilutions of the standard sample (previously known to express the gene of interest) were prepared and amplified. Based on the determined values of the standard curve, a linear trendline was generated by plotting the logarithm of the quantity against the Ct-value for each dilution. Thus, the linear trendline follows the equation  $y = mx$

+ b. With this equation the quantity of each gene was determined. The expression of the specific genes was normalized to the expression of 18S rRNA in the respective cDNA sample. The results were analyzed using SDS 2.2.1 (Applied Biosystems) and Microsoft EXCEL (Microsoft Co).

#### 4.10.3.4 Recombination Assay

The degree of recombination at the targeted *Ptch* locus in myeloid cells was estimated by quantitative real-time PCR in gDNA using primers and TaqMan probes as described previously<sup>108</sup>. All primers and probes used are listed in Table 12. The primer combination mPTCdelNx\_f/mPTCNx\_r amplifies a fragment after cre-mediated excision of the floxed locus i.e. of the deleted *Ptch*<sup>del</sup> allele. This fragment was detected using a 6-carboxylfluoreceine-labeled probe (mPTCdelNx\_S1). The primers mPTCNx\_f/mPTCNx\_r amplify a fragment of the *Ptch*<sup>lox</sup> locus, which was detected with a Yakima Yellow-labeled probe (mPTCNx\_S2). A pelota gene-specific quantitative PCR-assay (primer combination Pelo-F1/Pelo-R, probe Pelo-Sonde2) was used for data normalization. The standard curve method for relative quantification was used for data analysis. The deletion efficiency was calculated as the ratio of the values for the deleted allele to the total value from the floxed allele plus the deleted allele and is denoted in percent. Each sample was measured in triplicates.

#### 4.10.4 Agarose gel electrophoresis

To separate DNA fragments, gel electrophoresis was done. Depending on the size of the expected DNA fragments, gels in TBE buffer containing 1 to 2% (w/v) agarose and 0.2 µg/ml ethidium bromide were used. The electrophoresis chamber was filled with TBE buffer and the gels were loaded with DNA samples. In parallel a DNA ladder was loaded. The gels were run at a constant voltage of 30 to 100. A UV transilluminator (Intas, Göttingen, Germany) was used for documentation.

### 4.11 Cell biology methods

#### 4.11.1 Isolation of bone marrow cells and preparation of murine bone marrow-derived macrophages (BMDM)

Isolation of BM and BMDM was performed as previously described<sup>109</sup>, with minor modifications. To isolate BM, femurs were obtained from 8-13 week old mice. The femurs were dissected using scissors and were removed by cutting the tibia below the knee joints

and the pelvic bone close to the hip joint. Muscles connected to the bone were removed using clean gauze. The femurs were placed into a petri dish on ice until use. Under a tissue culture hood, the bones were sprayed with 70% ethanol and then both epiphyses were removed using sterile scissors and forceps.

To collect BM cells, BM were flushed with 2.5 ml sterile PBS using a syringe. Cells were then resuspended in 10 ml PBS. Cells were pelleted by centrifugation at 1200 rpm for 10 min at 4°C. Cells were resuspended in 5 ml PBS and counted.

In order to grow BMDM, the bones were flushed with 2.5 ml of Pluznik medium using a syringe. In order to allow the settling of adherent cells such as fibroblast, cells were grown overnight in a total of 10 ml Pluznik medium. The next day, non-adherent cells in the supernatant were centrifuged at 1200 rpm for 10 min at RT. The cells were resuspended in 40 ml of Pluznik medium and divided into 4 non-coated 10 cm culture petri dishes. Four days later, the medium was replaced by 10 ml/plate of fresh Pluznik medium. The cells were incubated for an additional 3 days. For further use, cells were washed with sterile PBS, enzymatically detached (using TrypLE express) and resuspended in BMDM culture media. Cells were counted and seeded at 8000 - 15000 cells/well in a 96-well culture plate for cell viability and proliferation assays (see below). BMDM were cultivated for at least 12 hours before further manipulation.

#### **4.11.2 Isolation of splenocytes**

Spleen was removed and pressed through a fine-mesh cell strainer (40 µm pore size) in a petridish containing 10 ml PBS. Single cell suspension was made by repeated suction with a syringe through a fine needle (gauge 22). The splenocytes were centrifuged at 300 g for 5 min at 4°C and resuspended in 5 ml of PBS. Cells were counted using the Neubauer chamber.

#### **4.11.3 Isolation of CD11b<sup>+</sup> and CD11c<sup>+</sup> cells**

Whole blood cells or 10<sup>7</sup> splenocytes (see 4.11.2) or were pelleted by centrifugation at 300g for 10 min. The pellet was resuspended in 90 µl of buffer (PBS pH 7.4 with 0.5% bovine serum albumin (BSA) and 2 mM EDTA). Then 10 µl of CD11b/CD11c MicroBeads (Miltenyi Biotec) was added to the cells and incubated for 15 min at 4°C. The cells were pelleted by adding 1 ml of buffer and centrifuged at 300 g for 10 min. The supernatant was removed and the cells were resuspended in 500 µl of buffer. The magnetic separation column

was prepared by placing the column in the magnetic field separator and rinsing the column with 500  $\mu$ l of buffer. After rinsing, the resuspended cells were loaded into the prepared column. At this stage, the unlabeled cells passed through the column while the magnetically labeled CD11b<sup>+</sup>/CD11c<sup>+</sup> cells remained attached to the column. The column was washed thrice with 500  $\mu$ l of buffer. To retrieve the CD11b<sup>+</sup>/CD11c<sup>+</sup> fraction, the column was removed from the separator and placed on a 2 ml collection tube. The CD11b<sup>+</sup>/CD11c<sup>+</sup> cells were immediately flushed out by firmly applying the plunger after adding 1 ml buffer on the column.

#### **4.11.4 Isolation of Thy1.2<sup>+</sup> cells**

10<sup>7</sup> whole blood cells were resuspended in 1 ml PBS in a 2 ml tube. Then 25  $\mu$ l of resuspended magnetic beads (Dynabeads, Invitrogen) was added to the cells and incubated for 20 min at 4°C. Then the tube was placed on a magnet for 2 min before carefully removing the supernatant. The cells were washed by removing the tube from the magnet and adding 1 ml of isolation buffer (PBS pH 7.4 with 0.1% BSA and 2 mM EDTA). The cells were vortexed shortly (2–3 sec) and the tube was placed again in the magnet for 2 min. While the tube was still in the magnet, the supernatant was carefully removed and discarded. The washing step was repeated once more before using the cells for isolation of RNA.

#### **4.11.5 Analysis of blood and bone-marrow-derived cells**

##### **4.11.5.1 Differential blood count and smears**

Whole blood isolated from mice was transferred directly into EDTA tubes and mixed well to prevent coagulation. The blood samples were stored until analysis at 4°C (maximally 6 h). The differential blood cell counting of non-coagulated whole blood was done on an AcT5 hematology analyzer. The blood smears were stained with Hemacolor before counting.

##### **4.11.5.2 Cytospin preparation from bone marrow**

BM cells were isolated as described in 4.11.1. Two hundred thousand cells of each sample were centrifuged (Cytospin 2) at 1500 rpm for 3 min onto microscope slides. Upon Pappenheim staining, the cells were analyzed by a train hematopathologist.

#### **4.11.6 Stimulation of BMDM with LPS or BLP**

After isolation and differentiation of BMDM, cells were counted and seeded at 15000 cells/well in a 96-well culture plate. Cells were allowed to adhere to the plate overnight. The following day, supernatants were removed and medium containing 100 ng/ml LPS or BLP (stock concentration is 1mg/ml in water) was added for 6 to 72 hr.

#### **4.11.7 Cell viability and cell proliferation assay**

To test the viability of BMDM, WST-1 reagent was used. Briefly, 15000 cells were seeded in 96-wells. Four hours before the end of treatment, supernatants were removed and cells were incubated with 10  $\mu$ l of WST-1 reagent in 100  $\mu$ l fresh media at 37°C for 3 to 4 h. During this time the tetrazolium salt WST-1 was cleaved to a soluble formazan dye. This bioreduction is largely dependent on the glycolytic production of NAD(P)H in viable cells. Therefore, the amount of formazan dye (quantitated by spectrophotometer at a wavelength of 450 nm) is proportional to living cells.

The proliferation of BMDM was analyzed using the BrdU Cell proliferation kit (Roche). The assay was done according to the manufacturer's instruction. Briefly, 8000 cells were seeded in 96-well plates. Twenty two hours prior to the end of treatment, BrdU reagent was added. Cells were then fixed. The cell membrane was denatured and probed with anti-BrdU-POD for 1 h. After thorough washing, BrdU incorporation was determined by adding peroxidase substrate and measurement of luminescence using a luminometer. The measured luminescence is proportional to the proliferation of cells.

#### **4.11.8 Flow cytometric analysis**

For flow cytometric analysis,  $1 \times 10^6$  splenocytes (see 4.11.2), cells were put in a brown 1.5 ml reaction tubes and incubated on ice for 20 min with the appropriate antibodies (diluted 1:50 in PBS; see also Table 15) in a 50  $\mu$ l total volume. Then the cells were washed by adding 300  $\mu$ l PBS and centrifuged for 5 min at 300 g and 4°C. The cell pellet was resuspended in 300  $\mu$ l PBS and stored (maximally 1 hr) on ice until flow cytometric measurement.

For flow cytometric analysis of whole blood cells derived from the retro-orbital venous plexus or from tumor ascites, 49  $\mu$ l of sample was incubated with 1  $\mu$ l antibodies for 20 min on ice. This was followed by lysis of erythrocytes by adding 1ml of ready-to-use lysis buffer (BD Pharmingen) for 10 min at 4°C. The cells were then centrifuged for 5 min at 300 g and

4°C to remove the lysis buffer and then washed twice with 1 ml PBS by centrifugation for 5 min at 300 g and 4°C. The cell pellet was resuspended in 300 µl PBS and stored (maximally 1 hr) on ice until flow cytometric measurement.

BD LSR II flow cytometer was used for data collection and analysis was performed using the BD FACSDiva™ software.

#### **4.11.9 Enzyme-linked immunosorbent assay (ELISA)**

Commercially available ELISA kits were used according to the manufacturer's instruction. In short, the supernatants of stimulated BMDM (see 4.11.2) were collected at different time points (6, 12 and 24 h after treatment) and centrifuged at 13000 rpm for 10 min to pellet the cellular debris. The levels of IL-6, IL-10 and MCP-1, MIP-1α, RANTES and KC were measured using the DuoSet ELISA Kit (R & D systems). TNFα and IL-12p40 were quantified using a kit from BioLegend and E Bioscience, respectively.

#### **4.11.10 Cellular transformation assay**

To test for cooperation of HH/GLI and PDGFRA signaling in oncogenic transformation,  $1 \times 10^4$  human non-tumorigenic HaCaT keratinocytes expressing *GLII* under the control of a tetracycline inducible promotor<sup>110</sup> were seeded as single cells in 12-well plates in 0.4% select agar on top of 0.5% bottom select agar (Invitrogen). Cells were either treated with 50 ng/ml doxycycline (Dox) (Sigma) to induce *GLII* expression, 50 ng/ml recombinant PDGF-BB (R&D Systems) or with a combination of Dox/PDGF-BB. To assay possible cooperation of HH/GLI with KIT signaling, the same *GLII*-expressing HaCaT cells were stably transduced with the constitutively active D816V KIT mutant (GNNK+ splice form)<sup>111</sup>. Empty-vector transfections served as controls. 3D transformation assays were incubated for 4 weeks at 37°C with 5% CO<sub>2</sub>. Anchorage independent clonogenic growth was documented with a Cell<sup>^</sup>D Image capture system and quantified by automated colony counting using Colony Counter software (Microtec Niton)<sup>112,\*</sup>.

### **4.12 Protein chemistry and immunohistochemistry methods**

#### **4.12.1 Protein isolation and quantification**

---

\*This method was done in collaboration with Prof. Fritz Aberger, University of Salzburg, Austria.

Tissues samples were collected, washed thoroughly with sterile PBS and homogenized in RIPA buffer. The protein concentration was measured using the Pierce BCA Protein Assay Kit according to manufacturer's instructions. Bovine serum albumin was used as the standard.

#### **4.12.2 Western blot**

For western blot analyses, 50 µg of total tissue protein lysates were denatured with sample buffer for 5 min at 96°C. Proteins were loaded on NuPAGE Novex Midi Gels in 1x running buffer (NuPAGE MES SDS buffer) and electrophoresed for 1.5 to 2 h at 160 mA. Four µl of pre-stained protein standard (SeeBlue Plus2) was loaded in parallel to estimate the molecular weight of the proteins. Proteins were transferred to a nitrocellulose membrane (GE Healthcare) using a semi-dry blotting device at 120 mA for 90 min. After blocking with 0.2% casein/PBST for 1.5 h at RT, membranes were probed with the appropriate primary antibodies (Table 13) at 4°C overnight. Subsequently, the membrane was washed 3x 10 min in PBS with 0.1% Tween 20 and then incubated in HRP-conjugated secondary antibody for 1 h at RT. After thorough washing in PBS with 0.1% Tween-20, 1.5 ml the detection reagent (Amersham ECL Plus Western Blotting Detection Reagents) was pipetted onto the membrane and incubated for 3 min at RT. For visualization, a Hyperfilm ECL was placed on the membrane and developed in a developing machine (Curix 60, Agfa).

#### **4.12.3 Hematoxylin-Eosin (HE) Staining**

For HE staining, paraformaldehyde-preserved tissue was embedded in paraffin and cut to 4-5 µm sections and mounted on glass slides. Sections were initially deparaffinized with xylene for 20 min and subsequently rehydrated using descending ethanol solutions (100% to 70% ethanol). After extensive washing with ddH<sub>2</sub>O, slides were placed in hematoxylin solution for 15 min. The color development was done with running lukewarm tap water for at least 5 min. Samples were then quickly dipped in 1% eosin solution (with freshly added 0.5% v/v glacial acetic acid). After staining, slides were again washed with ddH<sub>2</sub>O and dehydrated using ascending ethanol solutions (70% to 100% ethanol). Slides were placed again in xylene before mounting in Pertex. In order to solidify the mounting medium, the slides were placed in an oven at 55°C for at least 15 min.



#### 4.12.4 Electron microscopy

After perfusion of the tumor-bearing mice (see 4.13.3), tumor samples were taken and fixed in 2.5% glutaraldehyde. Samples were then postfixed with 1% osmium tetroxide (Serva, Heidelberg, Germany) and embedded in araldite (Serva). Ultrathin sections were cut using an ultramicrotome and contrasted with lead citrate (Serva) and uranyl acetate (Serva). Investigations were performed on a Zeiss EM10 transmission electron microscope (Zeiss, Oberkochen, Germany) equipped with a MegaView III imaging system (Olympus Soft Imaging Systems GmbH, Münster, Germany).<sup>†</sup>

#### 4.12.5 In situ hybridization

For *in situ* hybridization, all solutions were treated with 300 µl/L DEPC and autoclaved before use. Formalin-fixed tissue samples were embedded in paraffin and sectioned to 4-5 µm thickness. The probe sequences for mouse *Gli1* are reported in Wijgerde M *et al* <sup>113</sup>. The *Ptch* specific probes were a 477 bp fragment spanning exons 2 to 6, and a 250 bp fragment spanning exons 8 and 9 of the *Ptch* gene <sup>92</sup>. *In situ* hybridization was performed as previously described <sup>114</sup>. Briefly, sections were dried at 65°C for 30 min and deparaffinized with xylene. Sections were rehydrated through decreasing ethanol solutions (100% to 30%). After washing with PBS and saline, the sections were post-fixed in 4% PFA/PBS for 20 min on ice. After two additional washing steps in PBS, the tissue was permeabilized with 40 µg/ml proteinase K for 7.5 min and washed again in PBS. Subsequently, the sections were refixed in 4% PFA/PBS for 5 min on ice and transferred to 0.1 M triethanolamine, pH 8.0. After adding 0.25% (v/v) acetic anhydride, sections were incubated in the solution for 10 min then washed with PBS and 0.83% NaCl. Samples were dehydrated through increasing ethanol solutions (30% to 100%) and air dried. Sense and antisense (as negative control) probes were diluted in hybridization buffer and denatured for 2 min at 80°C, chilled on ice and 60 µl of the solution was pipetted on the tissue sections. The sections were covered with coverslips and incubated overnight at 59°C in a chamber with paper towels soaked in 50% formamide/5x SSC to prevent dehydration of the sections. The next day coverslips were removed with 5x SSC and slides were washed in 5x SSC at 55°C. This was followed by a high stringency wash in 50% formamide/2x SSC for 20 min at 63°C. Afterwards, the sections were washed once at RT and thrice at 37°C in STE-*in situ*-buffer for 10 min each.

---

<sup>†</sup> These experiments were done in collaboration with Prof. Dr. Walter Schultz-Schaeffer, Department of Neuropathology, University of Goettingen

Then the sections were incubated with 10 ng/ml RNase A in STE-*in situ*-buffer for 30 min at 37°C and then washed again for 15 min in STE-*in situ*-buffer at 37°C. Once again the slides were washed with 50% formamide/2x SSC for 20 min at 63°C then transferred to 2x SSC for 15 min and placed in NT-buffer for 10 min. Subsequently, sections were washed thrice for 5 min with MBSTL-buffer and incubated for 1 h with 0.2% I-block/PBS to block unspecific binding sites. Afterwards, anti-Dig/AP (1:1000 in 0.02% I-block/MBSTL-buffer) was pipetted onto the sections and incubated overnight at 4°C. On the following day, slides were washed six times for 15 min with MBSTL-buffer and thrice for 5 min with NTMLT-buffer. Finally, BM-Purple was pipetted onto the sections and the staining reaction was performed in the dark. To stop the staining reaction, slides were transferred to stop-buffer, washed 2 x 5 min PBS and fixed 1 to 2 h in 4% PFA/0.2% glutaraldehyde in PBS. Finally, the sections were washed with PBS and mounted using Glycer gel.

#### **4.12.6 LacZ staining**

LacZ activity was analyzed according to standard procedures. Briefly, tissues were fixed for 2 h in 4% paraformaldehyde/PBS, washed and soaked in 25% sucrose/PBS overnight. For cryosectioning, tissues were embedded in OCT compound and cut to 5 µm sections at -20 to -22°C. Next, cryosections or whole tissue blocks were fixed with 0.2% glutaraldehyde in PBS and washed in LacZ buffer. Both, cryosections and tissue blocks were stained in LacZ-staining solution overnight at 30°C. Reaction was stopped by washing the tissues or cryosections twice with PBS.

#### **4.12.7 Immunohistochemistry (IHC)**

LacZ-stained cryosections were further used for immunohistochemical analysis of Kit. The sections were washed in PBS, post-fixed in acetone for 10 min and air-dried before IHC staining was performed as described below.

LacZ-stained whole tissue samples were used for Pdgfra IHC. For this purpose, the tissue was embedded in paraffin and cut to 4 to 5 µm sections. IHC was performed using anti-Pdgfra antibody as described below.

For immunohistochemical staining, sections were deparaffinized and rehydrated. Whenever necessary, permeabilization treatment was done (see Table 14). Sections were blocked with 3% H<sub>2</sub>O<sub>2</sub> to inhibit endogenous peroxidase and blocked once again with 0.2% casein to block non-specific antibody binding. Thereafter, the sections were incubated with a primary and an appropriate secondary antibody (see Table 14) in a humid chamber. Antibody binding

was visualized using DAB+ (Envision+ system-HRP, Dako) or aminoethylcarbazol as chromogen. To stop the reaction, slides were rinsed with distilled water.

All LacZ/IHC doublestained sections were counterstained with hematoxylin.

For the quantification of Ki-67, pictures were taken from Ki-67-stained sections using the CellF software. 1000 cells were counted and analyzed for Ki-67 positivity. Ki-67 positive cells are given in percent.

#### **4.12.8 Assessment of skin thickness and nevi area**

The skin thickness was assessed as previously described <sup>115</sup>, with minor modifications. Briefly, 6 representative areas of HE stained (see 4.12.3) skin samples of each animal were examined. In each area, the thickness of the epidermis from the basal layer to the stratum granulosum and stratum spinosum but excluding the stratum corneum was measured using Cell F software. If the mice developed skin papillomas, only the thickness of the papilloma-free epidermis was measured. Data is presented as boxplot with mean  $\pm$ SE.

To measure the nevi area, 6 HE stained (see 4.12.3 ) skin samples per mouse were analyzed. Whole skin samples were examined for the tumor cells, which presented as black cells. The whole area including the stroma between the tumor cells were measured using Cell F software. The sum of nevi area per skin sample was normalized to the total skin area that was measured. Two independent investigators performed the measurement.

### **4.13 Animal Experiments**

All experiments using animals were performed in compliance with all relevant legal and ethical requirements.

#### **4.13.1 Breeding of mice**

The mouse strains used in this thesis were bred and maintained in the animal facility of the Institute of Human Genetics, University of Göttingen. Animals were housed in Makrolon cages type II and III, with a twelve-hour light-dark cycle (light period: 6.a.m.-6 p.m.), a temperature of  $20 \pm 2$  ° C and a relative humidity of  $50 \pm 10\%$ . Rodent pellets (complete diet for mice breeding) and tap water were given *ad libitum* to the animals.

#### 4.13.2 Tail biopsy and genotyping of mice

To identify the mice, tail biopsies (cut approx. 0.2 cm from the tip of the tail) were taken and ear markings were done in four week old mice.

The genotyping of mice was done by PCR on gDNA from tail biopsies. The oligonucleotides and PCR conditions are given in Table 9.

#### 4.13.3 Perfusion of mice

Mice were injected with a lethal dose of a mixture of Ketanest S (4 mg) and Rompun (0.9 mg). The chest of the animal was opened and the heart was exposed. The right atrium was cut open for bleeding. The left ventricle was punctured. Then the animal was infused with Ringer lactate solution for 10 min. Afterwards, the animal was infused with 2.5% glutaraldehyde for additional 10 min or until the animal was completely fixed. The organs or tissues were removed and put in 4% paraformaldehyde or 2.5% glutaraldehyde (for electron microscopy samples) and stored at 4°C until analysis.

#### 4.13.4 Isolation of tumors

Mice were closely monitored for the development of tumors twice a week. Furthermore, the animals were examined for other symptoms such as ataxia, cachexia and lethargy. When mice developed a distended abdomen they were killed by cervical dislocation. After killing the mice were fixed on the preparation table and disinfected with 70% ethanol. Every mouse was thoroughly examined for tumors or other abnormalities. All tumors were carefully removed and rinsed with PBS. In case of cystic tumors, the cystic fluid was removed and the solid tissue or sac was thoroughly washed with PBS. Normal reference tissue (mostly intestine) was also isolated.

#### 4.13.5 Adoptive transfer of BM

Nine week-old *Rag-2<sup>-/-</sup>γc<sup>-/-</sup>* mice were irradiated with 7 Gy to eliminate the existing BM cells. BM cells were isolated from 8-week-old *Ptch<sup>flox/flox</sup>LysMcre<sup>+/-</sup>* and *Ptch<sup>flox/flox</sup>* mice (as described in 4.11.1). After counting,  $2 \times 10^6$  cells were transplanted by tail vein injection into the irradiated mice. Reconstitution of the BM engraftment was analyzed by monitoring peripheral blood 6 weeks after transplantation by flow cytometry using anti-TCRβ-FITC, anti-CD3-PE-Cy5, anti-CD19-FITC and anti-B220-PE-Cy7 antibodies. *Rag-2<sup>-/-</sup>γc<sup>-/-</sup>* mice

reconstituted with control or *Ptch* mutant BM cells were observed for 250 days. Flow cytometry analysis procedure is described in section 4.11.8.

#### 4.13.6 Tumor xenografts

Xenograft experiments were performed essentially as described in Schnidar et al.<sup>112</sup>. In brief,  $1 \times 10^6$  Dox inducible GLI1-HaCaT cells transduced with the PDGFRAH650Q mutation (PDGFRA<sup>mut</sup>; generous gift from Steffen Koschmieder, Department of Haematology and Oncology, Universitäts klinikum Aachen, Germany) or with empty vector control (pBabe-puro) were injected subcutaneously into the flanks of nude mice. *In vivo* GLI1 expression was induced by Dox added to a final concentration of 2 mg/ml to the drinking water containing 2% sucrose. Tumor growth was monitored over a period of 3 weeks and tumor volume was calculated as described in Eberl et al.<sup>116</sup>. Statistical significance was calculated with Dunnett's multiple comparison test.<sup>‡</sup>

#### 4.13.7 Imatinib treatment of mice

Imatinib tablets were pulverized and dissolved in PBS. Stock solutions (15 mg/ml) were stored in aliquots in -20°C. Six or 8 weeks-old *Ptch*<sup>fl<sup>ox</sup>/fl<sup>ox</sup></sup>*LysMcre*<sup>+/-</sup> mice were randomized into 4 groups. Two groups were treated orally with 0.1 g/kg imatinib (dissolved in 200 µl PBS), as previously described<sup>117</sup>. The treatment was continued daily for 10 or 12 weeks. Vehicle-treated (PBS) mice served as controls. Mice were weighed once a week to monitor their conditions. Following the completion of the treatment all mice were sacrificed and screened for tumors.

Another cohort of 8 week-old *Ptch*<sup>fl<sup>ox</sup>/fl<sup>ox</sup></sup>*LysMcre*<sup>+/-</sup> mice was randomized into 2 groups. The first group received imatinib (0.1 g/kg) and the second group served as vehicle treated controls. After 10 weeks of daily oral treatment, the treatment was stopped and the animals were kept for additional 3 weeks before they were sacrificed and screened for tumors.

All tumors were embedded in paraffin and examined microscopically via HE stained sections.

#### 4.13.8 Transplantation of syngeneic melanoma cells

Eight to 9 week-old mice were transplanted with B16F10 cells. For this purpose, subconfluent B16F10 cells were detached with trypsin solution, counted and resuspended in PBS. For the induction of subcutaneous solid tumors,  $1 \times 10^4$  cells diluted in 100 µl PBS were

<sup>‡</sup> Xenograft experiments were done in collaboration with Prof. Fritz Aberger, University Salzburg, Austria.

injected subcutaneously. Tumor growth was monitored daily and calculated using the formula:  $\text{Length} \times \text{Width}^2 \times 0.4$ <sup>118</sup>. Mice were sacrificed when the tumor reached a size of 2 cm<sup>3</sup>. For analysis of the metastatic behavior of the cells,  $1 \times 10^5$  cells in 100  $\mu$ l PBS were injected into the tail vein. Twenty days post-injection, mice were sacrificed and tumor nodules in the lungs were counted.

#### **4.13.9 Transplantation of syngeneic ovarian carcinoma cells and bioimaging**

ID8 cells are transformed late-passage mouse ovarian surface epithelial cells from adult C57BL6 mice. Intraperitoneal injection of these cells into syngeneic mice results in tumor growth throughout the abdominal cavity and in production of a hemorrhagic ascitic fluid<sup>119</sup>. The ID8-LUC cells express luciferase (introduced by lentiviral infection<sup>120</sup>) and were kind gifts from Dr. Thorsten Hagemann (Queen Mary, University of London). Ten million ID8-LUC cells were injected i.p. into 8 week-old mice. In order to monitor tumor growth bioluminescence images were taken from mice injected i.p. with 150  $\mu$ g/g body weight D-luciferin in PBS. Mice were anaesthetized with Isoflouran vapor while images were taken. Grayscale images were acquired with low light with an exposure of 0.5 sec. Bioluminescence images were acquired in the dark 5 min later using an exposure time of 5 min in a CCD camera. For analysis of luminescence intensity, the Signal Meta Vue 6.1 image software (Universal Imaging Corporation) was used. Pseudo-colored overlay images of the bioluminescence signal intensities and the mice were generated using VCTEO2D Image analyze software.

Mice injected with ID8-LUC cells also developed an ascites between 13 and 16 weeks post injection. At that time animals were euthanized and the ascetic fluid and spleen were collected for further flow cytometric and gene expression analyses.

#### **4.13.10 Two-stage chemical carcinogenesis DMBA/TPA protocol**

The dorsal area of mouse skin was shaved 2 days prior to a single application of 200 nM (50  $\mu$ g, in 200  $\mu$ l acetone) of 7,12-dimethylbenzanthracene (DMBA). One week after DMBA application, 20 nM 12-O-tetradecanoyl-phorbol-13-acetate (TPA, in 50  $\mu$ l acetone) was applied topically twice a week for 32 weeks. This was done by fixing the neck and tail of the mouse by hand and topically applying the chemicals directly on the dorsal skin and waiting for 30 sec to allow the solvent to evaporate before releasing the mouse. The area was shaved regularly and the number of tumors per mouse was recorded weekly. The weight of the mice was also monitored once a week. Animals were sacrificed after the last TPA treatment.

#### 4.14 Softwares

**Table 16. List of softwares.**

Software	Distributor
ABI 3500	Applied Biosystems, Darmstadt, Germany
Cell F	Olympus Europa GmbH, Hamburg, Germany
Endnote	Thomson ISI ResearchSoft , California, USA
FlowJo	Tree Star Inc., Oregon, USA
Free Hand MX	Adobe Systems Incorporated, California, USA
ImageJ	National Health Institute, Maryland, USA
Intas GDC	Intas, Göttingen, Germany
MS Office	Microsoft Co., Redmont, USA
Photoshop CS3	Adobe Systems Incorporated, California, USA
SDS 2.1	Applied Biosystems, Darmstadt, Germany
Statistica 9	StatSoft GmbH, Hamburg , Germany

#### 4.15 Databases

**Table 17. List of database.**

MGI_3.43-mouse genome informatics	<a href="http://www.informatics.jax.org/">http://www.informatics.jax.org/</a>
National Center for Biotechnology Information (NCBI)/ (NCBI) GEO DataSets	<a href="http://www.ncbi.nlm.nih.gov/">http://www.ncbi.nlm.nih.gov/</a> <a href="http://www.ncbi.nlm.nih.gov/gds">http://www.ncbi.nlm.nih.gov/gds</a>
European Bioinformatics Institute (EBI)	<a href="http://www.ebi.ac.uk/Information/">http://www.ebi.ac.uk/Information/</a>
Ensembl	<a href="http://www.ensembl.org/index.html">http://www.ensembl.org/index.html</a>
GeneSapiens	<a href="http://www.genesapiens.org/">http://www.genesapiens.org/</a>

#### 4.16 Statistical Analysis

Statistical analyses were performed using the programs MS office Excel and Statistica softwares. GSEA analysis on GEO DataSets samples was done by Dr. Annalen Bleckman using R software. P values <0.05 are considered significant.

## 5 Results

### 5.1 Generation and phenotype of *Ptch*<sup>flox/flox</sup>*LysMcre*<sup>+/-</sup> mice

In order to define the role of *Ptch* in LysM-expressing cells that were expected to be mainly macrophages, DC and granulocytes, *Ptch* was deleted in these cells by breeding *Ptch*<sup>flox/flox</sup> mice to *LysMcre*<sup>+/-</sup> mice. The resulting *Ptch*<sup>flox/+</sup>*LysMcre*<sup>+/-</sup> were backcrossed to *Ptch*<sup>flox/flox</sup> to obtain *Ptch*<sup>flox/flox</sup>*LysMcre*<sup>+/-</sup> mice. *Ptch*<sup>flox/flox</sup>*LysMcre*<sup>+/-</sup> mice were obtained at the expected Mendelian ratio. The floxed *Ptch* locus is shown in Figure 3A. The presence of the *LysMcre* transgene was detected with the primers MLYS1, MLYS2 and Cre8, which resulted in a 350 bp and 700 bp fragment derived from the *LysM* wt and *LysMcre* locus, respectively (Figure 3B). Genotyping by PCR of wt *Ptch* (Figure 3C, lane 1), *Ptch*<sup>flox/+</sup>*LysMcre*<sup>+/-</sup> (Figure 3 B and C, lane 2) and *Ptch*<sup>flox/flox</sup> (Figure 3 C, lane 3) mice is shown Figure 3 B and C. As demonstrated in Figure 3A and B, the primer pair mPTCNx\_f and mPTCwt\_r amplified a 455 bp fragment derived from the wt *Ptch* allele, which is detected in *Ptch* wt and *Ptch*<sup>flox/+</sup> mice. The primer pair mPTCNx\_f and mPTCNx\_r amplified a smaller 150 bp fragment, which was indicative of the *Ptch*<sup>flox</sup> allele. The floxed allele was also detected by the primer combination Neo-F/p1011R.2, which resulted in a 1735-bp fragment. Moreover, the primer pair p910F.4/Neo-R, which resulted in a 843-bp fragment also amplifies the *Ptch*<sup>flox</sup> allele and will vanish when there is a complete cre mediated recombination of the floxed *Ptch* locus. The occurrence of a 950 bp fragment using the primer pair Exon 7-F and Neo-R is also indicative for the cre-mediated recombination event at the floxed *Ptch* locus. This so-called *Ptch*<sup>del</sup> allele occurred in the presence of *LysMcre*<sup>+/-</sup> allele in *Ptch*<sup>flox/+</sup>*LysMcre*<sup>+/-</sup> and *Ptch*<sup>flox/flox</sup>*LysMcre*<sup>+/-</sup> mice (Figure 3 C).

These data show that the presence of the *LysMcre* recombinase results in deletion of the floxed *Ptch* sequence in *Ptch*<sup>flox</sup>*LysMcre*<sup>+/-</sup> mice. However, due to DNA derived from many cells in which the *LysMcre* was not active, both the floxed and the deleted *Ptch* locus were detected by PCR in tail DNA isolated from *Ptch*<sup>flox/+</sup>*LysMcre*<sup>+/-</sup> and *Ptch*<sup>flox/flox</sup>*LysMcre*<sup>+/-</sup> mice.



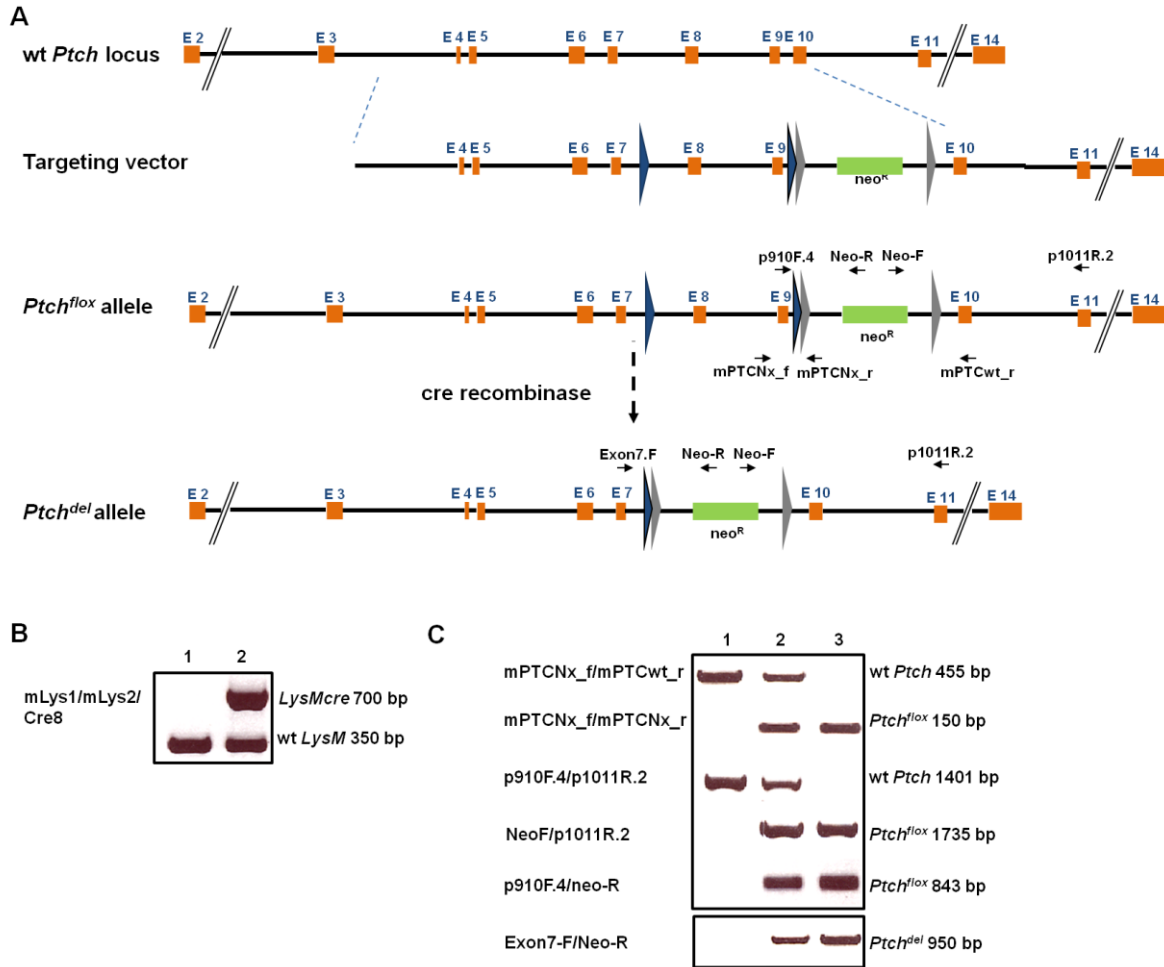


**Figure 3. Scheme and genotyping of the *Ptch* conditional knock-out mouse model.** (A) The figure shows the wt *Ptch* locus and the targeting vector used for homologous recombination. The resulting *Ptch*<sup>fllox</sup> allele was converted into the *Ptch*<sup>del</sup> allele in the presence of the cre recombinase. Blue triangles represent *loxP*-sequences in intron 7 and 9. The neomycin resistance cassette (*neoR*) is flanked by *frt* sites (grey triangles). The figure was adapted from <sup>83</sup>. The genotyping was done by PCR and performed using mouse tail gDNA (B). Primer combinations were as indicated on the left column of the figure. The existence or the absence of the *LysMcre* transgene was identified by PCR with a resulting 700 bp and 350 bp fragment, respectively, using the primer combination mLys1, mLys2 and Cre8. (C) The primer locations are indicated in (A) and the primer combinations were as indicated on the left column of the figure. Primer pairs mPTCNx\_f/mPTCwt\_r (455 bp) and p910F.4/p1011R.2 (1401 bp) identify the wt *Ptch* allele present in wt *Ptch* mice (lane 1) and *Ptch*<sup>fllox/+</sup> (lane 2). The *Ptch*<sup>fllox</sup> allele can be detected by primers mPTCNx\_f/mPTCNx\_r (150 bp), Neo-F/p1011R.2 (1735 bp) present in *Ptch*<sup>fllox/+</sup> (lane 2) and *Ptch*<sup>fllox/fllox</sup> mice (lane 3). The primer pairs p910F.4/Neo-R also detects the floxed allele (lane 2 and 3) and will disappear in the presence of the cre recombinase. The presence of a 950 bp band from primers Exon7-F/neo-R shows the *Ptch*<sup>del</sup> allele in *Ptch*<sup>fllox/+</sup> *LysMcre*<sup>+/-</sup> and *Ptch*<sup>fllox/fllox</sup> *LysMcre*<sup>+/-</sup> mice after cre-mediated excision of the floxed *Ptch* sequences.

In addition to genotyping of mice, the recombination efficiency at the *Ptch* locus was investigated in purified cells of the myeloid and lymphoid lineage. These were CD11c<sup>+</sup> (dendritic), CD11b<sup>+</sup> (macrophage) and Thy1.2<sup>+</sup> (T) cells. For this purpose, the cells were selected using antibody conjugated-magnetic beads (see 4.11.3 and 4.11.4 in the Material and Methods section). In addition, the recombination efficiency was analyzed in the whole bone marrow and peritoneal macrophages (PM).

As demonstrated in Figure 4, the *Ptch* deletion efficiency was 20% in purified Thy1.2<sup>+</sup> cells, 18% in CD11c<sup>+</sup> cells, 65% in CD11b<sup>+</sup> cells, 52% in (BM) and 85% in PM derived from *Ptch*<sup>flx/flx</sup>*LysMcre*<sup>+/-</sup> mice. These data indicate that a small portion of the T cells and the majority of the investigated subsets of myeloid cell lineages were recombined at the *Ptch* locus.

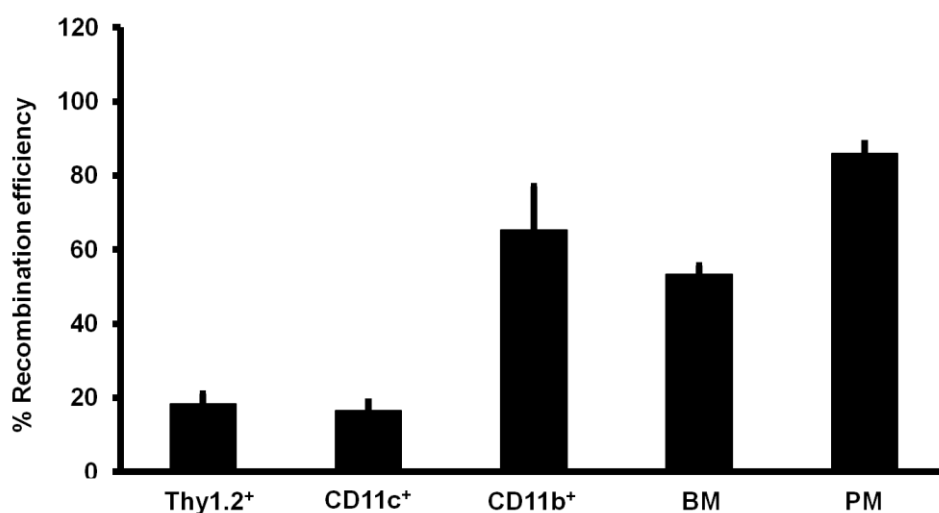


**Figure 4. Effective recombination of the floxed *Ptch* locus in myeloid cells of *Ptch*<sup>flx/flx</sup>*LysMcre*<sup>+/-</sup> mice.** Recombination efficiency was analyzed by qRT-PCR on gDNA obtained from purified cell subpopulations of *Ptch*<sup>flx/flx</sup>*LysMcre*<sup>+/-</sup> mice. The data show the mean values (± SEM) of at least 3 different animals.

Despite being a tumor suppressor gene, the *Ptch* deletion did not result in tumors of the hematopoietic lineage. Thus, the numbers and morphology of cells composing the peripheral blood or the BM of *Ptch*<sup>flx/flx</sup>*LysMcre*<sup>+/-</sup> mice were normal as revealed by analysis of whole blood values (see Table 18), BM and blood and BM smears (data not shown). Thus, the absolute number of the white blood cells and platelets of *Ptch*<sup>flx/flx</sup>*LysMcre*<sup>+/-</sup> mice remained comparable to the *Ptch*<sup>flx/flx</sup> controls. Although the erythrocyte count as well as the hemoglobin and hematocrit levels of *Ptch*<sup>flx/flx</sup>*LysMcre*<sup>+/-</sup> mice was slightly lower in comparison to the controls, the difference did not reach statistical significance. All other red

blood cell indices (MCV, MCH, MCHC) remained normal. The platelet indices (MPV, PDW and PCT) also remained comparable to the controls (Table 18).

In addition, blood smears of the mice did not show any indication of hematological defects, and BM smear analysis showed no signs of deviations in cell counts and the cells looked normal as analyzed by a hematopathologist<sup>§</sup>.

**Table 18. Hematologic parameters of *Ptch*<sup>flox/flox</sup> and *Ptch*<sup>flox/flox</sup>*LysMcre*<sup>+/-</sup> mice.**

	<i>Ptch</i> <sup>flox/flox</sup>		<i>Ptch</i> <sup>flox/flox</sup> <i>LysMcre</i> <sup>+/-</sup>		<i>P</i>
	Mean	SD	Mean	SD	
<b>WBC (10<sup>3</sup>/μl)</b>	7.987	1.507	8.580	1.899	0.693
<b>Neu</b>	1.497	0.497	1.500	0.056	0.991
<b>Lym</b>	6.310	0.934	6.903	1.877	0.650
<b>Mono</b>	0.123	0.079	0.135	0.066	0.846
<b>Eos</b>	0.006	0.004	0.009	0.007	0.502
<b>Baso</b>	0.049	0.021	0.046	0.052	0.931
<b>Ery (10<sup>6</sup>/μl)</b>	11.300	0.265	8.723	1.716	0.062
<b>Hgb, g/dl</b>	15.433	0.379	12.433	1.834	0.050
<b>Hct, %</b>	52.433	3.027	43.367	6.200	0.085
<b>MCV, fl</b>	46.533	2.196	50.100	4.233	0.265
<b>MCH, pg</b>	13.700	0.361	14.133	1.026	0.528
<b>MCHC, g/dl</b>	29.467	1.102	28.700	2.364	0.637
<b>RDW, %</b>	15.067	0.351	18.300	2.252	0.070
<b>Pl (10<sup>6</sup>/μl)</b>	0.986	0.085	1.042	0.167	0.634
<b>MPV, fl</b>	3.030	0.327	3.737	0.515	0.115
<b>PDW</b>	11.333	2.309	16.633	6.413	0.249
<b>PCT, %</b>	0.300	0.059	0.385	0.037	0.102

Blood cell numbers were determined by an automated hematological analyzer. WBC: white blood cells; Neu: neutrophils; Lym: Lymphocytes; Mono: monocytes; Eos: eosinophils; Baso: basophils; Ery: erythrocytes; Hgb: hemoglobin; Hct: hematocrit; MCV: mean corpuscular volume; MCH: mean corpuscular hemoglobin; MCHC: mean corpuscular hemoglobin concentration; RDW: red cell distribution width; Pl: platelet; MPV: mean platelet volume; PDW: platelet distribution width; PCT: plateletcrit. *P* value was calculated using student's t-test (n=3).

Whenever possible, the mice were monitored for at least 398 days after birth. Most interestingly, as the *Ptch*<sup>flox/flox</sup>*LysMcre*<sup>+/-</sup> mice grew older, many of them developed a distended belly. Upon autopsy, tumors located in the gastrointestinal tract were detected.

<sup>§</sup> Blood and BM smear analysis was done by Prof. Claudia Binder in the Dept. of Hematology and Oncology, University of Goettingen.

## 5.2 *Ptch*<sup>flox/flox</sup>*LysMcre*<sup>+/-</sup> mice develop GIST-like tumors

### 5.2.1 Histological characteristics of the tumors of *Ptch*<sup>flox/flox</sup>*LysMcre*<sup>+/-</sup> mice

None of the *LysMcre*<sup>+/-</sup>, *Ptch*<sup>flox/flox</sup>, *Ptch*<sup>flox/+</sup>*LysMcre*<sup>+/-</sup> mice developed any kind of abnormalities (Table 19). However, at a median age of 206 days, 82% of *Ptch*<sup>flox/flox</sup>*LysMcre*<sup>+/-</sup> animals presented with - mostly multiple - tumors arising from the wall of the stomach and/or the intestine and/or caecum (Figure 5A and B; Table 19). Larger tumors frequently presented as blood-filled cysts protruding into the peritoneal cavity (Figure 5B), whereas smaller, i.e. most likely earlier lesions had a solid appearance (Figure 5B and E). The gastrointestinal tumors that develop in *Ptch*<sup>flox/flox</sup>*LysMcre*<sup>+/-</sup> were initiated from lesions, which were localized between either the circular and longitudinal muscle layer or the longitudinal muscle layer and the serosa (Figure 5C and D). Although the tumors were located in close vicinity to the myenteric plexus, the plexus was frequently intact (Figure 5D). Upon growth (Figure 5E), the tumor cells showed a high cellularity, variably spindle-shaped cells, elongated nuclei, and a pale eosinophilic cytoplasm (Figure 5F). Histologically, the tumors therefore resembled GIST or LMS.

**Table 19. Absolute numbers and percentages of symptomatic and symptom-free animals used in this study.**

<i>genotype</i>	<i>n</i>	<i>Age</i> ( <i>days</i> ) <i>range</i> <sup>1</sup> ; <i>median</i>	<i>mice with GIST-like</i> <i>tumors</i>	<i>mice with other</i> <i>abnormalities</i>	<i>healthy</i>
<i>LysMcre</i> <sup>+/-</sup>	9	583-670; 604	-	-	9
<i>Ptch</i> <sup>flox/flox</sup>	17	96-524; 324	-	-	17
<i>Ptch</i> <sup>flox/+</sup> <i>LysMcre</i> <sup>+/-</sup>	18	398-693; 640	-	-	18
<i>Ptch</i> <sup>flox/flox</sup> <i>LysMcre</i> <sup>+/-</sup>	34	116-555; 206	28 (82%)	1	5

<sup>1</sup> from birth on

<sup>2</sup> mean ± SD

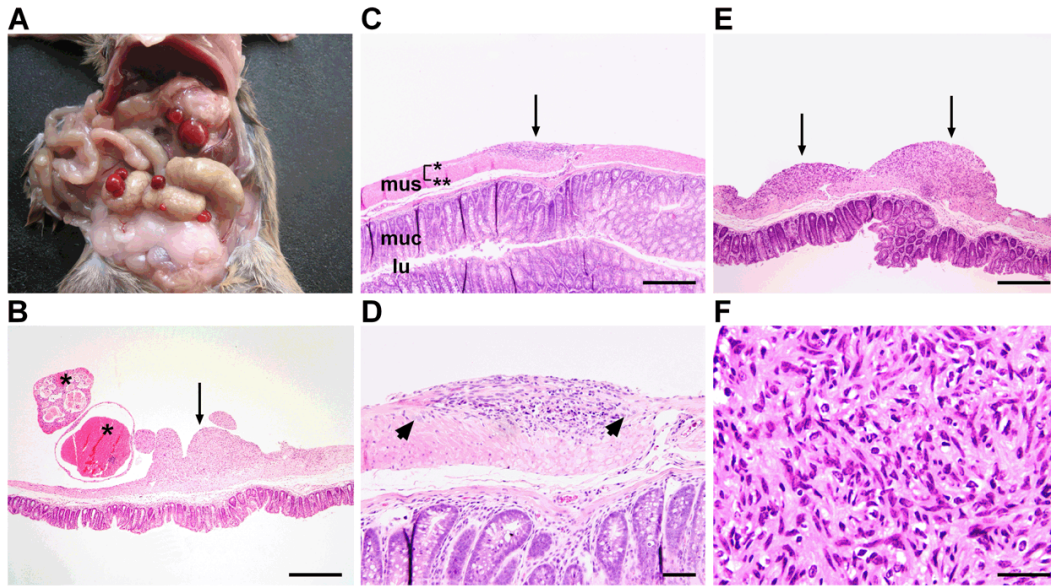


**Figure 5. *Ptch* mutant mice develop gastrointestinal tumors.** (A) Gross appearance of tumors of *Ptch*<sup>flox/flox</sup>*LysMcre*<sup>+/-</sup> mice. (B) Tumors either have a solid (arrow) or cystic appearance (asterisks). The cystic appearance is associated with intratumoral bleeding. (C) Shows a precursor lesion (arrow). mus, muscularis (\*: longitudinal muscle layer; \*\*: circular muscle layer); muc, mucosa; lu, lumen of the intestine. (D) Arrows point to the intact myenteric plexus. (E) When precursor lesions become larger (arrows) they adopt a (F) GIST-like histology. Scale bars in  $\mu\text{m}$ : (B,C and E) 500; (D) 100; (F) 50.

Electron microscopy of the tumor was done in collaboration with Walter Schulz-Schaeffer, pathologist of the department of Neuropathology, University Medical Center Göttingen. According to him the tumor cells resembled smooth muscle. This was revealed by the occurrence of myofilaments (Figure 6). Moreover, the tumor cells showed an increased numbers of mitochondria (marked by red arrows, Figure 6).



**Figure 6. Electron microscopy of the tumors of *Ptch*<sup>flox/flox</sup>*LysMcre*<sup>+/-</sup> mice.** Tumors from *Ptch*<sup>flox/flox</sup>*LysMcre*<sup>+/-</sup> mice resemble smooth muscle as shown by myofilaments. The red arrows mark mitochondria in the tumor cell. Magnification: 10000x.

### 5.2.2 Molecular characteristics of gastrointestinal tumors of *Ptch<sup>flx/flx</sup>LysMcre<sup>+/-</sup>* mice

In order to specify the tumors in more detail, the expression of several tumor-specific markers was analyzed. In general, the tumors did not overexpress markers of follicular dendritic tumors such as CD21, CD23, CD35 (Figure 7)<sup>121</sup> or the mesothelioma-specific marker keratin 7<sup>122</sup> (Figure 7).

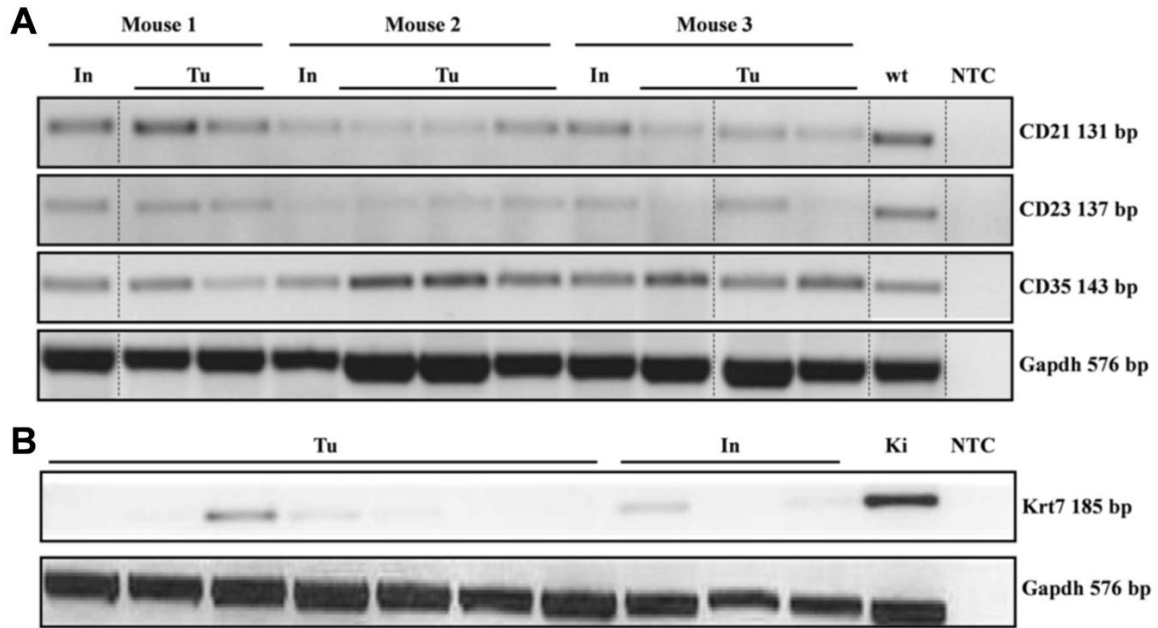


**Figure 7. Investigation of specific markers in tumors of *Ptch<sup>flx/flx</sup>LysMcre<sup>+/-</sup>* mice.** A) In comparison to normal intestine, tumors do not overexpress CD21, CD23 and CD35, which are markers for follicular dendritic tumors. B) Tumors also do not generally overexpress the mesothelioma-specific marker keratin 7 (Krt7). Expression was analyzed by semi-quantitative PCR. Tu: tumor; In: intestine; and Ki: kidney (as positive control) from *Ptch<sup>flx/flx</sup>LysMcre<sup>+/-</sup>* mice.

In agreement with histology (GIST- or LMS-like), the tumors were positive for the smooth muscle marker alpha-smooth muscle actin ( $\alpha$ SMA; Figure 8A), which can be expressed by both GIST and LMS<sup>123, 124</sup>. They moderately expressed the LMS-specific marker desmin (Figure 8B) and were negative for the GIST-specific marker CD34 (Figure 8C)<sup>43</sup>. However, as revealed by qRT-PCR analysis, the tumors clearly overexpressed the GIST-specific marker *Dog1* (Figure 8D).



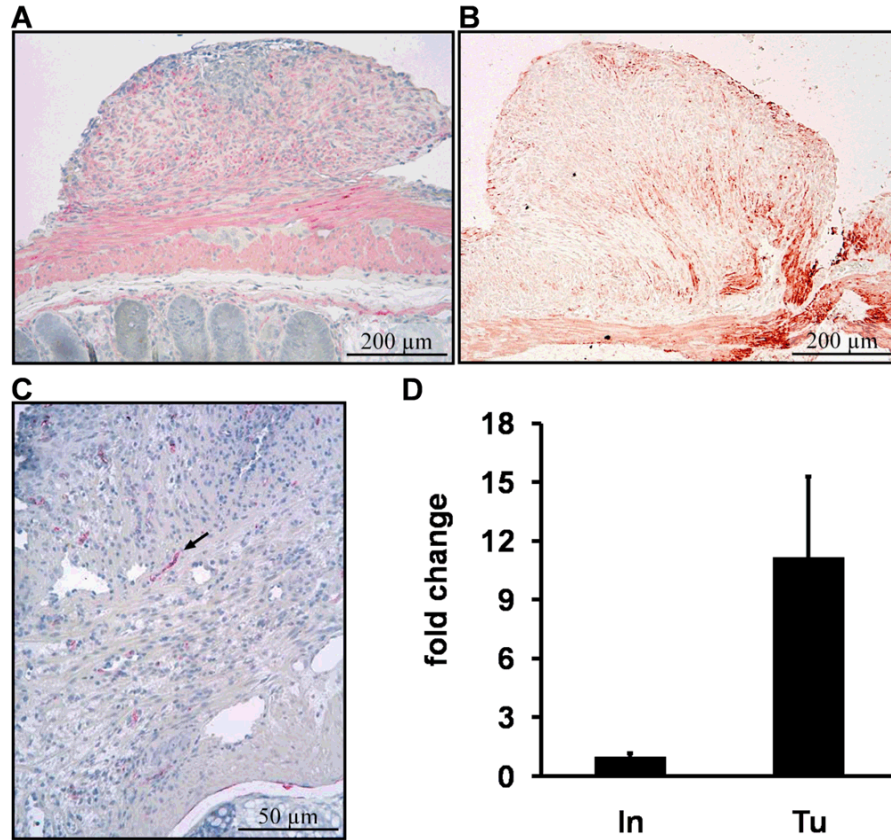


**Figure 8. Tumors express GIST and/or LMS markers.** Immunohistochemical analyses showed that tumors are positive for the smooth muscle marker  $\alpha$ SMA (A) and moderately expressed desmin (B), which can be expressed by both GIST and LMS. Although the tumors were negative for the GIST-specific marker CD43 (C; see CD34 positive vessels marked by arrow heads), the tumors (Tu, n=3) strongly expressed the GIST-specific marker *Dog1* (D) in comparison to normal intestine (In; n=3). Normalized qRT-PCR data ( $\pm$  SEM) are shown in relation to normal intestine, which was set to 1.

Together these data show that the tumors from *Ptch*<sup>flox/flox</sup>*LysMcre*<sup>+/-</sup> mice are rather GIST-like than LMS-like.

Considering the GIST-like appearance of the tumors, the expression status of Kit and *Pdgfra* in the tumors was investigated. As revealed by immunofluorescence and immunohistochemistry, all tumors were negative for Kit (Figure 9A and D). However, the tumors strongly expressed *Pdgfra* (Figure 9B and D), but were negative for *Pdgrβ* (Figure 9C).

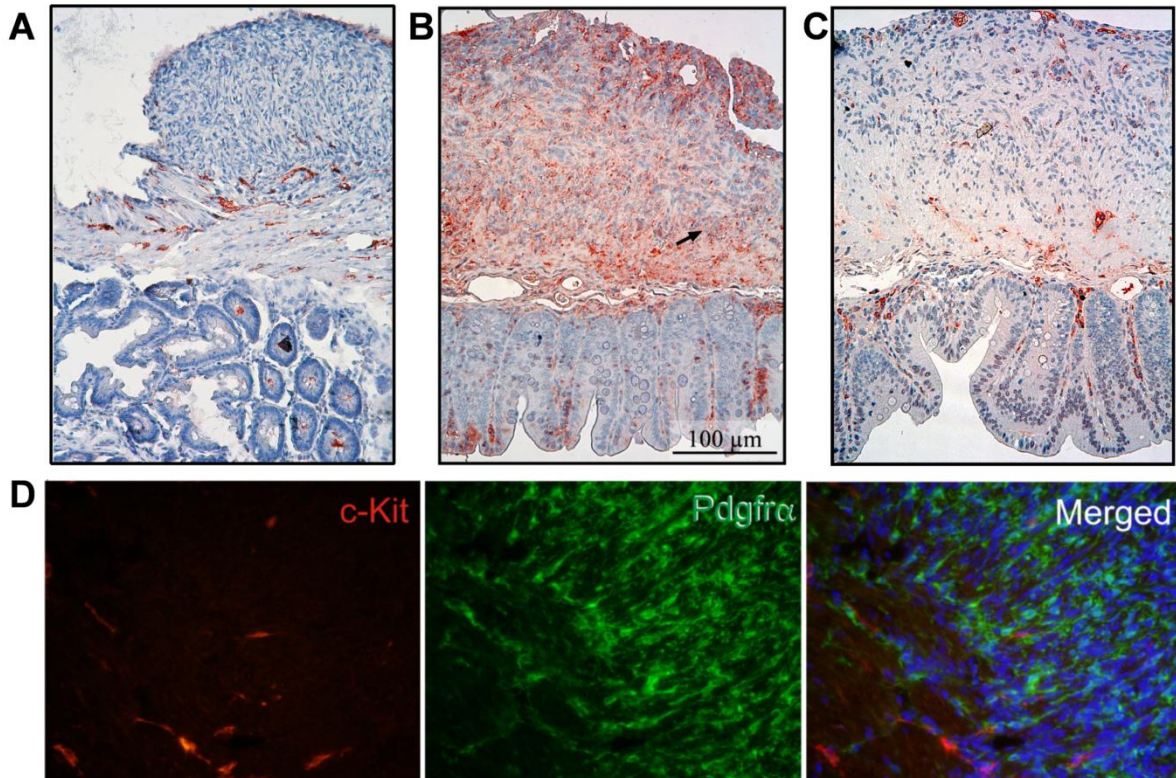


**Figure 9. Tumors of *Ptch* mutant mice express *Pdgfra* but not *Pdgfrβ* or *Kit*.** Immunohistochemical and immunofluorescence analyses of tumors of *Ptch*<sup>flx/flx</sup>*LysMcre*<sup>+/-</sup> mice using an anti-Kit (A and D) anti-*Pdgfra* (B, and D) and anti-*Pdgfrβ* (C) antibodies. Analyses showed that tumors are negative for Kit but positive for *Pdgfra*. No *Pdgfra*/Kit double-positive cells were detected in the tumors (D, merged right panel). Immunohistochemical analysis further showed that the tumor is negative for *Pdgfrβ* (C).

In addition, the tumors and normal intestine of *Ptch*<sup>flx/flx</sup>*LysMcre*<sup>+/-</sup> mice were subjected to westernblot analyses. The results supported the immunohistochemical stainings and showed that the tumors were negative for phospho-Kit and thus, Kit activity. As positive control, a lysate from the cell line GIST-T1 was used that was established from a KIT<sup>+</sup> GIST<sup>125</sup> (Figure 10). However, in contrast to Kit, the tumors of *Ptch*<sup>flx/flx</sup>*LysMcre*<sup>+/-</sup> mice strongly expressed *Pdgfra* (Figure 10B). In addition, *Pdgfra* was substantially phosphorylated in tumors when compared to normal intestine (Figure 10B).

In order to see whether the activation of *Pdgfra* was ligand-dependent, the expression of the *Pdgfra*-specific ligands- *Pdgfa*, *Pdgfb* and *Pdgfc* were analyzed by qRT-PCR. Indeed, the results showed that all 3 ligands were overexpressed in tumor tissue (Figure 10C).



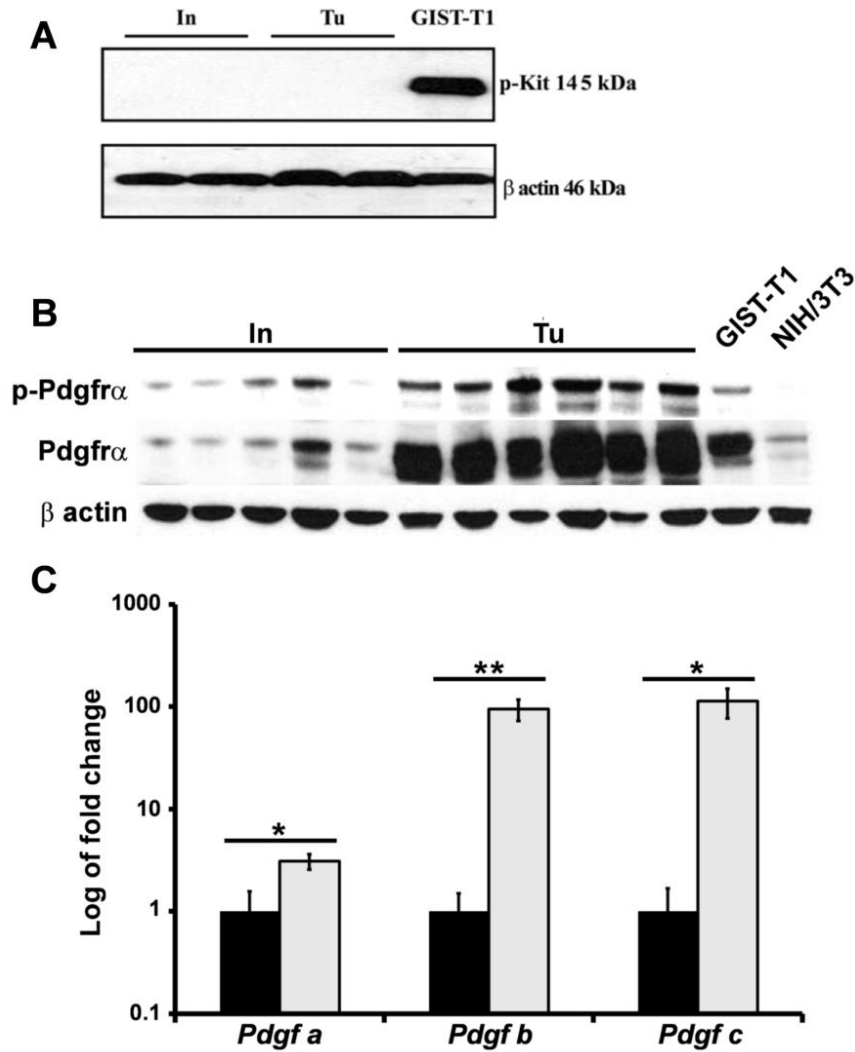


**Figure 10. Tumors of *Ptch* mutant mice overexpress *Pdgfra* and its ligands.** (A and B) Western Blot analyses of tumors (Tu) and normal small intestine (In) of *Ptch*<sup>flx/flx</sup>*LysMcre*<sup>+/-</sup> mice using anti-Kit, anti-Pdgfra and anti-pPdgfra (phosphorylated Pdgfra) antibodies. GIST-T1 and NIH/3T3 cells were used as control samples. (C) qRT-PCR analysis of *Pdgfa*, *Pdgfb* and *Pdgfc* in normal intestine and in tumors. Expression levels in tumors are shown in relation to normal intestine, which was set=1. (black bars: intestine; grey bars: tumors).

In summary, these results show that the tumors of *Ptch*<sup>flx/flx</sup>*LysMcre*<sup>+/-</sup> mice are negative for Kit and Pdgfrβ but strongly overexpress Pdgfra. In addition, Pdgfra seems to be active in the tumors, which correlates with high expression of the Pdgfra ligands.

### 5.2.3 Activation of Hh signaling in gastrointestinal tumors of *Ptch*<sup>flx/flx</sup>*LysMcre*<sup>+/-</sup> mice

Next, the Hh activity in the tumors was investigated. As explained in the introduction section, tumors associated with *Ptch* mutations are expected to show activation of the Hh signaling pathway. Since a reliable marker for Hh pathway activity is the expression of *Gli1*, tumors and corresponding normal intestine were subjected to a *Gli1*-specific qRT-PCR analysis. The results show that *Gli1* was significantly overexpressed in the tumors in comparison to normal

intestine (Figure 11). In addition, the expression of the two other *Gli* transcription factors *Gli2* and *Gli3* was analyzed. Although the expression of these two genes was increased in comparison to the small intestine, the increase did not reach statistical significance. Besides *Gli1* the tumor samples also overexpress mutant *Ptch<sup>del</sup>* transcripts when compared to normal intestine (Figure 12A and B). This was revealed by RT-PCR (Figure 12A; in the mutant *Ptch<sup>del</sup>* transcripts exon 7 is spliced into exon 10 due to the cre-mediated deletion of exon 8 and 9 of the *Ptch* gene) and by *in situ* hybridization (Figure 12B). The latter method confirmed that the tumors overexpressed *Gli1* and additionally shows that wt *Ptch* transcripts are missing, whereas the mutant *Ptch* transcripts are strongly overexpressed in the tumors (Figure 12B). Consistent with an aberrant Hh pathway activation in tumor cells, the normal intestine only showed a few cells positive for *Gli1* or *Ptch*.

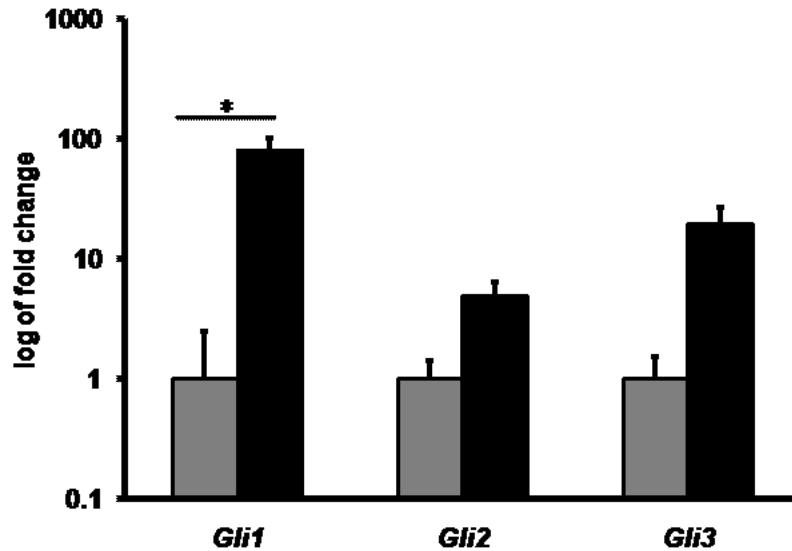


**Figure 11. *Gli* expression in tumors of *Ptch* mutant mice.** Quantitative RT-PCR analysis of *Gli1*, *Gli2* and *Gli3* in normal intestine (n=6) and in tumors (n=8) of *Ptch<sup>flx/flx</sup>LysMcre<sup>+/-</sup>* mice. Expression levels ( $\pm$  SEM) in tumors are shown in relation to normal intestine, which was set to 1. Grey bars: intestine; black bars: tumors. Asterisk indicates  $P < 0.05$  by unpaired t-test ( $P_{Gli1} = 0.015$ ;  $P_{Gli2} = 0.131$ ;  $P_{Gli3} = 0.054$ ).

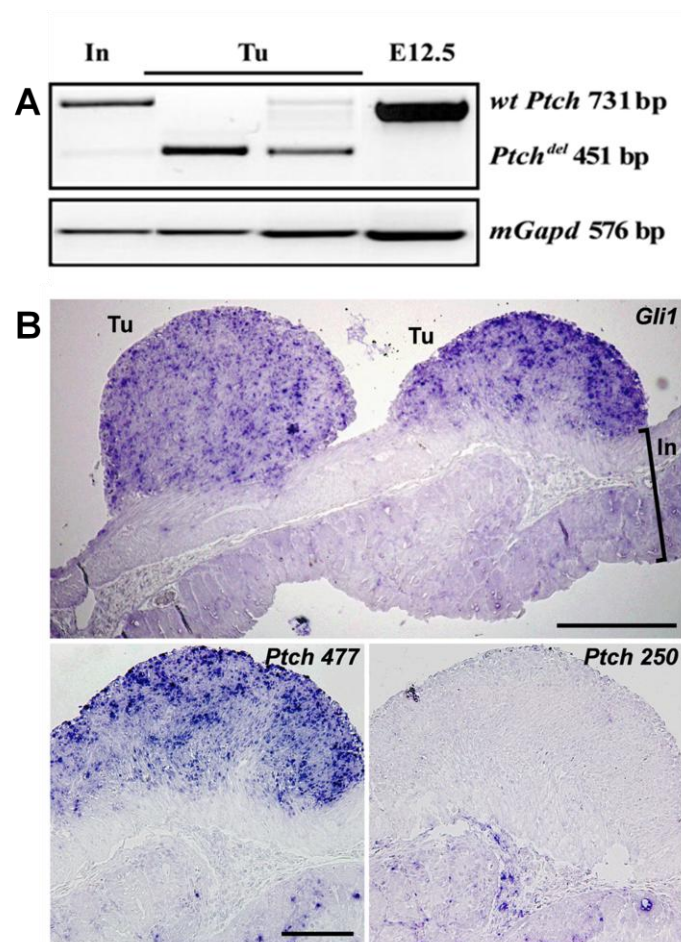


**Figure 12. Activation of Hh signaling in tumors of *Ptch* mutant mice.** (A) RT-PCR analysis of tumors showing the disappearance of wt *Ptch* (731 bp) and the appearance of the *Ptch*<sup>del</sup> (451 bp) transcript. Similar results were obtained by *in situ* hybridization of the Hh target genes *Gli1* (B, upper panel) and *Ptch* (B, lower panel). The 477 bp *Ptch* probe identifies both the wt and the mutant *Ptch*<sup>del</sup> transcripts (B, lower panel left), in which exon 7 is spliced to exon 10 due to cre-mediated deletion of exon 8 and 9. The 250 bp *Ptch* probe exclusively binds to wt *Ptch* transcripts (B, lower panel, right). The figure demonstrates that the tumors overexpress exclusively mutant *Ptch*<sup>del</sup> transcripts, since wt *Ptch* transcripts were not detected. Scale bar in  $\mu\text{m}$ : 200.

These data indicate that the Hh signaling pathway is activated in the tumors but not the normal tissue surrounding the tumors of *Ptch*<sup>flx/flx</sup>*LysMcre*<sup>+/-</sup> mice.

### 5.3 Differentiation of the tumors of *Ptch*<sup>flx/flx</sup>*LysMcre*<sup>+/-</sup> mice from LMS

#### 5.3.1 Comparison of gene expression profiles between human GIST, human and murine LMS and tumors of *Ptch*<sup>flx/flx</sup>*LysMcre*<sup>+/-</sup> mice

Based on histology and localization, the tumors in *Ptch*<sup>flx/flx</sup>*LysMcre*<sup>+/-</sup> mice strikingly resembled GIST tumors in humans. Since LMS is an important tumor entity in the differential diagnosis of GIST, we next investigated whether the tumors of *Ptch*<sup>flx/flx</sup>*LysMcre*<sup>+/-</sup> mice were more related to GIST or to LMS.

According to the GEO database, GIST overexpress the main HH targets *PTCH* (4-fold) as well as other downstream HH target genes *FOXF1* (20-fold), *HAND2* (2-fold) and *NKX3.2* (130-fold) when compared to LMS (Figure 13).

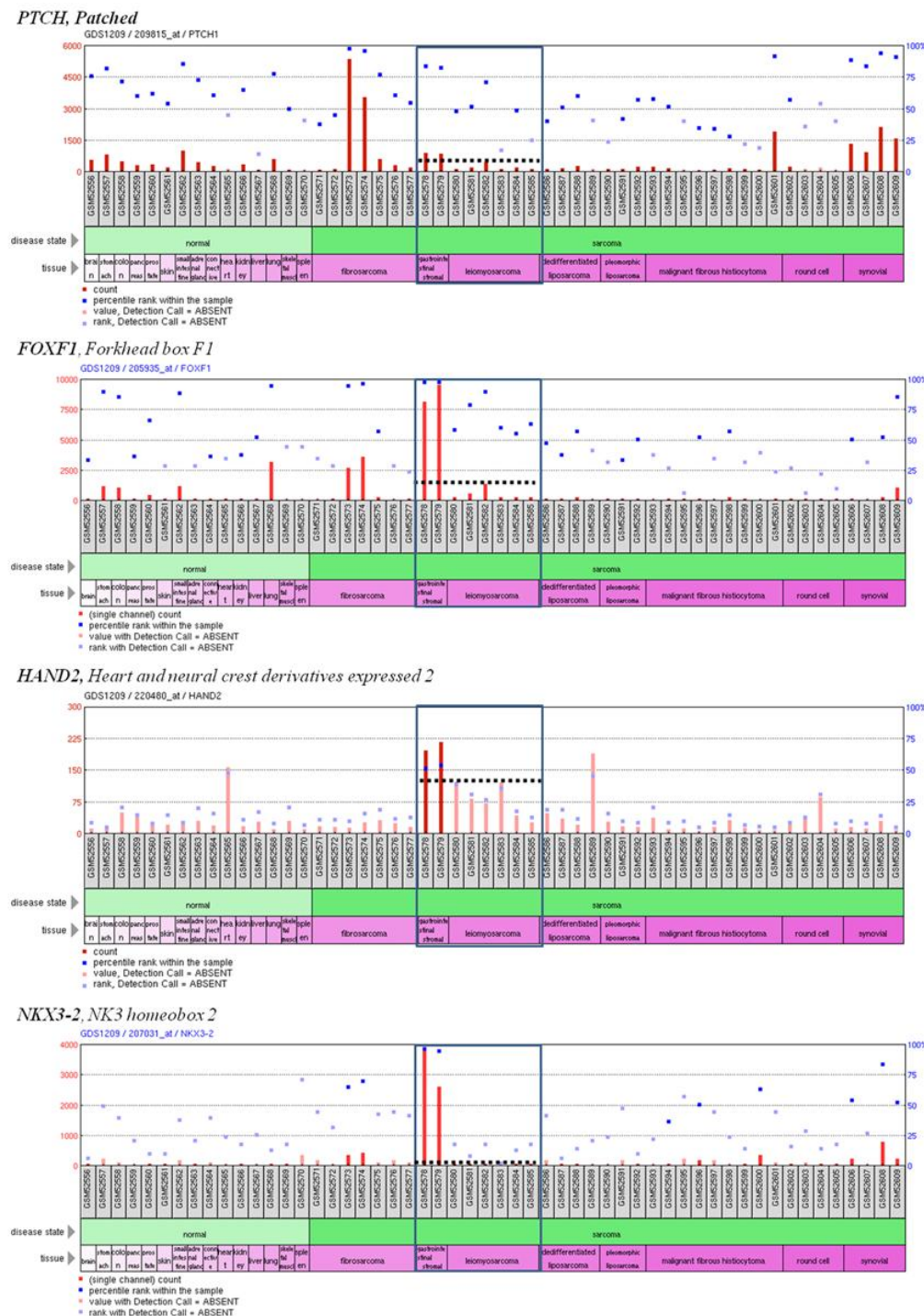


**Figure 13. According to the GEO database, GIST overexpress HH target genes when compared to LMS.** Data are from GEO GDS1209 (<http://www.ncbi.nlm.nih.gov/sites/GDSbrowser?acc=GDS1209>).

Due to the data from GEO database, the expression levels of the Hh downstream target genes *Gli2*, *Ptch*, *Hand2* and *Foxf1* were analyzed by qRT-PCR analysis in tumors of

*Ptch<sup>flox/flox</sup>LysMcre<sup>+/-</sup>* mice and in murine LMS derived from *Pten/p53* double-mutant mice (ref<sup>126</sup> and Guijarro and Hernando, unpublished). The data was compared to 20 human GIST and 7 human LMS samples. The human tumor samples were from the Department of Pathology at the Leiden University Medical Center. Indeed, the analysis showed higher levels of the Hh target genes *GLI2/Gli2*, *PTCH/Ptch*, *HAND1/Hand1*, *FOXF1/FoxF1* and *Nkx3.2* in human GIST and in tumors of *Ptch<sup>flox/flox</sup>LysMcre<sup>+/-</sup>* mice when compared to the respective LMS samples (Figure 14; an expression analysis of murine *Nkx3.2* was not possible in our hands).

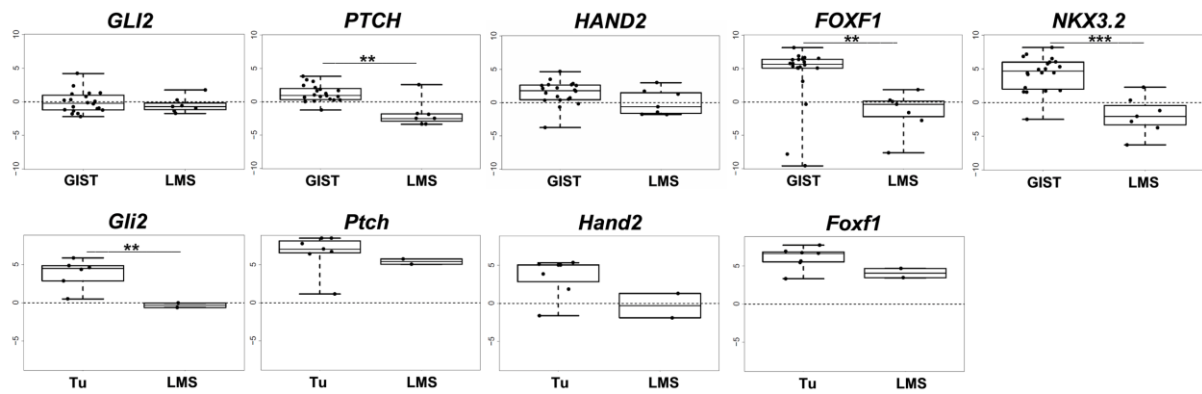


**Figure 14. Differentiation of the tumors from LMS.** Quantitative qRT-PCR analysis of HH/Hh-target genes in 20 human GIST compared to 7 human LMS samples (upper panel), and in tumors of *Ptch<sup>flox/flox</sup>LysMcre<sup>+/-</sup>* mice (Tu) compared to murine LMS derived from mice harboring a *Pten/p53* mutation (lower panel). Expression levels in human and murine samples were normalized to the expression of  $\beta$ -actin and *18S rRNA*, respectively. Data shows Box-Whisker-Plots of the relative gene expression. (\* $P<0.05$ , \*\* $P<0.01$ , \*\*\* $P<0.001$  by unpaired t-test).

Together, these data demonstrate that HH/Hh signaling activity is increased in human GIST and tumors found in of *Ptch<sup>flox/flox</sup>LysMcre<sup>+/-</sup>* mice when compared to human and murine LMS. Thus, these data confirmed that the murine tumors of *Ptch<sup>flox/flox</sup>LysMcre<sup>+/-</sup>* mice are GIST-like rather than LMS-like.

Since *Pdgfra*, and not *Kit*, was strongly expressed in the tumors of *Ptch<sup>flox/flox</sup>LysMcre<sup>+/-</sup>* mice and thus correlated with active Hh signaling, we next analyzed the correlation between high *PDGFRA* expression and HH-signaling activity in human GIST.

To this end, the published microarray data set GSE8167 (accession number at the GEO database<sup>127</sup>) was analyzed by our collaborators of the Department of Medical Statistics, Annalen Bleckmann and Tim Beissbarth. Indeed, in this set a relation between *PDGFRA* expression and HH signaling was evident, when low and high *PDGFRA*-expressers were



distinguished using a cut-off according to the median gene expression of *PDGFRA*. Gene set enrichment analysis (GSEA) revealed that HH pathway genes are enriched in the *PDGFRA*-high expressers (Figure 15; enrichment score according to Wilcoxon and Kolmogorov-Smirnov test:  $p=0.01811$  and  $p=0.04923$ , respectively).

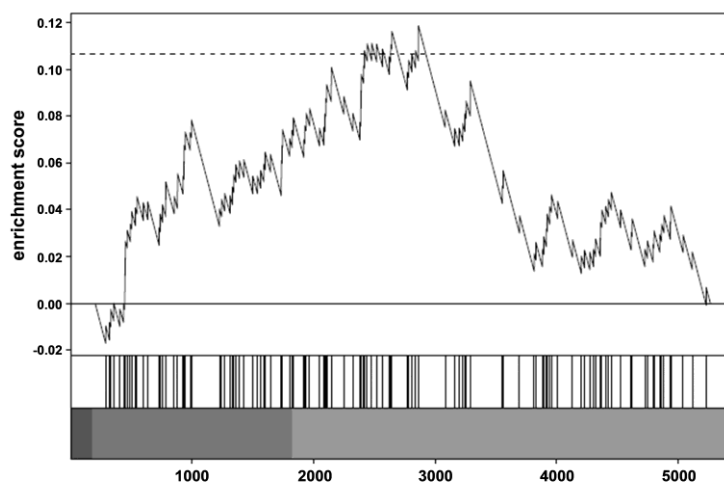


**Figure 15. Positive correlation between HH signaling and *PDGFRA* expression in human GIST.** Enrichment plot in *PDGFRA* high-expresser GIST samples (performed on GEO database set GSE8167): shown is the profile of the running enrichment score and the positions of the Hh pathway gene set members on the rank ordered list.

Next, GIST with a known *KIT* and *PDGFRA* mutational status were analyzed for the expression of *PDGFRA* and the HH target *GLII* (for samples see Table 20). As shown in Figure 16 (left panel), tumors showing high *PDGFRA* expression are *PDGFRA* mutant GIST. This was in agreement with recently published data<sup>128, 129</sup>. Importantly, as revealed by *GLII* expression, *PDGFRA* mutant GIST generally show higher HH signaling activity when compared to *KIT* mutant or wildtype GIST (Figure 16, right panel). Thus, the positive correlation between HH activity and *PDGFRA* expression and the mutational status of *PDGFRA* seems to be a common phenomenon in GIST.

**Table 20. Characteristics of human GIST used for analysis.**

<i>Case no.</i>	<i>KIT/PDGFR mutation</i>
<b>24</b>	KIT deletion N579
<b>26</b>	KIT point mutation V559D
<b>1936</b>	KIT point mutation V560D
<b>1964</b>	KIT duplication PTQLPYDHKWEFP573-585
<b>1984</b>	KIT point mutation V560D
<b>2594</b>	KIT deletion WK557-558
<b>2648</b>	KIT insertion AY502-503
<b>2822</b>	KIT point mutation W557R
<b>2833</b>	KIT point mutation W557G
<b>2860</b>	KIT deletion WKVVE557-561 and point mutation D820Y
<b>2932</b>	KIT deletion WK557-558
<b>2970</b>	KIT point mutation V822K
<b>3033</b>	KIT insertion AY502-503
<b>4</b>	PDGFRA point mutation D842V
<b>9</b>	PDGFRA point mutation D842V
<b>484</b>	PDGFRA point mutation D842E and deletion IMHD843-846
<b>485</b>	PDGFRA point mutation V561D
<b>486</b>	PDGFRA point mutation D842V
<b>508</b>	PDGFRA point mutation D842V
<b>1468</b>	PDGFRA point mutation D842V
<b>12</b>	KIT wildtype E 9, 11, 13, 17; PFDGFRA wildtype E 12, 18
<b>13</b>	KIT wildtype E 9, 11, 13, 17; PFDGFRA wildtype E 12, 18
<b>1971</b>	KIT wildtype E 9, 11, 13, 14, 17; PDGFR wildtype E 12, 18
<b>2014</b>	KIT wildtype E 9, 11; PDGFR wildtype E 12, 18
<b>2272</b>	KIT wildtype E 9, 11, 13, 14, 17 ; PDGFR wildtype E 12, 18
<b>3500</b>	KIT wildtype E 9, 11; PDGFR wildtype E 12, 18
<b>2014</b>	KIT wildtype E 9, 11; PDGFR wildtype E 12, 18
<b>3501</b>	KIT wildtype E 9, 11, 13, 14, 17, PDGFR wildtype E 12, 18

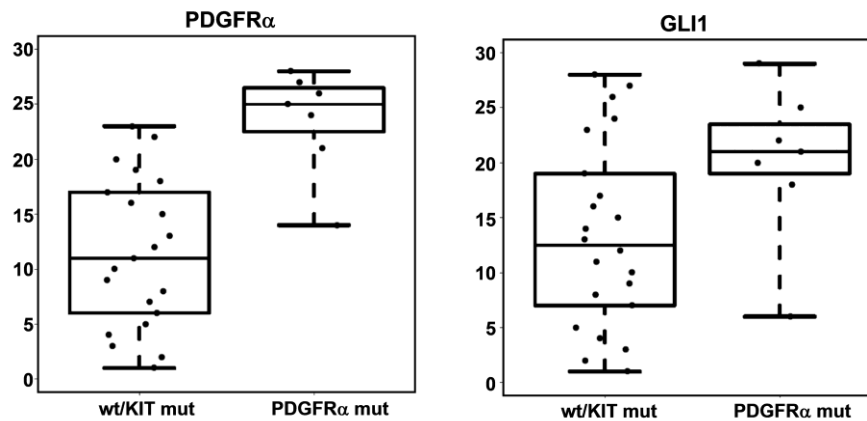


**Figure 16. HH activity is increased in *PDGFRA* mutant GIST that highly express *PDGFRA*.** Figure shows qRT-PCR analysis of *PDGFRA* (left panel) and of the main HH-target *GLI1* (right panel) in GIST that are either wildtype or *KIT* mutant (wt/*KIT* mut) or have a *PDGFRA* mutation (*PDGFRA* mut). The samples used for the study are shown in Table 20. Data is represented by Box-Whisker-Plots.

Together, these results demonstrate that the tumors of *Ptch<sup>fllox/fllox</sup>LysMcre<sup>+/-</sup>* mice are indeed GIST-like rather than LMS-like. In addition, they confirm the previously reported data showing that HH signaling is aberrantly activated in human GIST<sup>46</sup>. Furthermore, the data showed that *PDGFRA* mutant GIST have relatively high *PDGFRA* and *GLI1* expression indicating increased HH activity in comparison to wt or *KIT* mutant GIST.

### 5.3.2 Gastrointestinal tumors of *Ptch<sup>fllox/fllox</sup>LysMcre<sup>+/-</sup>* mice are responsive to imatinib

An important characteristic of most human GIST is the responsiveness to imatinib, which inhibits the activity of both the KIT and PDGFR tyrosine kinases<sup>130</sup>. Therefore, the effect of imatinib was tested on the growth of GIST-like tumors in symptom-free *Ptch<sup>fllox/fllox</sup>LysMcre<sup>+/-</sup>* mice. For this purpose, 6 or 8 week old mice were randomly divided into 6 groups. The first 2 groups received 0.1g/kg/day imatinib orally over a period of 10 or 12 weeks. One additional group received the same dose (0.1g/kg/day) for 10 weeks and was observed for 3 additional weeks before autopsy. All 3 imatinib-treated groups had a corresponding vehicle-treated control group. All the treatment schemes were tolerated well by the animals. When the animals were sacrificed and subjected to autopsy all mice included in the analysis have developed GIST-like tumors. Both the 10 and 12 week treatment decreased the total number of tumors: Whereas the average tumor number was  $5.2 \pm 1.7$  and  $5.2 \pm 1.5$  in the vehicle-treated groups, imatinib treatment for 10 or 12 weeks significantly decreased the number of tumors to an average of  $2.6 \pm 1.3$  ( $P=0.01$ ) and  $2.6 \pm 1.3$  ( $P=0.0080$ ) per animal, respectively (Figure 17 and Table 21). In addition, the effect of imatinib seems to be reversible when the treatment was halted. Thus, 3 weeks after the end of the 10 week-imatinib treatment, the



imatinib-treated animals had a comparable tumor number when compared to the vehicle-treated mice with  $4.0 \pm 1.73$  and  $5.0 \pm 3.61$  tumors per mouse, respectively (Table 21). The effect of imatinib on tumor growth of *Ptch*<sup>flox/flox</sup>*LysMcre*<sup>+/-</sup> mice can be attributed to the inhibition of *Pdgfra* activity. Furthermore, these results confirm the GIST-like identity of the tumors.



**Figure 17. Tumors of *Ptch*<sup>flox/flox</sup>*LysMcre*<sup>+/-</sup> mice respond to imatinib treatment.** Shown are representative GI tracts of *Ptch*<sup>flox/flox</sup>*LysMcre*<sup>+/-</sup> mice after treatment with vehicle (left) or imatinib (right). Imatinib treatment decreased the number of tumors (also see Table 21) in comparison to vehicle-treated animals.

**Table 21. Effect of imatinib on tumor multiplicity in *Ptch*<sup>flox/flox</sup>*LysMcre*<sup>+/-</sup> mice.**

genotype	n	Age (days) <sup>1</sup> median	Treatment	mice with GIST-like tumors	P value
<i>Ptch</i> <sup>flox/flox</sup> <i>LysMcre</i> <sup>+/-</sup>	7	127	0.1 g/kg/d imatinib orally starting at 8 weeks of age for 10 weeks	7/7; tumor multiplicity <sup>2</sup> : $2.6 \pm 1.3$	0.01
<i>Ptch</i> <sup>flox/flox</sup> <i>LysMcre</i> <sup>+/-</sup>	6	127	vehicle (200 $\mu$ l PBS) orally starting at 8 weeks of age for 10 weeks	6/6; tumor multiplicity <sup>2</sup> : $5.2 \pm 1.7$	
<i>Ptch</i> <sup>flox/flox</sup> <i>LysMcre</i> <sup>+/-</sup>	7	127	0.1 g/kg/d imatinib orally starting at 6 weeks of age for 12 weeks	7/7; tumor multiplicity <sup>2</sup> : $2.6 \pm 1.3$	0.008
<i>Ptch</i> <sup>flox/flox</sup> <i>LysMcre</i> <sup>+/-</sup>	5	127	vehicle (200 $\mu$ l PBS) orally starting at 6 weeks of age for 12 weeks	5/5; tumor multiplicity <sup>2</sup> : $5.2 \pm 1.5$	
<i>Ptch</i> <sup>flox/flox</sup> <i>LysMcre</i> <sup>+/-</sup>	3	174	0.1 g/kg/d imatinib orally starting at 8 weeks of age for 10 weeks plus 3 weeks of no treatment	3/3; tumor multiplicity <sup>2</sup> : $4.0 \pm 1.73$	1.0
<i>Ptch</i> <sup>flox/flox</sup> <i>LysMcre</i> <sup>+/-</sup>	3	174	vehicle (200 $\mu$ l PBS) orally starting at 8 weeks of age for 10 weeks plus 3 weeks of no treatment	3/3; tumor multiplicity <sup>2</sup> : $5.0 \pm 3.61$	

<sup>1</sup> from birth on

<sup>2</sup> mean  $\pm$  SD; Due to frequent clustering of tumor nodules, each cluster was counted as one separate tumor.

#### 5.4 GIST-like tumors of *Ptch*<sup>flox/flox</sup>*LysMcre*<sup>+/-</sup> mice are derived from LysM<sup>+</sup> cells of the GI tract

The histology, the localization within the gut wall, the development i.e. in the same location as do tumors in mice overexpressing a Kit K641E mutation (normally found in the caecal area), and the responsiveness to imatinib were suggestive of GIST<sup>131</sup>. However, this was inconsistent with the *Ptch* deletion in the myeloid lineage, as GIST are considered to arise from KIT- or PDGFRA-expressing precursor cells of the smooth muscle layer of the GI tract. To resolve this discrepancy, we investigated if the tumors in *Ptch*<sup>flox/flox</sup>*LysMcre*<sup>+/-</sup> mice were indeed derived from LysM-targeted cells. For this purpose, *Ptch*<sup>flox/flox</sup>*LysMcre*<sup>+/-</sup>*R26R-LacZ*<sup>+/-</sup> mice were generated by crossing *Ptch*<sup>flox/flox</sup>*LysMcre*<sup>+/-</sup> with *R26R-LacZ*<sup>+/-</sup> mice. In *Ptch*<sup>flox/flox</sup>*LysMcre*<sup>+/-</sup>*R26R-LacZ*<sup>+/-</sup>, *LysMcre* not only induces recombination at the *Ptch*<sup>flox</sup> locus, but also at the *R26R* locus. Therefore, all progeny of LysM-expressing cells are expected to be marked by the permanent expression of LacZ. As demonstrated in Figure 18, the LacZ-positive cells localized to the tumor mass. This confirmed that the tumor originated from LysM<sup>+</sup> cells.

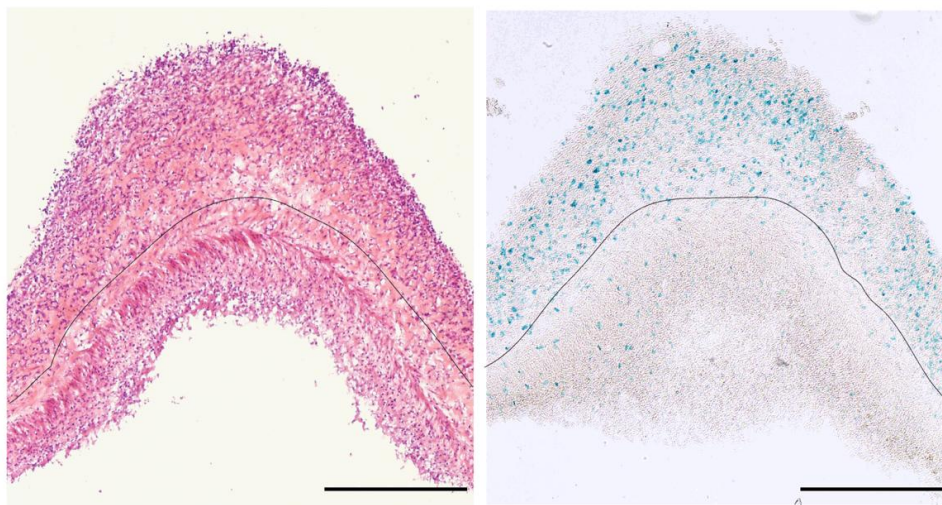


**Figure 18. LysM-expressing cells in tumors of *Ptch* mutant mice.** In *Ptch*<sup>flox/flox</sup>*LysMcre*<sup>+/-</sup>*R26R-LacZ*<sup>+/-</sup>, cre not only induces recombination at the *Ptch*<sup>flox</sup> locus, but also at the *R26R* locus. This marks LysM<sup>+</sup> cells by permanent LacZ expression. The figure shows LacZ expression in tumors of *Ptch*<sup>flox/flox</sup>*LysMcre*<sup>+/-</sup>*R26R-LacZ*<sup>+/-</sup> mice. Left: HE staining, Right: LacZ staining. Dotted line marks the tumor (Tu)/normal muscle border. Scale bar (μm):500.

In order to assess whether the LysM-positive tumor cells were derived from the BM, yet another lineage-tracing experiment was performed. For this purpose lethally irradiated *Rag-2*<sup>-/-</sup>*γc*<sup>-/-</sup> mice were transplanted with BM isolated from either *Ptch*<sup>flox/flox</sup>*LysMcre*<sup>+/-</sup> or *Ptch*<sup>flox/flox</sup>

control mice. Since *Rag-2*<sup>-/-</sup>*γc*<sup>-/-</sup> mice lack T, B and natural killer cells<sup>132</sup>, the successful repopulation of the mice with donor BM was monitored by flow cytometry analysis of T and B cells in the whole blood. T cells are TCRβ<sup>+</sup>CD3<sup>+</sup>, whereas B cells are B220<sup>+</sup> and CD19<sup>+</sup>. The analysis demonstrated that the *Rag-2*<sup>-/-</sup>*γc*<sup>-/-</sup> mice were successfully repopulated with the BM derived from both *Ptch*<sup>flx/flx</sup>*LysMcre*<sup>+/-</sup> and *Ptch*<sup>flx/flx</sup> control mice (Figure 19). However, despite successful reconstitution with the transplanted mutant BM, the *Rag-2*<sup>-/-</sup>*γc*<sup>-/-</sup> mice did not develop any tumor, not even after 250 days post-transplantation. Thus, these data suggested that the GIST-like tumors did not originate from LysM<sup>+</sup> myeloid cells of the BM.

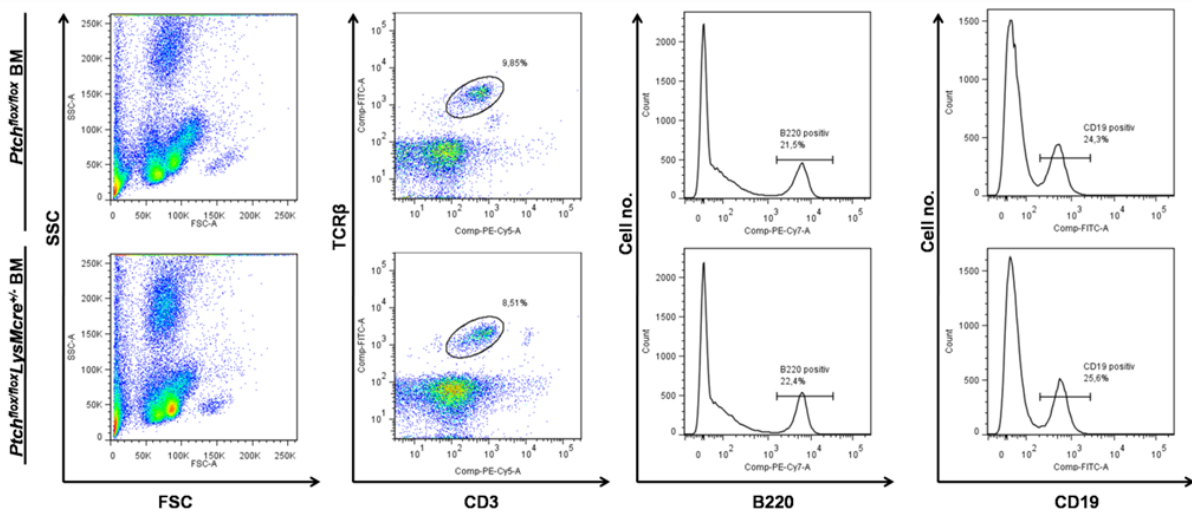


**Figure 19. Repopulation of *Rag-2*<sup>-/-</sup>*γc*<sup>-/-</sup> mice after transplantation with BM derived from *Ptch*<sup>flx/flx</sup> or *Ptch*<sup>flx/flx</sup>*LysMcre*<sup>+/-</sup> mice.** BM cells (2x10<sup>6</sup> cells/animal) from *Ptch*<sup>flx/flx</sup> or *Ptch*<sup>flx/flx</sup>*LysMcre*<sup>+/-</sup> mice were injected intravenously into lethally irradiated *Rag-2*<sup>-/-</sup>*γc*<sup>-/-</sup> mice. After 6 weeks, peripheral blood cells were analyzed by flow cytometry. Cells were analyzed by staining with antibodies against either CD3 or TCRβ to identify the T cell population, and antibodies against B220 and CD19 to identify the B cells.

Since these data suggested that GIST-like tumors of *Ptch*<sup>flx/flx</sup>*LysMcre*<sup>+/-</sup> mice were derived from a LysM<sup>+</sup> cell located in the intestinal muscle layer, the intestines from *LysMcre*<sup>+/-</sup>*R26R-LacZ*<sup>+/-</sup> mice were stained for LacZ. Indeed, as shown in Figure 20, LacZ-positive cells were detected between the longitudinal muscle layer and the serosa, and between the circular and the longitudinal muscle layers (Figure 20) i.e these cells were detected in the same location where tumors normally develop (see Figure 5C).

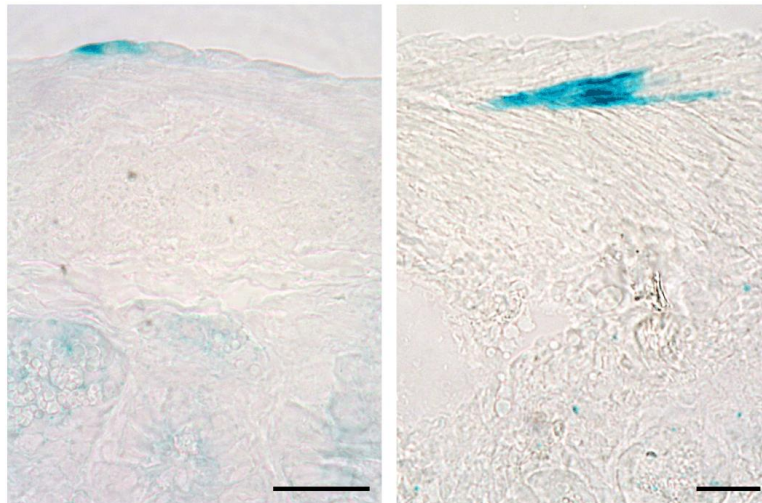


**Figure 20. LacZ-staining of normal intestine derived from  $LysMcre^{+/-}R26R-LacZ^{+/-}$  mice.** In the muscularis LacZ-positive cells are detected between the longitudinal muscle layer and the serosa (left panel) and the circular and longitudinal muscle layer (right panel). Scale bars ( $\mu\text{m}$ ): 50.

Together, these data suggested that *Ptch*-associated GIST are derived from a BM-independent  $LysM^{+}$  cell population in the muscular wall of the intestine.

#### 5.4.1 $LysM^{+}$ cells of the GI tract can express *Pdgfra* but not *Kit*

Since the tumors of  $Ptch^{flox/flox}LysMcre^{+/-}$  mice had a GIST-like appearance and expressed *Pdgfra* but not *Kit*, we hypothesized that the respective cell of origin i.e. the  $LysM^{+}$  cell in the intestinal wall, also should express *Pdgfra* but not *Kit*. In order to prove this assumption, the expression status of *Kit* and *Pdgfra* in  $LacZ^{+}$  cells in the intestine of  $Ptch^{flox/flox}LysMcre^{+/-}R26R-LacZ^{+/-}$  mice was investigated. Immunohistochemical analyses revealed that some  $LacZ^{+}$  cells in the muscle layer co-expressed *Pdgfra* (Figure 21, left and middle panel). In contrast, no  $LacZ^{+}$  cells expressing *Kit* were detected. However, the  $LacZ^{+}$  cells frequently were juxtaposed to  $Kit^{+}$  cells (Figure 21, right panel). These data showed that the GIST-like tumors of  $Ptch^{flox/flox}LysMcre^{+/-}$  mice were not derived from  $LysM^{+}$  cells that concomitantly express *Kit*. Rather the tumors of  $Ptch^{flox/flox}LysMcre^{+/-}$  mice originate from  $LysM^{+}$  cells that are negative for *Kit* and concomitantly may express *Pdgfra*.



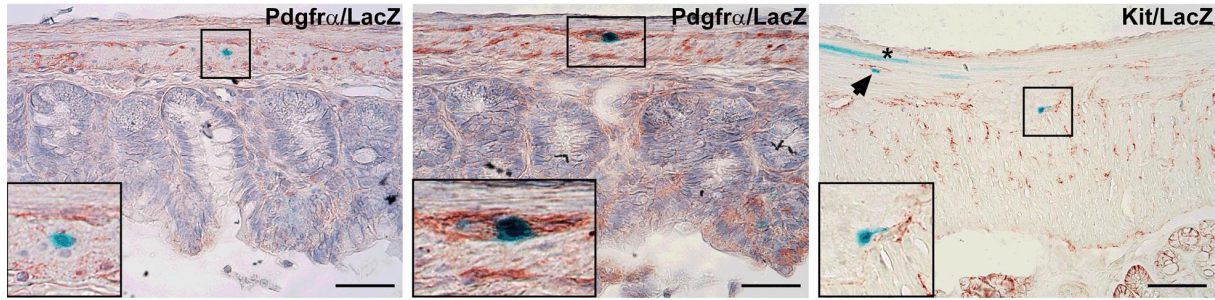


**Figure 21. LacZ and Pdgfra or Kit co-stainings of intestines derived from *Ptch<sup>flox/flox</sup>LysMcre<sup>+/-</sup>R26R-LacZ<sup>+/-</sup>* mice.** Sections were co-stained with antibodies against Pdgfra (left and middle panel) or Kit (right panel). Inset in the left panel shows a LacZ-positive, but Pdgfra-negative cell. Inset in the middle panel shows a LacZ/Pdgfra double-positive cell. Inset in the right panel shows a LacZ-positive cell juxtaposed to a Kit-positive cell (a similar cell is marked by an arrowhead). The asterisk in the right panel indicates a LacZ-positive muscle fiber not juxtaposed to Kit-positive cells. Scale bars ( $\mu\text{m}$ ): left and middle panel: 50; right panel: 25.

Still another question was of whether Hh signaling was activated in  $\text{LysM}^+$  or in  $\text{LysM}^+\text{Pdgfra}^+$  cells of *Ptch<sup>flox/flox</sup>LysMcre<sup>+/-</sup>* mice. This was expected since the *Ptch* mutation in LysM-expressing cells was the driving force for tumor development. To answer this question, I tried to co-stain intestines derived from *Ptch<sup>flox/flox</sup>LysMcre<sup>+/-</sup>R26R-LacZ<sup>+/-</sup>* mice for Pdgfra (by IHC) or LacZ with either the *Gli1* or *Ptch in situ* probes (see 4.12.5 and 4.12.6). However, this was not possible in my hands. Nevertheless, the *Gli1* and *Ptch in situ* hybridization of intestines derived from wt mice showed that the distribution of *Gli1*-positive or *Ptch*-positive cells was the same as the distribution of  $\text{LacZ}^+$  or  $\text{Pdgfra}^+$  cells i.e. they were found between the serosa and the longitudinal muscle layer, the longitudinal muscle layer and the circular muscle layer and within the circular muscle layer. A representative staining using the 477 *Ptch* probe (see 4.12.5) is shown in Figure 22.

Therefore, it is likely that Hh signaling was active in either  $\text{LysM}^+$  or  $\text{LysM}^+\text{Pdgfra}^+$  cells of the intestine.

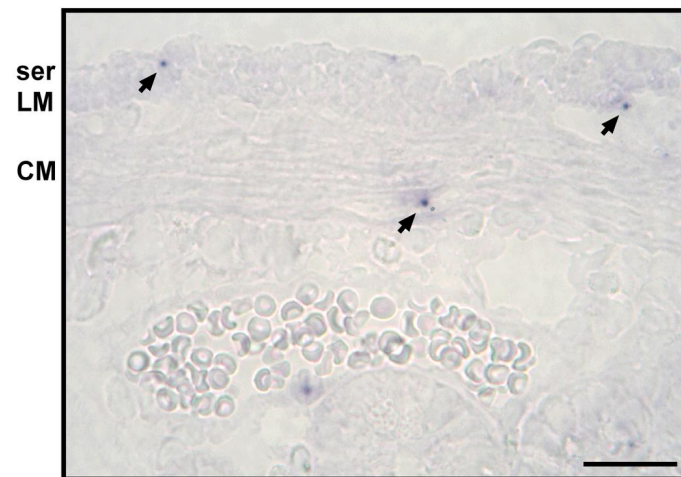


**Figure 22.** *Ptch*-positive cells are found in the same location as *LacZ*<sup>+</sup> or *Pdgfra*<sup>+</sup> cells. *In situ* hybridization of *Ptch* in the normal intestine of a wt mouse using the 477 bp *Ptch* probe. The figure demonstrates *Ptch* expression in single cells (shown by arrows) between the serosa (ser) and the longitudinal muscle layer (LM) of the normal intestine, the LM and the circular muscle layer (CM) and within the circular muscle layer. Scale bar in  $\mu\text{m}$ : 20.

### 5.5 HH signaling cooperates with PDGFRA signaling, but not with KIT signaling, in cellular transformation

So far the analysis indicated that the GIST-like tumors of *Ptch*<sup>flox/flox</sup>*LysMcre*<sup>+/-</sup> mice were derived from a *LysM*<sup>+</sup> cell of the intestine, in which Hh signaling was activated due to mutations in *Ptch*. In addition, this cell may express *Pdgfra*, but not *Kit*.

Recently it has been shown that HH signaling frequently cooperates with other signaling pathways in cellular transformation<sup>133, 112</sup>. The positive correlation of the expression and activation of PDGFRA and HH signaling in the GIST array data set (see Figure 15) as well as the potential activation of Hh signaling in *Pdgfra*<sup>+</sup> cells of the intestine of *Ptch*<sup>flox/flox</sup>*LysMcre*<sup>+/-</sup> mice prompted us to test the possibility of signal cooperation between Hh and *Pdgfra* signaling in oncogenic transformation. For this purpose, human non-tumorigenic HaCaT keratinocytes expressing GLI1 under the control of Dox-inducible promotor (Dox-inducible GLI-HaCaT) were employed. This is a well established assay system that facilitates analysis of proteins that modulate the oncogenic activity of GLI proteins<sup>112</sup>. HaCaT keratinocytes were seeded on plates with agar and treated with Dox and/or the PDGFRA ligand PDGFB. To assay a possible cooperation of HH/GLI with KIT signaling, the same GLI1-expressing HaCaT cells were stably transduced with the constitutively active D816V KIT mutant. The codon 816 in exon 17 is a mutation hot spot for KIT gene and one of the most common substitutions D816V, causes constitutive activation of *KIT*<sup>134</sup>.

The data revealed that the Dox-induced expression of GLI1 cooperated with the PDGFRA ligand PDGFB to induce cellular transformation. This was evidenced by significant growth of the transformed cells in 3D cultures (Figure 23, left panel). By contrast, neither GLI1 nor PDGFB alone was able to elicit appreciable growth. As PDGFB induced phosphorylation of PDGFRA (Figure 23, right panel) and activated both ERK and the JUN oncogene, we conclude that PDGFRA signaling can cooperate with HH/GLI in oncogenic transformation. In contrast, simultaneous expression of GLI1 and dominant active KIT (D816V mutant) did not enhance transformation (Figure 23, left panel). These data suggest that *Pdgfra*, in cooperation with Hh activation, may be the cause of GIST-like tumors in *Ptch<sup>flox/flox</sup>LysMcre<sup>+/-</sup>* mice.

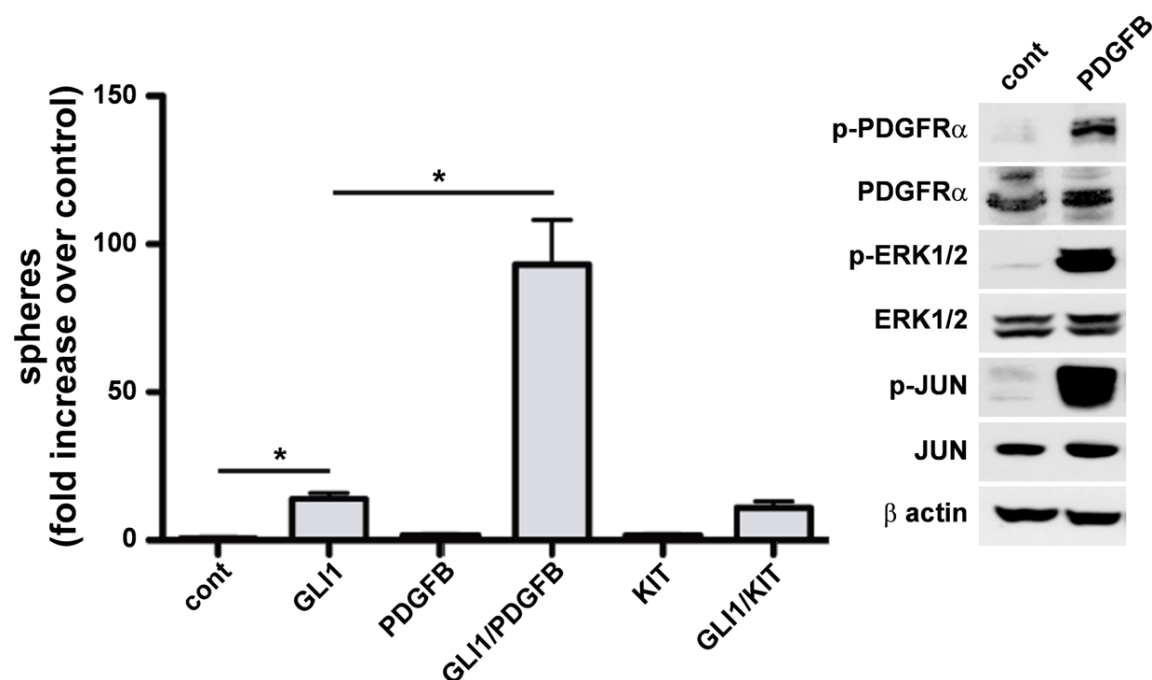


**Figure 23. HH signaling cooperates with PDGFRA signaling in cellular transformation.** (Left panel) Quantification of anchorage-independent clonogenic growth of human non-tumorigenic GLI1-HaCaT keratinocytes after activation of either HH signaling (by Dox treatment; see text GLI1)) or KIT signaling (overexpression of the constitutively active Kit D816V mutant; KIT) or stimulation of PDGFR signaling by PDGFB. Either signal alone has little or no activity towards cellular transformation, whereas GLI1 in combination with PDGFB treatment (GLI1/PDGFB), but not in combination with KIT activation (GLI1/KIT), leads to formation of clonogenic colonies (spheres) in 3D cultures (asterisks indicate  $p < 0.03$  by unpaired t-test). (Right panel) Western Blot analysis of HaCaT cells after incubation with PDGFB using anti-Pdgfra and anti-p-Pdgfra (phosphorylated Pdgfra) as well as anti-Erk, anti-p-Erk(1/2) (phospho-Erk1/2), anti-Jun and anti-p-Jun (phosphorylated Jun) antibodies.

Next we tested whether the cooperative effect was also apparent in a xenograft assay. For this purpose GLI1-HaCaT cells were retrovirally transfected with PDGFRAH650Q (PDGFRA<sup>mut</sup>). The PDGFRAH650Q mutation results in phosphorylation and activation of PDGFRA, but shows only weak intrinsic transforming activity<sup>135</sup>. This characteristic ensured that the potential cooperative transforming activity was not overlooked, what might have happened when expressing a PDGFRA mutation with strong transforming activity. Therefore, this mutation was more suitable for studying potential cooperative transforming effects than PDGFRA mutations with strong transforming activity.

To see whether this *in vitro* transformation led to tumor growth *in vivo*, 1x10<sup>6</sup> GLI1-HaCaT cells transfected with PDGFRA<sup>mut</sup> were injected s.c into the hind flank of nude mice. As controls, GLI1-HaCaT cells or HaCaT cells transfected with PDGFRA<sup>mut</sup> transfection were also transplanted. To induce and maintain GLI1 expression in the xenografts, Dox (10 mg/ml) was added to the drinking water supplemented with 5% sucrose. The tumor growth was monitored for 24 days. The *in vivo* tumor growth analysis revealed that in comparison to growth induced by GLI1 and PDGFRA<sup>mut</sup>, the growth of GLI1-PDGFRA<sup>mut</sup> cells were strongly enhanced. These data show that PDGFRA signaling in cooperation with GLI1 strongly increased growth of GLI1-HaCaT transfected with PDGFRA<sup>mut</sup>. Altogether, these data point to the possibility that PDGFRA signaling can cooperate with HH/GLI in oncogenic transformation.



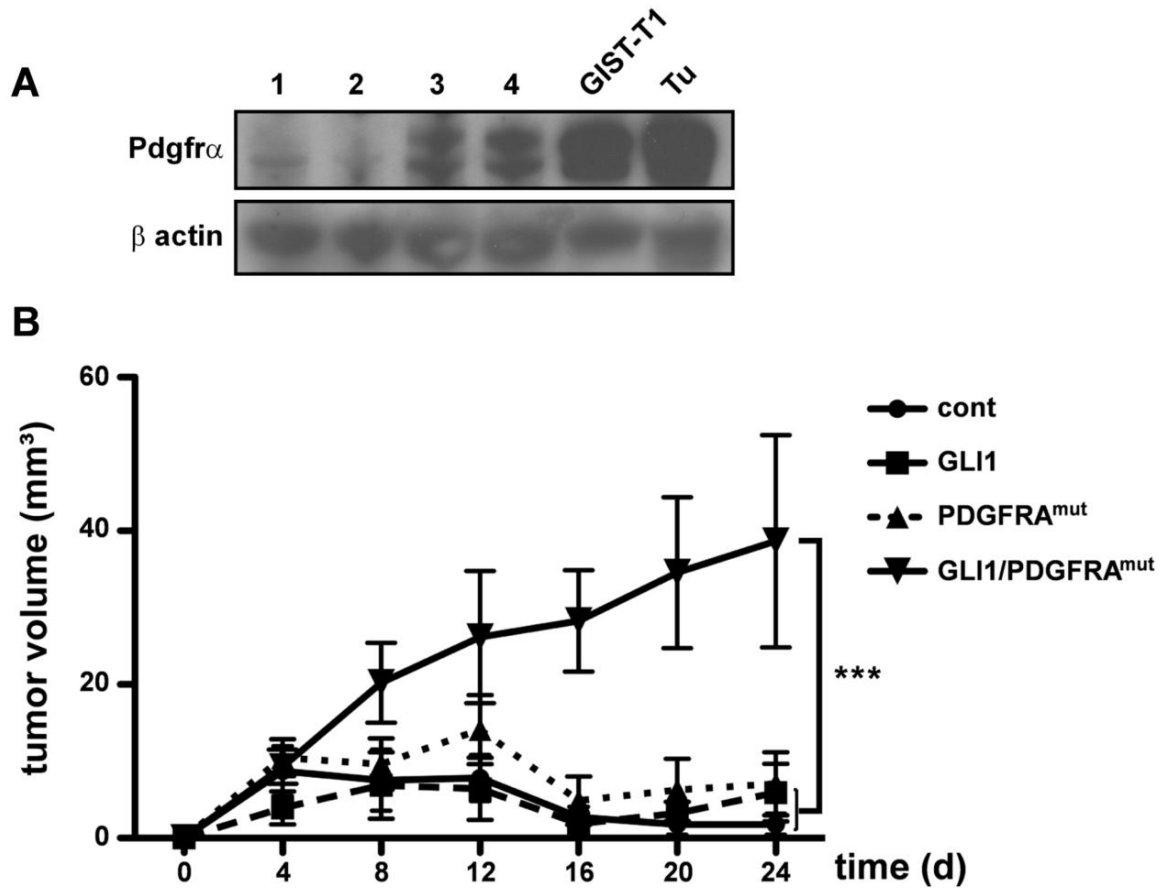


**Figure 24. HH signaling cooperates with PDGFRA signaling in cellular transformation *in vivo*.** (A) Westernblot analysis of PDGFRA expression in GLI1-HaCaT keratinocytes expressing *GLI1* under the control of a Dox-inducible promotor. Retrovirally-expressed PDGFRAH650Q (PDGFRA<sup>mut</sup>) results in overexpression of PDGFRA. Lane 1: control-transduced GLI1-HaCaT; Lane 2: control-transduced GLI1-HaCaT + Dox; Lane 3: PDGFRA<sup>mut</sup>-transduced GLI1-HaCaT; Lane 4: PDGFRA<sup>mut</sup>-transduced GLI1-HaCaT + Dox. The cell line GIST-T1 and GIST-like tumor (Tu) were used as control samples. (B) In vivo tumor growth analysis of Dox inducible GLI1-HaCaT cells transduced with constitutively active PDGFRA (PDGFRA<sup>mut</sup>) or empty vector control (n=6 for each setting). Cont: tumor growth in control mice injected with control-transduced inducible GLI1-HaCaT cells without Dox treatment (i.e. no GLI1 expression), GLI1: tumor growth of inducible and control-transduced GLI1-HaCaT cells in mice treated with Dox. PDGFRA<sup>mut</sup>: tumor growth of PDGFRA<sup>mut</sup>-transduced inducible GLI1-HaCaT without Dox treatment (i.e. PDGFRA<sup>mut</sup> only). GLI1/PDGFRA<sup>mut</sup>: tumor growth of PDGFRA<sup>mut</sup>-transduced inducible GLI1-HaCaT in Dox treated mice (\*\*\*P<0.001 by Dunnett's multiple comparison test).

## 5.6 Functional analysis of immune cells of *Ptch*<sup>flox/flox</sup>*LysMcre*<sup>+/-</sup> mice

Another line of investigation dealt with the functional analysis of *Ptch*-deficient cells of the innate immune system. Although the blood analysis shown in section 5.1 did not reveal any differences in the counts and morphology of white blood cells in *Ptch*<sup>flox/flox</sup>*LysMcre*<sup>+/-</sup> mice,

it was possible that the function of LysM-expressing cells ( i.e. of granulocytes, macrophages and DC) may have been compromised by the *Ptch* mutation in *Ptch<sup>flox/flox</sup>LysMcre<sup>+/-</sup>* mice.

In immune cells, Hh components are expressed in B and T cells as well as in myeloid cells. It is now established that Hh signaling plays an important role in the differentiation and proliferation of early thymocyte progenitors, and also in modulating T cell receptor signaling during repertoire selection, with implications for positive selection for CD4 versus CD8 lineage commitment, and clonal deletion of autoreactive cells (reviewed in<sup>136</sup>). Recent data showed that Hh signaling is dispensable for B cell development but that the Hh pathway within stromal cells promotes B lymphopoiesis in a non-cell-autonomous fashion<sup>137</sup> (see also introduction). However, very little is known about the role of Hh signaling in myeloid cells and almost no data are available about its role in innate immunity.

To this end, I have explored the response of BMDM isolated from *Ptch<sup>flox/flox</sup>LysMcre<sup>+/-</sup>* and *Ptch<sup>flox/flox</sup>* control mice to TLR activation. Activation of TLR not only leads to the induction of inflammatory responses but also to the development of antigen-specific adaptive immunity. The TLR-induced inflammatory response is dependent on a common signaling pathway that is mediated by the adaptor molecule MyD88<sup>138, 139</sup>.

In order to mimic TLR-induced inflammatory responses in *Ptch*-deficient BMDM, I used bacterial lipopolysaccharide (LPS) and Pam<sub>3</sub>CSK<sub>4</sub> (BLP). LPS is an essential component of the surface of gram-negative bacteria that activates the TLR 4 receptors which is present on the surface of many myelomonocytic cells. In contrast BLP is a triacylated lipopeptide that elicits responses mediated by TLR 1/2.

In order to study the role of *Ptch*-deficient macrophages (and other myeloid cells) in tumor immune surveillance, tumors (other than GIST) were induced in *Ptch<sup>flox/flox</sup>LysMcre<sup>+/-</sup>* mice. First, I transplanted the syngeneic B16F10 melanoma cell line and ID8-LUC ovarian carcinoma cell line into *Ptch<sup>flox/flox</sup>LysMcre<sup>+/-</sup>* and control *Ptch<sup>flox/flox</sup>* mice and monitored the tumor growth. In the case of the ovarian carcinoma model, I analyzed the expression of the M2 macrophage markers *Arg1* and *Trem2* in the tumor environment and the splenic recruitment of macrophages and granulocytes. Secondly, I chemically induced skin tumors using the two-step chemical carcinogenesis (DMBA/TPA) method and analyzed tumor growth and proliferation of the treated skin as well as the recruitment of macrophages and T cells to the tumor microenvironment.

It should be emphasized that the presented results, especially those of the *in vitro* experiments, are only preliminary. The respective experiments have to be repeated in the future.

### 5.6.1 Analysis of *Ptch*-deficient BMDM

In order to get some insight into the function of *Ptch*-deficient macrophages, BMDM from *Ptch*<sup>flx/flx</sup>*LysMcre*<sup>+/-</sup> and *Ptch*<sup>flx/flx</sup> control mice were isolated as described in section 4.11.1. To make sure that the BMDM from *Ptch*<sup>flx/flx</sup>*LysMcre*<sup>+/-</sup> were *Ptch*-deficient, recombination assay was performed. The results showed that almost 100% of BMDM were recombined at the floxed *Ptch* locus (Figure 25). However, the *Ptch* and *Gli1* expression in BMDM of *Ptch*<sup>flx/flx</sup>*LysMcre*<sup>+/-</sup> mice remained comparable to BMDM derived from *Ptch*<sup>flx/flx</sup> mice (Figure 26). This indicates that the *Ptch* mutation in BMDM apparently did not result in activation of Hh-signaling.

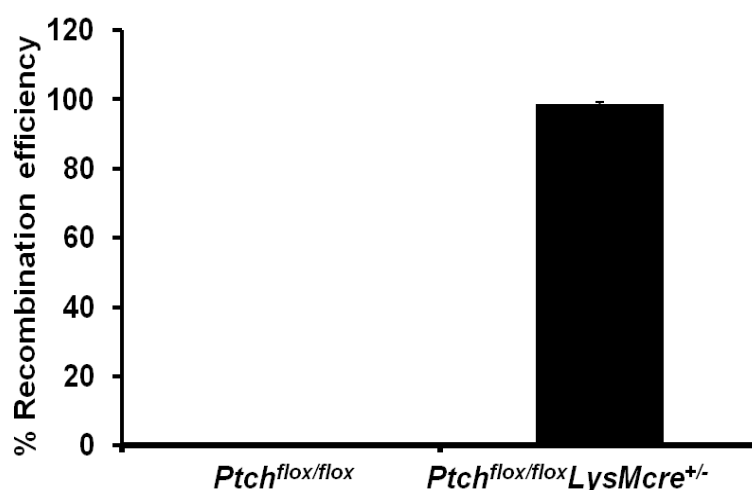


**Figure 25. Effective recombination of the floxed *Ptch* locus in the BMDM of *Ptch*<sup>flx/flx</sup>*LysMcre*<sup>+/-</sup> mice.** Recombination efficiency was analyzed by qRT-PCR on the gDNA obtained from BMDM of *Ptch*<sup>flx/flx</sup> and *Ptch*<sup>flx/flx</sup>*LysMcre*<sup>+/-</sup> mice. The data show the mean values ( $\pm$  SEM) of 3 different animals.

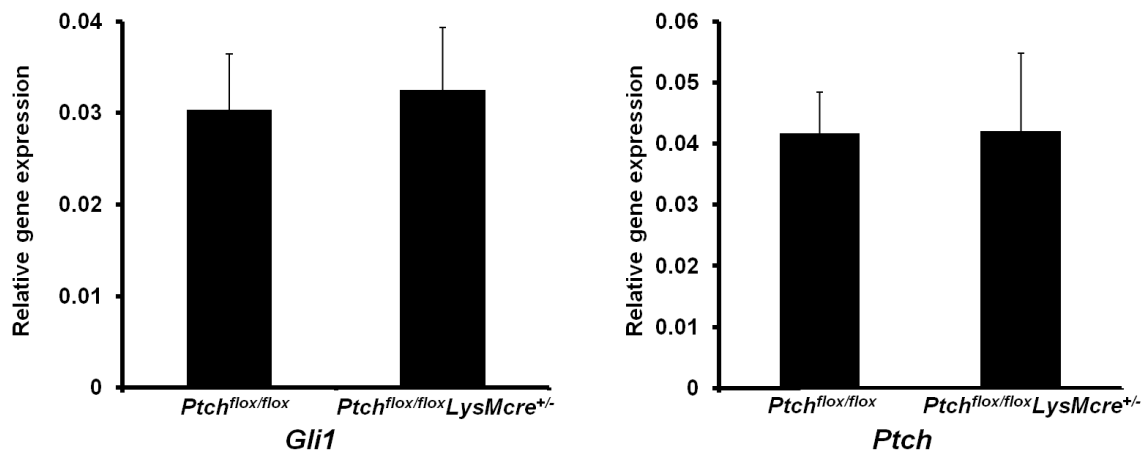


**Figure 26.** *Ptch* and *Gli1* expression in BMDM of *Ptch*<sup>flox/flox</sup>*LysMcre*<sup>+/-</sup> mice is not overexpressed. Quantitative PCR analyses showed no difference in the expression of *Gli1* (left panel) and *Ptch* (right panel) in BMDM isolated from *Ptch*<sup>flox/flox</sup> and *Ptch*<sup>flox/flox</sup>*LysMcre*<sup>+/-</sup> mice. The data show the mean values ( $\pm$  SEM).

After having shown that BMDM are indeed recombined at the *Ptch* locus, the cells were treated with 100 ng/ml LPS to see whether *Ptch* has a role in inflammatory response. First it was assessed whether the metabolic activity of BMDM was influenced by *Ptch*-deficiency after LPS stimulation. For this purpose, BMDM derived from *Ptch*<sup>flox/flox</sup>*LysMcre*<sup>+/-</sup> and *Ptch*<sup>flox/flox</sup> control mice were incubated with 100 ng/ml LPS for 24 h and subjected to a WST-1 assay. The reduction of WST-1 results in a colored formazan compound that can be measured via colorimetric measurement (at A<sub>450nm</sub>) and is a direct parameter of the cellular metabolic activity and viability. As shown in Figure 27, the *Ptch* mutation did not influence the basal metabolic activity when compared to wt cells. It also did not influence the viability of the BMDM after LPS stimulation.

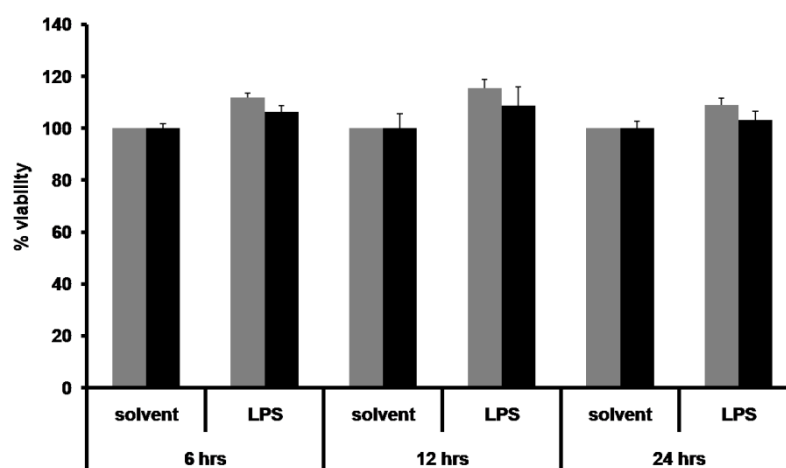


**Figure 27.** *Ptch* mutation does not have an effect on metabolic activity of BMDM. WST-1 assay of BMDM derived from *Ptch*<sup>flox/flox</sup>*LysMcre*<sup>+/-</sup> and *Ptch*<sup>flox/flox</sup> control mice with or without stimulation with LPS (100 ng/ml) at different time points (6, 12 and 24 h). WST-1 reagent was added 4 h before absorbance reading. Grey bars: *Ptch*<sup>flox/flox</sup>; black bars: *Ptch*<sup>flox/flox</sup>*LysMcre*<sup>+/-</sup>.

Next, the cytokine and chemokine release of BMDM from *Ptch*<sup>flx/flx</sup>*LysMcre*<sup>+/-</sup> and *Ptch*<sup>flx/flx</sup> control mice with or without LPS stimulation were quantified by ELISA. As shown in Figure 28, the cytokines IL-10 and IL-12p40 and chemokines KC (CXCL1), MCP-1 (CCL2) and MIP1-a (CCL3) as well as the pro-inflammatory cytokines RANTES (CCL5), tumor necrotic factor  $\alpha$  (TNF $\alpha$ ) and IL-6 were increased in the presence of LPS both in *Ptch*<sup>flx/flx</sup>*LysMcre*<sup>+/-</sup> and *Ptch*<sup>flx/flx</sup> mice. However, *Ptch* did not influence the release of the cytokines and chemokines because the values between *Ptch*-deficient and *Ptch*-wt BMDM were almost identical (Figure 28). These data clearly demonstrate that the *Ptch* mutation did not affect cytokine or chemokine release of LPS-stimulated macrophages at any of the time points examined.

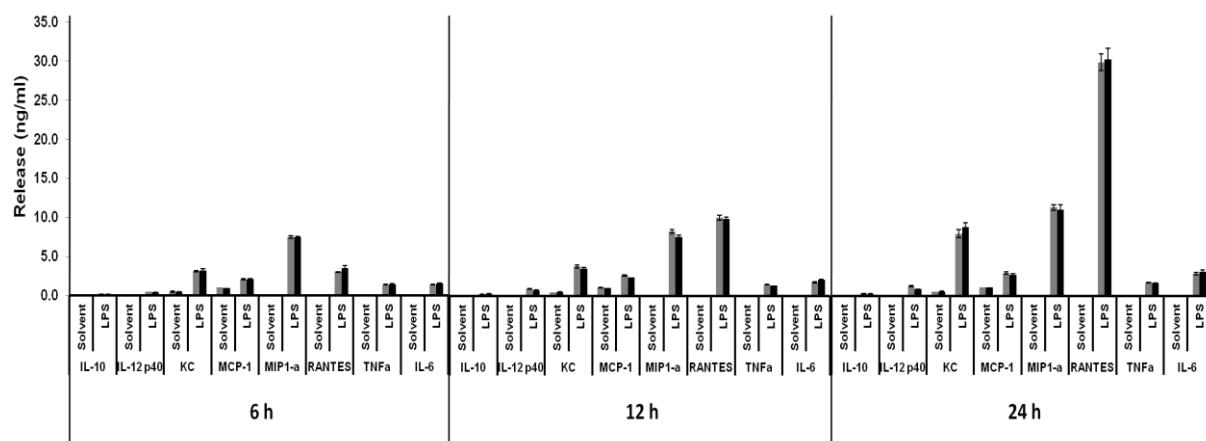


**Figure 28. *Ptch*-deficiency does not influence cytokine release of BMDM.** BMDM were treated with 100 ng LPS/ml or solvent. Supernatants were collected after 6, 12 and 24 h of incubation. The concentrations of cytokines were determined by ELISA. The data are expressed as mean  $\pm$  SEM. Grey bars: *Ptch*<sup>flx/flx</sup>; black bars of *Ptch*<sup>flx/flx</sup>*LysMcre*<sup>+/-</sup>.

To check whether the dose of LPS may have an effect on the BMDM's cytokine release, the pro-inflammatory cytokines RANTES, TNF $\alpha$  and IL-6 as well as IL12p40 were examined. ELISA showed that 1 to 100 ng/ml of LPS stimulated the release of all cytokines. There was no strong dose-dependency of the release of the cytokines at any time point examined. Again, there was no significant difference between *Ptch*-deficient and *Ptch*-wt BMDM (Figure 29).

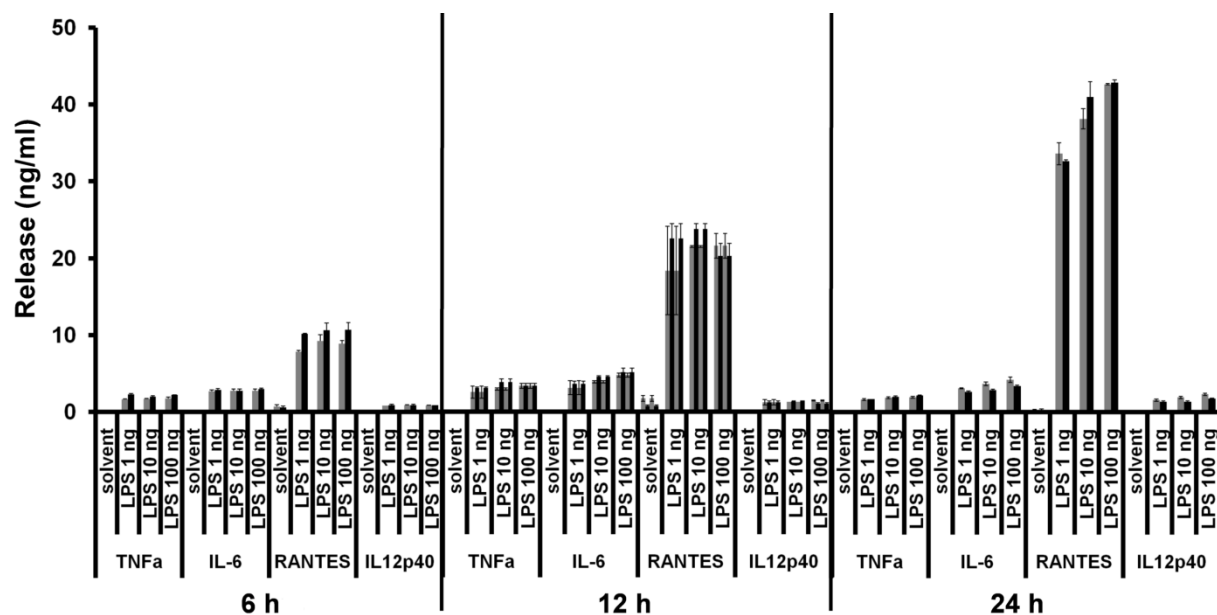


**Figure 29. *Ptch* does not influence the dose-dependent response of BMDM after LPS stimulation.** Quantification of the cytokine release after stimulation with different doses of LPS (1, 10 and 100 ng/ml) was done by ELISA. The supernatants were collected at different time points (6, 12 and 24 h after stimulation). The data are expressed as mean  $\pm$  SEM. Grey bars: *Ptch*<sup>flox/flox</sup>; black bars of *Ptch*<sup>flox/flox</sup> *LysMcre*<sup>+/-</sup>.

In a parallel approach, the mRNA expression levels of the cytokines *TNFα*, *IL-6* and *RANTES* were investigated in BMDM after stimulation with LPS. These cytokines were chosen since these are the most common read-outs for a pro-inflammatory response. As shown in Figure 30, stimulation with LPS resulted in increased levels of *TNFα*, *IL-6* and *RANTES*. The effects of LPS were strongest on *RANTES* transcription and weakest on *IL-6* transcription. In addition, the data indicate that the factors are regulated in a dose-dependent manner. However, no significant differences between *Ptch*-deficient and control BMDM were observed. These data correlated with the ELISA data, showing that *Ptch*-deficiency also did not influence cytokine protein release.

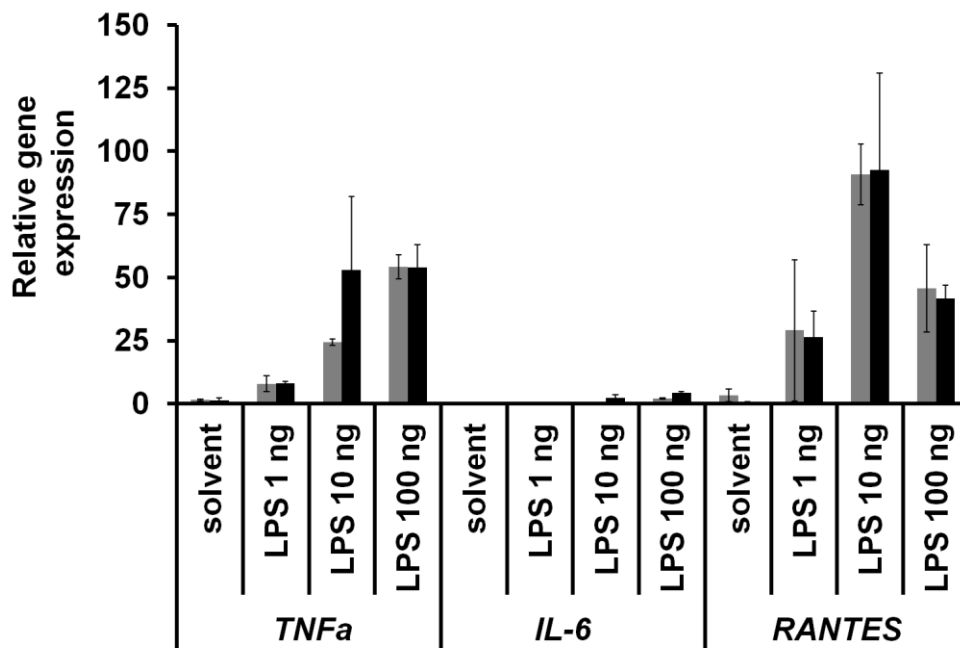


**Figure 30. *Ptch*-deficiency does not affect *TNFα*, *IL-6* and *RANTES* mRNA expression in BMDM.** Quantitative PCR analyses showed no difference in the expression of *TNFα*, *IL-6* and *RANTES* in macrophages isolated from *Ptch*<sup>fllox/fllox</sup> and *Ptch*<sup>fllox/fllox</sup>*LysMcre*<sup>+/-</sup> mice 12 h after LPS stimulation (100 ng/ml). Grey bars: *Ptch*<sup>fllox/fllox</sup>; black bars of *Ptch*<sup>fllox/fllox</sup>*LysMcre*<sup>+/-</sup>.

Taken together, these data suggest that *Ptch*-deficiency does not influence cytokine production in BMDM, even not after stimulation with LPS.

Next, *Ptch*-deficient and control BMDM were treated with BLP. In contrast to LPS, BLP is a TLR1/2 agonist and possibly exerts its inflammatory activity by additional activation of TNF-dependent macrophage-specific mechanism as shown in inflammatory disease models<sup>141</sup>. Interestingly, the stimulation of the BMDM for 24 h with 100 ng/ml BLP resulted in a significant 2-fold ( $P=0.13$ ) upregulation of *IL-6* mRNA expression levels in the *Ptch* mutant BMDM when compared to the wt control. The expression levels of the two other cytokines *RANTES* and *TNFα* remained comparable between the two genotypes (Figure 31). However, these data is based on single experiment and need to be verified in additional experiments.

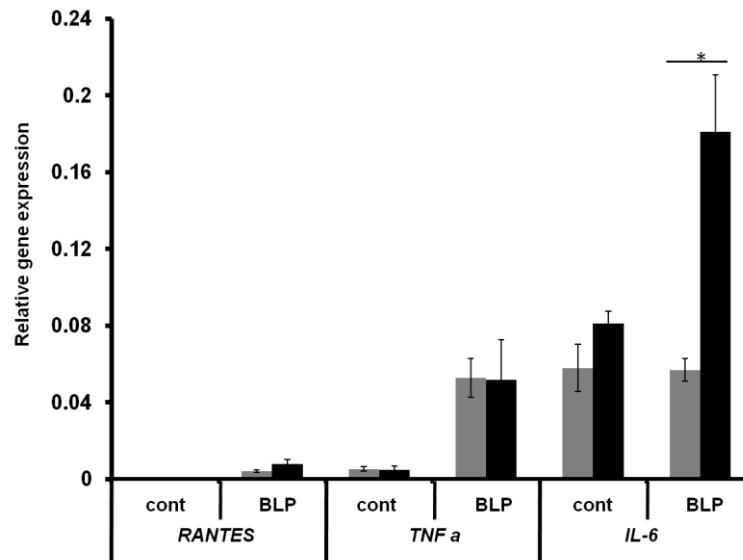


**Figure 31. *Ptch*-deficiency increases the *IL-6* expression of macrophages after BLP treatment.** Quantitative PCR analyses in BMDM isolated from *Ptch<sup>flox/flox</sup>* and *Ptch<sup>flox/flox</sup>LysMcre<sup>+/-</sup>* mice showed no difference in the expression of *RANTES* and *TNFα* after a 12 h stimulation with 100 ng/ml BLP. However, the BLP treatment resulted in an increased expression of *IL-6* in BMDM isolated from *Ptch<sup>flox/flox</sup>LysMcre<sup>+/-</sup>* mice. Grey bars: *Ptch<sup>flox/flox</sup>*; black bars: *Ptch<sup>flox/flox</sup>LysMcre<sup>+/-</sup>*.

Finally, the BrdU-incorporation rate of *Ptch*-deficient and wt BMDM was analysed both with and without stimulation with either LPS or BLP. In a first experiment, cells were stimulated with the TRL agonists for 48 or 72 hours. The rationale for this relatively long incubation time is the fact that macrophages are relatively slow-proliferating cells compared to most other cells. The basal BrdU-incorporation rate (without the LPS or BLP stimulus) did not differ between BMDM derived from *Ptch<sup>flox/flox</sup>LysMcre<sup>+/-</sup>* and *Ptch<sup>flox/flox</sup>* control mice cultured for 48 h and 72 h (Figure 32;  $P=0.61$  and  $P=0.098$  for 48 h and 72 h, respectively). However, the stimulation with both LPS and BLP for 72 h revealed a striking difference between the genotypes: Although after that time, both *Ptch* mutant and *Ptch* control BMDM showed a significant decrease in growth, the decrease was significantly more pronounced in BMDM derived from *Ptch<sup>flox/flox</sup>* mice (Figure 33,  $P=0.04$ ). This significant effect was already seen after 48 h in the BLP treated group (Figure 34,  $P=0.003$ ). Unfortunately, thus far I have not analysed apoptosis or metabolic activity of BMDM after treatment with BLP or LPS for 48 h or 72 h. Therefore it is hard to tell whether the above-mentioned differences in BrdU-incorporation indeed mirror a different proliferative capacity of *Ptch*-deficient BMDM or rather a resistance to toxic or pro-apoptotic effects of BLP/LPS.



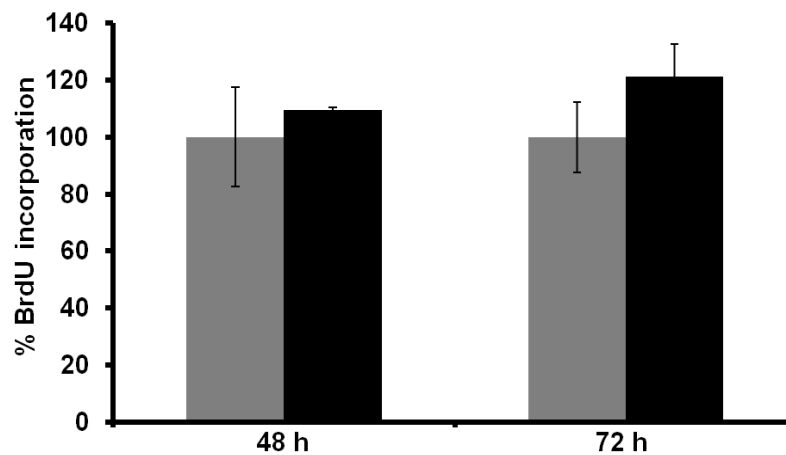


**Figure 32. *Ptch*-deficiency has no effect on the BrdU-incorporation rate of macrophages.** BMDM derived from *Ptch<sup>flox/flox</sup> LysMcre<sup>+/-</sup>* and *Ptch<sup>flox/flox</sup>* mice were cultured for 48 h or 72 h. 20 h before the end of the experiment, BrdU was added to the cells. BrdU incorporation was measured using a luminometer. BrdU-incorporation rate of BMDM isolated from *Ptch<sup>flox/flox</sup>* mice was set to 100%. Assay was done in triplicates and is presented as mean values  $\pm$  SEM.  $P=0.61$  and  $P=0.098$  for 48 and 72 h, respectively.

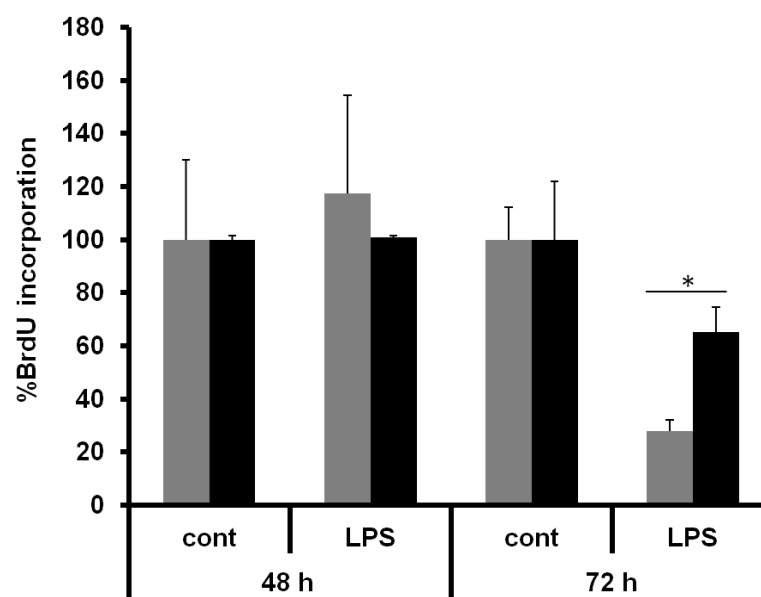


**Figure 33. *Ptch*-deficiency modulates the BrdU-incorporation rate of LPS-stimulated macrophages.** BMDM derived from *Ptch<sup>flox/flox</sup>* (grey bars) and *Ptch<sup>flox/flox</sup> LysMcre<sup>+/-</sup>* (black bars) mice were treated with 100 ng/ml LPS for 48 or 72 h as indicated. 20 h before the end of treatment, BrdU was added to the cells. BrdU-incorporation was measured using a luminometer. BrdU-incorporation rate of untreated cells was set to 100%. Assay was done in triplicates and presented as mean values  $\pm$  SEM. \*:  $P=0.04$ .

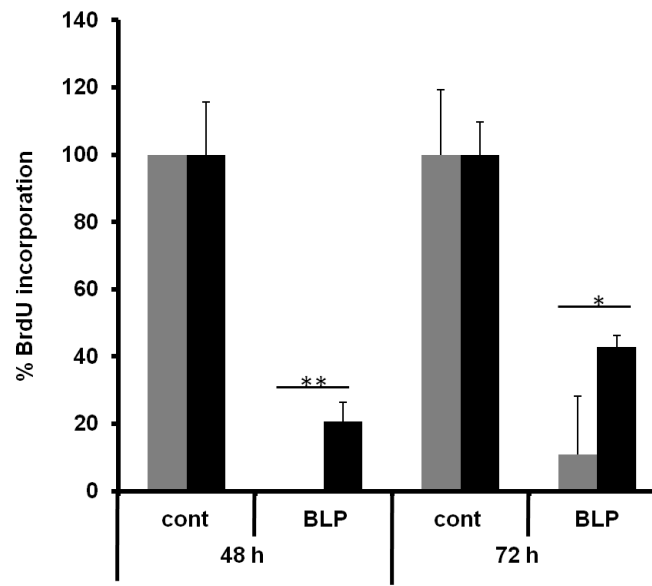


**Figure 34. *Ptch*-deficiency modulates the BrdU-incorporation rate of BLP-stimulated macrophages.** BMDM derived from *Ptch*<sup>flox/flox</sup> (grey bars) and *Ptch*<sup>flox/flox</sup>*LysMcre*<sup>+/-</sup> (black bars) mice were treated with 100 ng/ml BLP for 48 or 72 h. 20 h before the end of treatment, BrdU was added to the cells. BrdU incorporation was measured using a luminometer. BrdU-incorporation rate of untreated cells was set to 100%. Assay was done in triplicates and presented as mean values  $\pm$  SEM. \*\*:P=0.003; \*: P=0.012.

### 5.6.2 Effects of *Ptch*-deficient LysM<sup>+</sup> cells on tumor surveillance

As already explained in the introduction section, macrophages, granulocytes and DC (i.e. the main cell lineages in the mouse that express LysM) play an important role in tumor surveillance. In order to assess the role of *Ptch* in these cells during tumor growth, *Ptch*<sup>flox/flox</sup>*LysMcre*<sup>+/-</sup> and control *Ptch*<sup>flox/flox</sup> mice were transplanted s.c. with the syngeneic melanoma cell line B16F10. After transplantation, tumor growth was measured every day using a caliper. Tumor volume was calculated using the formula  $L \times W^2 \times 0.4$ . When the tumor volume of the animals reached  $\geq 2\text{cm}^3$  the animals were sacrificed due to the general condition of the mice because of the heavy tumor burden. As seen in Figure 35, all animals included in the study developed melanoma and the tumor growth rate was not influenced by the *Ptch* status in LysM-expressing cells (Figure 35; P=0.56 by Log Rank test).

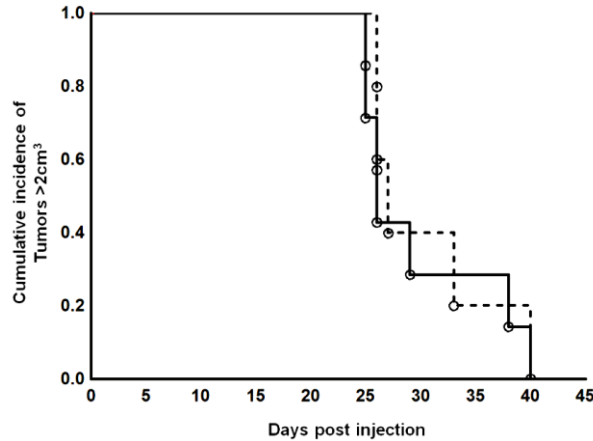


**Figure 35. *Ptch*-deficiency in  $LysM^{+}$  cells does not influence the growth of B16F10.** Animals were injected s.c. with  $10^4$  B16F10 melanoma cells. Kaplan-Meier curve shows the cumulative incidence of tumors larger  $\geq 2\text{cm}^3$ . Tumor growth was monitored every day using a caliper and the tumor area was calculated as explained in the text. The animals were euthanized when tumors reached  $\geq 2\text{cm}^3$ . Solid line:  $Ptch^{flox/flox} LysMcre^{+/-}$  (n=7); Dashed line:  $Ptch^{flox/flox}$  (n=5).

In addition, B16F10 melanoma cells were injected i.v. into  $Ptch^{flox/flox}$  and  $Ptch^{flox/flox} LysMcre^{+/-}$  animals. According to the literature this should result in homing of the B16F10 cells to the lung, which is frequently referred to “metastasis”<sup>142</sup>. Twenty days after transplantation of the cells, the lungs of the mice were subjected to autopsy and tumor nodules were counted. The results show that  $Ptch^{flox/flox} LysMcre^{+/-}$  animals have more tumor nodules in the lungs ( $5.0 \pm 8$  nodules/lung) when compared to  $Ptch^{flox/flox}$  control animals ( $2.5 \pm 2$  metastasis nodules/lung). However, these differences were not significant (Figure 36,  $P=0.45$  by t-test). Together, these data suggest that *Ptch*-deficiency in  $LysM^{+}$  cells does affect neither local nor metastatic B16F10 melanoma growth.

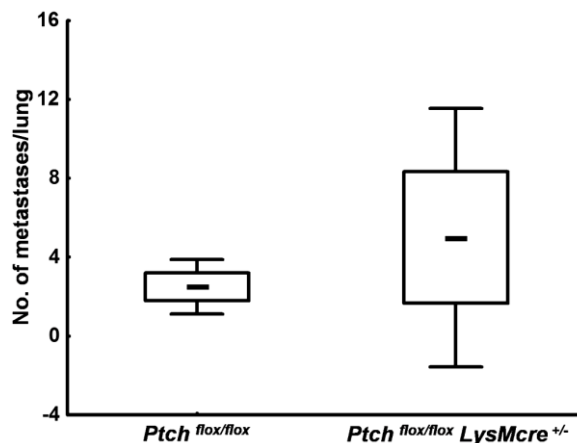


**Figure 36. *Ptch*-deficiency in  $LysM^{+}$  cells does not influence the homing of B16F10 cells to the lung.**  $Ptch^{flox/flox}$  (n=8) and  $Ptch^{flox/flox} LysMcre^{+/-}$  (n=7) mice were injected i.v. with  $1 \times 10^5$  B16F10 cells. Twenty days post-injection, animals were sacrificed and lungs were analyzed for tumor numbers. Box plots show mean values  $\pm$  SE.

### 5.6.2.1 Growth of syngeneic ID8-LUC ovarian carcinoma cells in *Ptch*<sup>flox/flox</sup>*LysMcre*<sup>+/-</sup> and control *Ptch*<sup>flox/flox</sup> mice

Since there was a tendency of *Ptch*<sup>flox/flox</sup>*LysMcre*<sup>+/-</sup> mice to have a higher tumor load in the lungs after transplantation of B16F10 cells, we also transplanted ID8-LUC cells. The ID8 cell line is an ovarian carcinoma cell line derived from C67Bl/6 mice and is rather slow-growing. Due to the slow-growing nature of this tumor cell line, we hoped to not overlook small differences in tumor growth, which might have occurred during the studies using the fast-growing tumor cell line B16F10.

ID8-LUC cells were injected i.p. into the peritoneal cavity and the growth was visualized using a CCD camera after injection of D-Luciferin substrate. The relative luminescence values are proportional to the ovarian carcinoma growth in the mice. According to our collaboration partner Thorsten Hagemann, the injection of  $1 \times 10^7$  ID8-LUC cells should result in detectable tumors starting by week 4 after transplantation. Indeed, 4 weeks after transplantation the relative luminescence intensity increased steadily, which indicated growth of the tumors (Figure 37). A comparison between ovarian carcinoma growth in *Ptch*<sup>flox/flox</sup> and *Ptch*<sup>flox/flox</sup>*LysMcre*<sup>+/-</sup> mice showed no significant difference between the two genotypes (Figure 37 and Figure 38). As demonstrated in Figure 37, the tumor growth seemed to cease in *Ptch*<sup>flox/flox</sup> mice at week 7 after transplantation. Unfortunately, all mice were killed at week 8 after transplantation and thus, it remains open whether the stagnation of tumor growth in the wt animals was reached. However, since all data available so far described progressive disease after implantation of ID8-LUC cells in wt mice<sup>143</sup>, the latter assumption is rather unlikely.

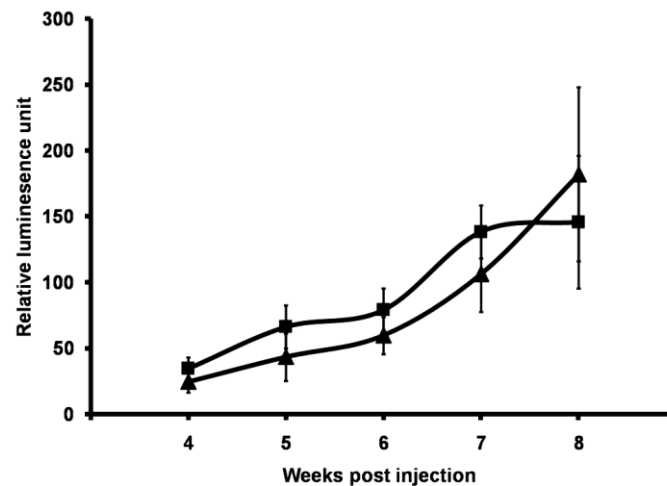


**Figure 37.** Growth of ID8-LUC cells in  $Ptch^{flox/flox}$  and  $Ptch^{flox/flox}LysMcre^{+/-}$  mice. ID8-LUC cells were transplanted into the peritoneal cavity of  $Ptch^{flox/flox}$  (■) and  $Ptch^{flox/flox}LysMcre^{+/-}$  (▲) mice and the tumor growth was monitored using a CCD camera and quantification of luminescence. Data shown are the average luminescence units  $\pm$  SEM.

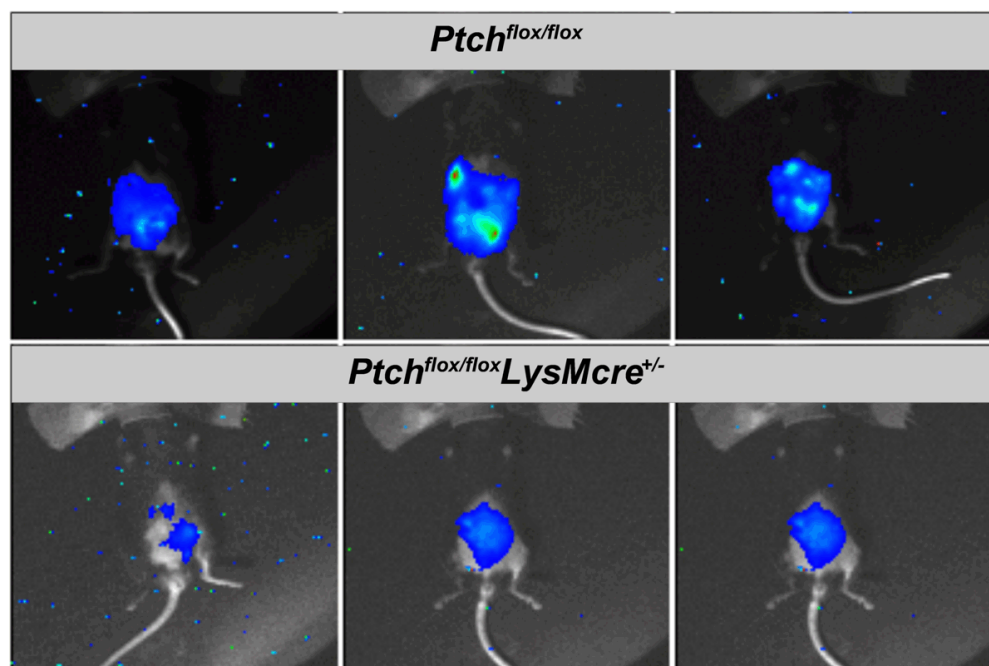


**Figure 38.** Representative bioluminescence images of mice 7 weeks after injection with ID8-LUC cells. Images were taken 5 min after D-Luciferin administration. Luminescence was normalized to a background image of the mice taken before the injection of D-Luciferin. Shown are representative pictures of pseudo colored overlay images of the bioluminescence signal intensity superimposed on mice.

As already stated in the Materials and Methods section (see 4.13.9), transplantation of ID8-LUC cells leads to the development of an ascites approximately 13 to 16 weeks after the transplantation of the cells. Indeed, the ID8-LUC transplanted  $Ptch^{flox/flox}$  and  $Ptch^{flox/flox}LysMcre^{+/-}$  animals developed ascites between 14 to 16 weeks. The cells within the

ascitic fluid in the ID8-transplantation model frequently serve as a source for the analysis of the “tumor microenvironment”<sup>144</sup>. In order to analyze the composition of the “tumor microenvironment” of ID8-LUC cells, the ascitic fluid of transplanted animals was subjected to flow cytometric and expression analyses. Unfortunately, flow cytometry for the analysis of the cellular composition of the ascites was not successful, since there were too many erythrocytes present in the ascites despite Ficoll gradient separation and/or addition of erythrocyte lysis buffer to the samples. Nevertheless, cells from the ascites were subjected to gene expression analysis to see whether *Ptch* influences the expression of M2 macrophage-specific genes. Analysis of *Arg1* and *Trem2* in the ascites of *Ptch*<sup>flx/flx</sup> and *Ptch*<sup>flx/flx</sup>*LysMcre*<sup>+/-</sup> animals showed that *Ptch*-deficiency does not influence on the expression of these two genes (Figure 39) in the tumor microenvironment of ovarian carcinoma.

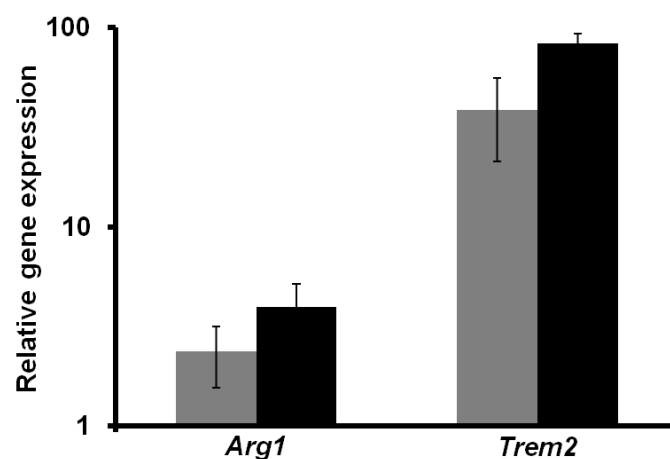


**Figure 39. *Ptch*-deficiency in LysM<sup>+</sup> cells does not influence the expression of alternative macrophage markers in the tumor microenvironment of ovarian carcinoma.** Quantitative PCR analysis of *Arg1* and *Trem2* in cells derived from the ascites of *Ptch*<sup>flx/flx</sup>*LysMcre*<sup>+/-</sup> and *Ptch*<sup>flx/flx</sup> mice. Shown are mean ± SEM. Grey bars: *Ptch*<sup>flx/flx</sup>; black bars *Ptch*<sup>flx/flx</sup>*LysMcre*<sup>+/-</sup>.

To this end, flow cytometric analysis of the spleen during ascites formation was carried out. The splenic granulocytes (Gr-1<sup>+</sup> cells) and macrophages (CD11b<sup>+</sup> cells) have been investigated. In addition, the cells were stained for F4/80 and IL-4Rα<sup>+</sup> because CD11b<sup>+</sup> Gr-1<sup>+</sup> IL-4Rα<sup>+</sup> F4/80<sup>-</sup> cells represent myeloid-derived suppressor cells (MSDC)<sup>145</sup>.

A previous report showed that MDSC derive from the ascites and the spleen in mice lymphoma tumor model had similar morphology and phenotype<sup>146</sup>. Moreover, the spleen acts as a reservoir of granulocytes, tumor-associated macrophages and MDSC during tumor progression<sup>147</sup>. Therefore, the number of cells in the spleen thought to reflect the number of

granulocytes, tumor-associated macrophages and MDSC in the tumor- microenvironment. The analysis revealed that *Ptch* has no impact on the numbers of splenic MDSC (Figure 40) or granulocytes and macrophages (Figure 41). These data suggest that *Ptch* does not influence tumor growth by modulation of these cell populations.

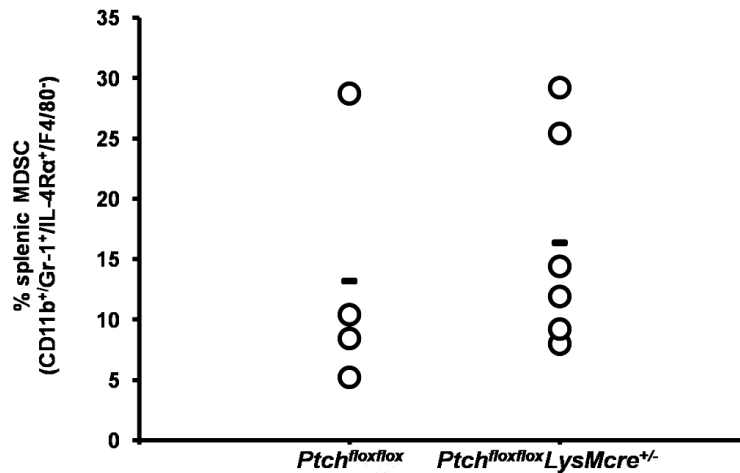


**Figure 40. *Ptch* in *LysM*<sup>+</sup> cells does not affect the number of MDSC in the spleen.** Flow cytometry analysis of splenic CD11b<sup>+</sup> Gr-1<sup>+</sup> IL-4Rα<sup>+</sup> F4/80<sup>-</sup> myeloid derived suppressor cells did not reveal a difference between ID8-LUC transplanted *Ptch*<sup>flox/flox</sup> and *Ptch*<sup>flox/flox</sup>*LysMcre*<sup>+/-</sup> mice.

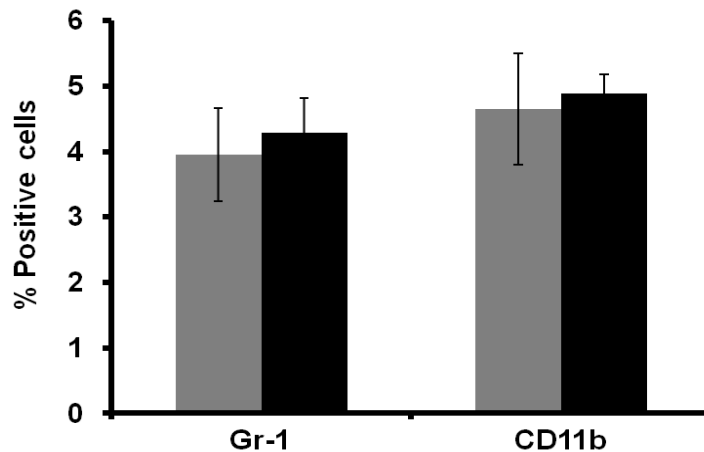


**Figure 41. *Ptch* mutation does not influence the number of granulocytes and macrophages in the spleen.** Flow cytometry analysis of splenic Gr-1<sup>+</sup> granulocytes and CD11b<sup>+</sup> macrophages did not reveal a difference between ID8-LUC transplanted *Ptch*<sup>flox/flox</sup> and *Ptch*<sup>flox/flox</sup>*LysMcre*<sup>+/-</sup> mice. Grey bars: *Ptch*<sup>flox/flox</sup>; black bars *Ptch*<sup>flox/flox</sup>*LysMcre*<sup>+/-</sup>.

Taken together, these data show that the *Ptch*-deficiency in *Ptch*<sup>flox/flox</sup>*LysMcre*<sup>+/-</sup> mice does neither influence the expression of *Arg1* and *Trem2* in the tumor microenvironment of ovarian carcinoma nor the splenic granulocytes (Gr-1<sup>+</sup>), macrophages (CD11b<sup>+</sup>) or MDSC numbers during ascites formation.

### 5.6.2.2 Growth of chemically induced tumors in *Ptch*<sup>flox/flox</sup>*LysMcre*<sup>+/-</sup> and control *Ptch*<sup>flox/flox</sup> mice

The two-step chemical tumorigenesis model using DMBA/TPA has been widely applied to study initiation, promotion and progression (malignant conversion) of mouse skin tumors<sup>148</sup>. Initiation of the skin tumors is accomplished with one single dose of DMBA. Continuous TPA treatment twice per week further results in tumor promotion and finally resulting in the development of papilloma, SSC and melanoma-like nevi in mice.

This protocol was applied to induce skin tumors in *Ptch*<sup>flox/flox</sup> and *Ptch*<sup>flox/flox</sup>*LysMcre*<sup>+/-</sup> animals. Development of papillomas was closely monitored twice per week and only papillomas larger than 1 mm diameter were counted. As shown in Figure 42, both *Ptch*<sup>flox/flox</sup>*LysMcre*<sup>+/-</sup> and *Ptch*<sup>flox/flox</sup> control mice developed papillomas. The data represent the number of papilloma at the end of the study. Although the control *Ptch*<sup>flox/flox</sup> animals showed a relatively higher papilloma number ( $3.12 \pm 2.47$  papillomas/animal) in comparison to *Ptch*<sup>flox/flox</sup>*LysMcre*<sup>+/-</sup> mutant mice ( $2.38 \pm 0.96$  papillomas/animal) (Figure 42) the difference was not significant ( $P=0.34$ ). In addition, the time span until the appearance of the first papilloma was monitored. The first papillomas were noticed after  $13.8 \pm 5.5$  weeks in *Ptch*<sup>flox/flox</sup> mice, whereas the first papillomas were noticed after  $16.5 \pm 3.3$  weeks in *Ptch*<sup>flox/flox</sup>*LysMcre*<sup>+/-</sup> mice. However, this difference was also not significant between the two genotypes (Figure 42;  $P=0.27$ ).

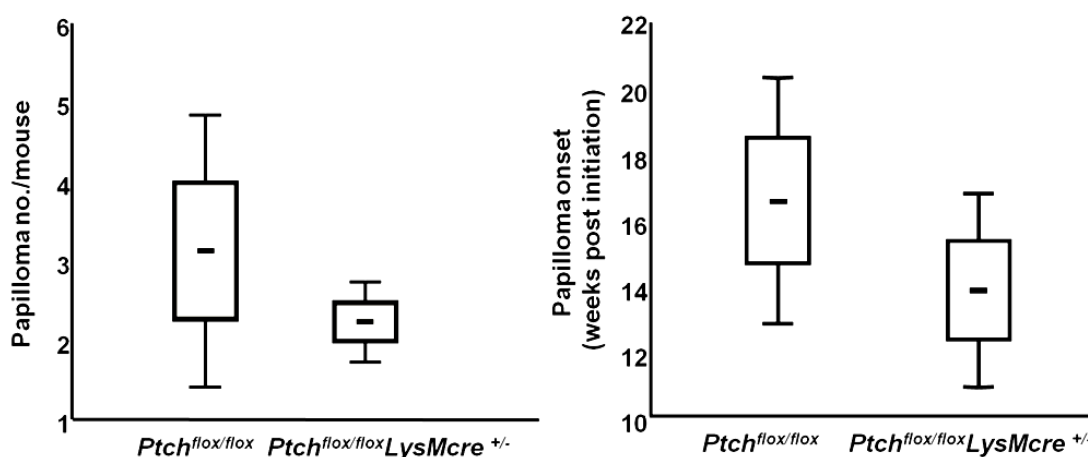


**Figure 42. Average papilloma numbers and onset of papilloma development of DMBA/TPA treated *Ptch*<sup>flox/flox</sup> and *Ptch*<sup>flox/flox</sup>*LysMcre*<sup>+/-</sup> mice.** Tumor initiation with DMBA and tumor promotion with TPA for 220 days resulted in papilloma in both *Ptch* mutant and control animals. Left panel shows the average number of visible papilloma (ca.  $\geq 1$  mm in diameter) that has developed per animal in the DMBA/TPA treated skin area at the end of the study. In the right panel the time at which the papillomas first became visible (ca.  $\geq 1$  mm in diameter) is plotted. Box plots show mean values  $\pm$  SE.



Although there was no difference in the papilloma number in both cohorts, the DMBA/TPA treatment has resulted in epidermal hyperplasia in *Ptch<sup>flx/flx</sup>LysMcre<sup>+/-</sup>* mice. Indeed, the epidermis of these mice was significantly thicker in comparison to the controls (Figure 43A;  $P=0.03$ ). The skin thickness of DMBA/TPA treated skin samples was analyzed as described in the Material and Methods section (4.12.8). Furthermore, IHC staining for the proliferation marker Ki-67 showed an increased proportion of proliferating cells in the treated *Ptch<sup>flx/flx</sup>LysMcre<sup>+/-</sup>* skin ( $27.01 \pm 2.38\%$  out of 1000 cells counted) compared to *Ptch<sup>flx/flx</sup>* skin ( $23.34 \pm 3.09\%$  out of 1000 cells counted). However, the difference in the percentage of Ki-67 positive cells did not reach statistical significance ( $P=0.21$ ; Figure 43B).

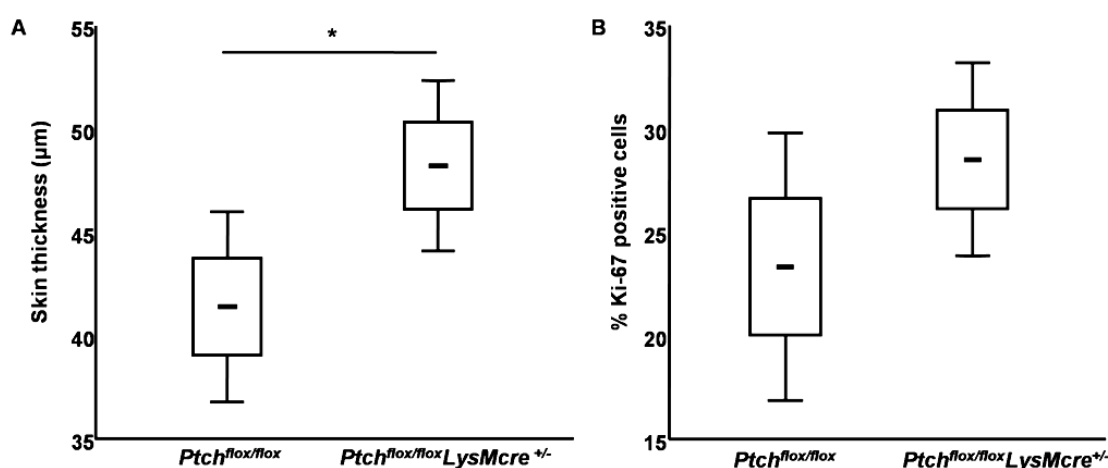


**Figure 43. Average thickness of the epidermis of DMBA/TPA treated *Ptch<sup>flx/flx</sup>* and *Ptch<sup>flx/flx</sup>LysMcre<sup>+/-</sup>* mice.** (A) Skin thickness of the animals after tumor initiation with DMBA and tumor promotion with TPA for 220 days. For each site of skin, the thickness of the epidermis (from the basal layer up to the stratum granulosum but excluding the stratum corneum) was measured using the Cell F program. (B) The figure shows the percentage of Ki-67<sup>+</sup> cells in the epidermal layer of DMBA/TPA treated skin ( $P=0.21$ ). For this purpose, Ki-67 positive cells were counted in at 1000 epidermal cells each from at least 8 animals. The positive cells are presented as the percentage of the total number of counted cells.

Since DMBA/TPA treatment can lead to development melanoma-like nevi, the number of the nevi in the skin of the treated animals was counted. The analysis revealed that the number of nevi between *Ptch<sup>flx/flx</sup>LysMcre<sup>+/-</sup>* ( $25 \pm 19$  nevi per animal) and *Ptch<sup>flx/flx</sup>* ( $16 \pm 9$  nevi per animal) mice was not different ( $P=0.234$ ). Then the nevi size in the skin of *Ptch<sup>flx/flx</sup>LysMcre<sup>+/-</sup>* and *Ptch<sup>flx/flx</sup>* mice was measured using Cell F software. The contour of the nevi in every image taken was traced using freehand tools. The actual nevi size was measured as described in 4.12.8 in the Material and Methods section. The nevi size was calculated by summing up the individual nevi area measured from each sample (3 skin

samples from each animal; at least 8 animals per group) and normalization to the total area of the analyzed skin samples. Most interestingly, the analysis revealed that the mean nevi size in *Ptch*<sup>flox/flox</sup>*LysMcre*<sup>+/-</sup> was significantly larger than that of *Ptch*<sup>flox/flox</sup> mice.

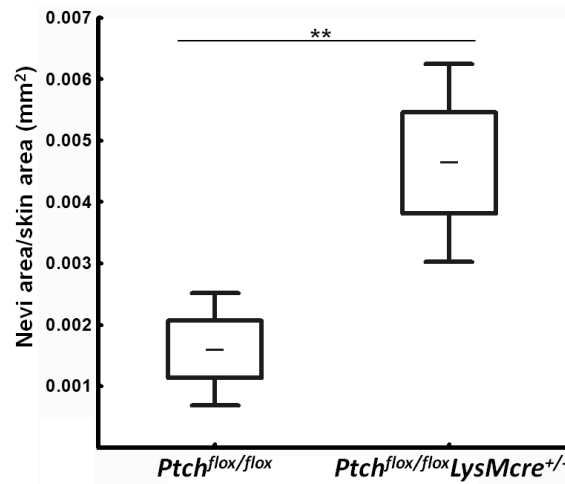


**Figure 44.** Average nevi size of DMBA/TPA treated *Ptch*<sup>flox/flox</sup> and *Ptch*<sup>flox/flox</sup>*LysMcre*<sup>+/-</sup> mice. Melanoma-like nevi size was calculated by tracing the contour of each nevus by freehand and measured using Cell F program. The nevi size was calculated by summing up the individual nevus area measured from each sample (3 skin samples from each animal; at least 8 animals per group) and normalizing it to the total area of the analyzed skin samples. The data shows boxplot and mean values  $\pm$  SE. of 6 sections derived from atleast 8 individual animals per group (P=0.007).

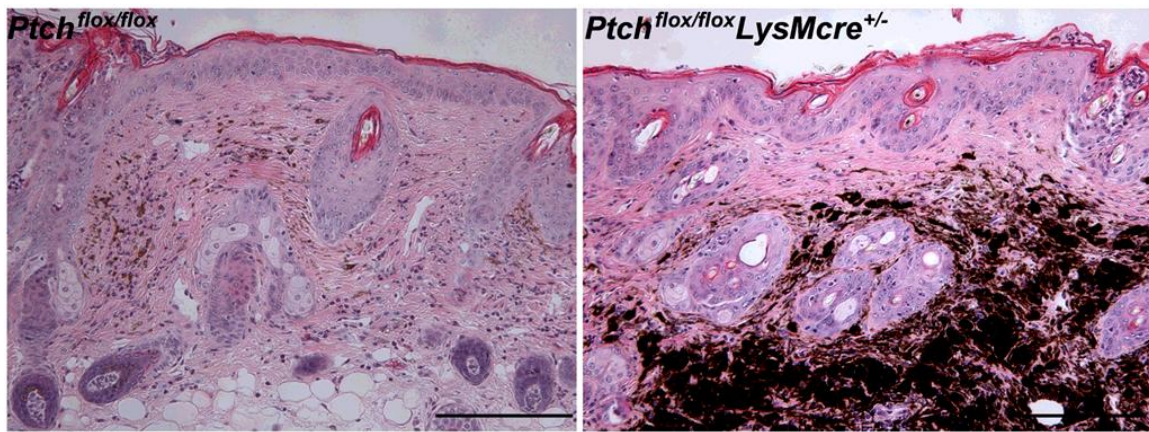


**Figure 45.** Representative HE staining of nevi in skin of DMBA/TPA treated *Ptch*<sup>flox/flox</sup> and *Ptch*<sup>flox/flox</sup>*LysMcre*<sup>+/-</sup> mice. Image shows HE stained mouse skin after tumor initiation with DMBA and tumor promotion with TPA for 220 days. Melanoma-like nevi cells appear as “black” cells due to high melanin content. Scale bar (µm): 200.

Finally, the nevi-bearing skin of *Ptch*<sup>flox/flox</sup> and *Ptch*<sup>flox/flox</sup>*LysMcre*<sup>+/-</sup> mice was stained with F4/80 and MHCII to visualize the numbers of tumor-associated macrophages and DC, respectively. After staining with the respective antibodies the sections were scored by two independent investigators. For the analysis the positive cells were counted in and around the

melanoma area. The scores were ranked between + (low), ++ (intermediate) and +++ (high), depending on the number of positive cells in and around the melanoma area. The + score indicates that there were <10% positive cells, the score ++ indicates that 10-20% of cells were positive, while the score +++ indicates that >20% cells were positive. The results are shown in Table 22 which gives the percentage of animals with particular scores. The results suggest that MHCII<sup>+</sup> and F4/80<sup>+</sup> cells were recruited to the nevi after DMBA/TPA treatment. Interesting, whereas none of the nevi in of *Ptch*<sup>flx/flx</sup> mice were strongly infiltrates with MHCII<sup>+</sup> cells, about 10% of the nevi of *Ptch*<sup>flx/flx</sup>*LysMcre*<sup>+/-</sup> mice showed a high infiltration with this cell population. Similarly, F4/80<sup>+</sup> macrophages were low in nevi-bearing skin of all *Ptch*<sup>flx/flx</sup> examined, whereas 38% of *Ptch*<sup>flx/flx</sup>*LysMcre*<sup>+/-</sup> mice showed an intermediate number of macrophages in and around the nevi. Finally, the sections were stained for CD3, which is a marker for T cells. As shown in Table 22, CD3<sup>+</sup> T cells recruitment to the nevi area was low in *Ptch*<sup>flx/flx</sup>*LysMcre*<sup>+/-</sup> mice (83%) when compared to *Ptch*<sup>flx/flx</sup> mice (50%). Moreover, 17% of *Ptch*<sup>flx/flx</sup>*LysMcre*<sup>+/-</sup> mice with nevi showed an intermediate score for CD3<sup>+</sup> cells, whereas the percentage of *Ptch*<sup>flx/flx</sup> mice showing this score was 50%. These data indicate that T cell recruitment to the melanoma-like nevi area is stronger in *Ptch*<sup>flx/flx</sup> mice when compared to *Ptch*<sup>flx/flx</sup>*LysMcre*<sup>+/-</sup> mice.

Together, the immunohistochemical analyses indicate that chemically induced melanoma-like nevi in *Ptch*<sup>flx/flx</sup>*LysMcre*<sup>+/-</sup> mice are larger than those induced in *Ptch*<sup>flx/flx</sup> mice, which is associated with an increased recruitment of macrophages and DC, but a decreased recruitment of T cells.

**Table 22. Immunohistochemical score for MHCII, F4/80 and CD3 in chemical induced melanoma of *Ptch*<sup>flx/flx</sup>*LysMcre*<sup>+/-</sup> and *Ptch*<sup>flx/flx</sup> mice.**

	MHC <sup>+</sup>				F4/80 <sup>+</sup>				CD3 <sup>+</sup>			
	+	++	+++	n	+	++	+++	n	+	++	+++	n
<i>Ptch</i> <sup>flx/flx</sup>	62.5	37.5	0.0	8	100.0	0.0	0.0	5	50.0	50.0	0.0	4
<i>Ptch</i> <sup>flx/flx</sup> <i>LysMcre</i> <sup>+/-</sup>	54.5	36.4	9.1	11	62.5	37.5	0.0	8	83.3	16.7	0.0	6

Immunohistochemical analysis of skin from DMBA/TPA treated animals were scored by 2 independent individuals; +(low): <10% of the tumor surrounding cells were positive; ++(intermediate): >10% to 20% of the tumor surrounding cells were positive; +++(high): >20% of the tumor surrounding cells were positive.

## 6 Discussion

This thesis originally aimed to elucidate the role of *Ptch* in macrophages. For this purpose *Ptch*<sup>flx/flx</sup> mice were crossed with *LysMcre* mice, which express cre recombinase under control of the murine *lysozyme M* promotor. This should result in specific and highly efficient cre-mediated deletion of *Ptch* in macrophages, DC and granulocytes<sup>104</sup>. Indeed, as demonstrated by a probe-based TaqMan assay, the *Ptch* deletion efficiencies in cells of the myeloid lineage were 65% in CD11b<sup>+</sup> cells (CD11b mainly marks macrophages/monocytes, to a lower extent granulocytes and NK cells), 52% in whole BM and 85% in peritoneal macrophages, 18% in CD11c<sup>+</sup> cells (CD11c mainly marks monocytes and macrophages, neutrophils, myeloid DC and a small subset of lymphocytes) and 20% in Thy1.2<sup>+</sup> cells (Thy1.2 mainly marks T cells), i.e. the degree of recombination was similar to those reported for *LysMcre*-mediated recombination of other floxed genes<sup>103, 104, 149</sup>. However, the targeted disruption of *Ptch* in mice did not lead to any disruption in the development of myeloid-derived blood cells and affected neither the peripheral blood nor the BM of *Ptch*<sup>flx/flx</sup>*LysMcre*<sup>+/-</sup> mice. Thus, the cell count, cell morphology and other hematologic parameters remained comparable in *Ptch*<sup>flx/flx</sup>*LysMcre*<sup>+/-</sup> and control mice. Although the erythrocyte count as well as Hb, Hct, and RDW were lower in *Ptch*<sup>flx/flx</sup>*LysMcre*<sup>+/-</sup> mice, the values did not reach significance. Nevertheless, this anemia could be attributed to the tumors that developed in *Ptch*<sup>flx/flx</sup>*LysMcre*<sup>+/-</sup> mice.

These data strongly suggest that *Ptch* is dispensable in myeloid cell differentiation and development, unlike its role in lymphoid-derived cells, where it was proved to have vital a role in the differentiation and maintenance process of T cells<sup>82</sup>. Furthermore, despite *Ptch* being a tumor suppressor gene, the data shows that *Ptch* inactivation in LysM<sup>+</sup> cells in *Ptch*<sup>flx/flx</sup>*LysMcre*<sup>+/-</sup> mice does not result in malignancies of the hematopoietic system.

### 6.1 GIST-like tumors in *Ptch* mutant mice

The development of GIST-like tumors in adult *Ptch*<sup>flx/flx</sup>*LysMcre*<sup>+/-</sup> mice was surprising. While it was expected that the tumors from *Ptch*<sup>flx/flx</sup>*LysMcre*<sup>+/-</sup> mice would show a deregulated Hh signaling cascade, i.e. an overexpression of the Hh target genes *Gli1* and mutant *Ptch*, *PTCH* mutations per se were not previously implicated in human GIST. In most instances human GIST are considered to arise due to gain-of-function mutations in

*KIT*. In addition, half of the cases which are negative for *KIT* mutations carry gain-of-function mutations in the *PDGFRA* gene<sup>50, 150</sup>.

In addition, human GIST are considered to originate from ICC harboring gain-of-function mutations in *KIT*. However, GIST-like tumors in *Ptch<sup>flox/flox</sup>LysMcre<sup>+/-</sup>* mice do not originate from the *Kit<sup>+</sup>* ICC, but from *LysM<sup>+</sup>* or *LysM<sup>+</sup>Pdgfra<sup>+</sup>* cells localized in the muscular wall of the GI tract. Thus, the *Ptch<sup>flox/flox</sup>LysMcre<sup>+/-</sup>* mouse model is not only the first murine model in which endogenous GIST develop independently of *Kit* mutations, but also gives insights into the nature of the cell of origin of GIST different from *KIT<sup>+</sup>* ICC. In addition, this model implicates an important role of the HH signaling pathway in the pathogenesis of GIST in humans.

### 6.1.1 Differentiation of the tumors from *Ptch<sup>flox/flox</sup>LysMcre<sup>+/-</sup>* mice from LMS

We based the similarity of the the gastrointestinal tumors in *Ptch<sup>flox/flox</sup>LysMcre<sup>+/-</sup>* mice to human GIST on the following investigations and experiments:

Firstly, the tumors of *Ptch<sup>flox/flox</sup>LysMcre<sup>+/-</sup>* mice exhibit a GIST-typical localization between either the circular and longitudinal muscle layer or the longitudinal muscle layer and the serosa of the gut wall. Moreover, the tumors were predominantly localized in the wall of the stomach, the colon and caecum. This location was similarly to that of GIST in mice that overexpress the *KitK641E* or *KitV558del* mutation originally identified in sporadic human GIST or in the germ line of familial GIST syndrome patients<sup>106, 131</sup>. Interestingly, the localization of GIST in mice is different than in humans. Sporadic human GIST are most common in the stomach (50-60%) followed by the proximal small intestine (20-30%). Human GIST of the large intestine are very rare<sup>151</sup>. Human patients who carry germ line *Kit K642E* mutations develop both gastric and small bowel GIST<sup>152</sup>. The reason for the differences in the distribution of GIST between mice and humans is not clear, but it was proposed that the differences in the density of ICC progenitor cells (which are thought to be the cell of origin of human GIST) in the two different species may influence the location of these tumors<sup>131</sup>. However, our observation that the GIST-like tumors of *Ptch<sup>flox/flox</sup>LysMcre<sup>+/-</sup>* mice do not develop from ICC argues against this proposition.

Secondly, the histology and molecular features of these tumors resemble GIST rather than other tumors of the gut, including LMS, the most important differential diagnosis of GIST.

The differentiation between GIST and LMS is important because these two tumor entities have different response to therapy <sup>153</sup>. Although tumors from *Ptch<sup>flox/flox</sup>LysMcre<sup>+/-</sup>* mice showed the occurrence of myofilaments and were negative for GIST-specific markers such as Kit and CD34, they stained positive for other GIST-specific markers. These were desmin, *Pdgfra* and importantly *Dog1*. The name *Dog1* stands for “discovered on GIST” and encodes for a protein of unknown function. However, its expression is specific for GIST because it is absent in non-GIST tumors and because it is expressed in GIST independent of the mutation type <sup>154</sup>. Furthermore, the tumors of *Ptch<sup>flox/flox</sup>LysMcre<sup>+/-</sup>* mice, but not LMS derived from *Pten/p53* double mutant mice, show activation of Hh signaling. This is also similar to human GIST, which in contrast to LMS express the HH target genes *GLI*, *HAND2*, *FOXM1* and others. Indeed, overexpression of HH target genes in GIST, but not in LMS, has not only been shown in the study presented here but also by data available in the GEO database.

Thirdly, the tumors of *Ptch<sup>flox/flox</sup>LysMcre<sup>+/-</sup>* mice are responsive to imatinib. Imatinib (also well-known as Glivec ®) is a synthetic TRK inhibitor, which now has an established role in the management of CML, which arise due to a fusion protein consisting of BCR-ABL <sup>155</sup>. Imatinib also inhibits the KIT tyrosine kinase at a concentration similar to the concentration required for the inhibition of BCR-ABL and can block *in vitro* kinase activity of both wild-type KIT and mutant KIT isoforms commonly found in GIST <sup>156</sup>. Several clinical trials have shown a significant response to imatinib in patients with advanced GIST <sup>157</sup>. Imatinib is now approved for the treatment of patients with KIT-positive unresectable and/or malignant GIST. Indeed, imatinib has resulted in response rates of 50% for patients with GIST. Conversely, patients with advanced LMS do not benefit from imatinib therapy <sup>158</sup>. Therefore, the responsiveness of tumors of *Ptch<sup>flox/flox</sup>LysMcre<sup>+/-</sup>* mice indicates that they are more GIST-like than LMS-like.

### 6.1.2 GIST-like tumors of *Ptch<sup>flox/flox</sup>LysMcre<sup>+/-</sup>* mice express *Pdgfra*, but not Kit

As already indicated in the introduction section, approximately 75-80 % of GIST show *KIT* mutations and 5-10 % are driven by mutations in *PDGFRA* <sup>159</sup>. Furthermore, several percent of GIST are referred to as “wild-type”, as they show neither *KIT* nor *PDGFRA* mutations <sup>50,</sup>

160, 129



Most GIST overexpress KIT protein<sup>48</sup>. The 4-6% KIT-negative GIST frequently overexpress PDGFRA protein and are more likely to have *PDGFRA* mutations<sup>160,150</sup>. It also has been reported that *KIT* mutant, KIT-positive GIST additionally express low levels of active PDGFRA and that, *vice versa*, PDGFRA-positive GIST with *PDGFRA* mutations express low levels of active KIT<sup>161</sup>. This indicates that, in addition to exclusive KIT and PDGFRA subtypes, some GIST can show activation in both pathways (either mutation- or ligand-dependent activation), which may replace each other in the course of tumor progression.

Our data shows that the tumors of *Ptch<sup>flox/flox</sup>LysMcre<sup>+/-</sup>* mice do not overexpress Kit, but instead overexpress *Pdgfra*. Thus, these tumors appear to constitute a first mouse model of the PDGFRA-positive KIT-negative GIST subtype in humans.

The overexpression of *Pdgfra* in the *Ptch<sup>flox/flox</sup>LysMcre<sup>+/-</sup>* model may have been induced by aberrant Hh signaling. This is due to the fact that *Pdgfra* is a downstream Hh target gene, at least in BCC<sup>162</sup>. In addition, it is possible that the overexpression of *Pdgfra* and the lack of Kit expression reflect the origin of the tumors from a cell line that is different from the Kit<sup>+</sup> ICC (see below).

In addition to *Pdgfra* overexpression, *Pdgfra* signaling also seems to be activated in the tumors of *Ptch<sup>flox/flox</sup>LysMcre<sup>+/-</sup>* mice. This was not only revealed by the responsiveness of the tumors to imatinib, but also by phosphorylation of *Pdgfra* in the tumors. In humans, aberrant PDGFRA pathway activity in GIST can be attributed to PDGFRA mutations or to an increased PDGF ligand expression<sup>161</sup>. The latter could explain the *Pdgfra* pathway activity in the *Ptch<sup>flox/flox</sup>LysMcre<sup>+/-</sup>* model.

### 6.1.3 GIST-like tumors of *Ptch<sup>flox/flox</sup>LysMcre<sup>+/-</sup>* mice are derived from LysM<sup>+</sup> cells of the intestine

The *LysMcre* driver used in this study targets LysM-expressing cells, which up to date are considered to be mainly macrophages, DC and granulocytes<sup>104</sup>. This, at first glance, would imply the origin of the GIST-like tumors from these cells which settled within the gut wall. Another possibility would be that a *Ptch*-deficient, LysM<sup>+</sup> transplanted BM-derived HSC (which also can express LysM; see 2.5 of introduction) has settled into the normal intestine. Indeed, contribution of HSC in the regeneration in the normal intestine, as previously

reported<sup>163</sup>. However, the absence of tumor formation in *Rag-2<sup>-/-</sup>γc<sup>-/-</sup>* mice reconstituted with BM cells from *Ptch<sup>flox/flox</sup>LysMcre<sup>+/-</sup>* mice, while not formally excluding, does not support these possibilities. It follows that the GIST-like tumors rather arose from non-myeloid cells that permit activation of the LysM promoter.

The existence of such cells is indeed evidenced by the data presented in this study. Thus, we found rare LysM<sup>+</sup> cells located between the serosa and the longitudinal muscle layer, or between the longitudinal and the circular muscle layers. Most importantly, using reporter mice, rare LysM-expressing cells were identified in the same localization where GIST-like tumors develop in consequence of the LysM-driven *Ptch* inactivation, i.e. between the serosa and the longitudinal muscle layer and between the longitudinal and circular muscle layer.

#### 6.1.4 GIST-like tumors of *Ptch<sup>flox/flox</sup>LysMcre<sup>+/-</sup>* mice are derived from Kit negative cells of the intestine

Besides being derived from a LysM-expressing cell, the tumors of *Ptch<sup>flox/flox</sup>LysMcre<sup>+/-</sup>* mice are not derived from the Kit-positive ICC. This was revealed by a costaining of LysM-positive cells with either Kit or Pdgfra. The analysis revealed that approximately 20% of LysM-expressing (i.e. LacZ-positive cells in *Ptch<sup>flox/flox</sup>LysMcre<sup>+/-</sup>R26R-LacZ<sup>+/-</sup>* mice) cells in the muscle layer co-expressed Pdgfra (see results section Figure 21, middle panel). In contrast, we did not detect any distinct LysM-positive (i.e. LacZ-positive) cells expressing Kit, but found that many LacZ-positive and Kit-positive cells were juxtaposed (see results section Figure 21, right panel).

In most instances human GIST are considered to originate from ICC, which have gain-of-function mutations in KIT. ICC are mesenchymal cells located within the muscular wall of the gastrointestinal tract, where they actively propagate electrical slow waves in the GI muscles and function as pacemakers (reviewed in<sup>164</sup>). Alternatively, PDGFRα<sup>+</sup>KIT<sup>-</sup> GIST could arise from distinct, PDGFRα<sup>+</sup>KIT<sup>low</sup> or PDGFRα<sup>+</sup>KIT<sup>-</sup> cells recently identified in the gut wall<sup>61, 62, 63, 64</sup>.

Although the co-expression of Pdgfra in LysM-positive cells may be a coincidence, it is tempting to speculate that the LysM-expressing Pdgfra-positive cells may serve as an origin for the GIST-like tumors in *Ptch<sup>flox/flox</sup>LysMcre<sup>+/-</sup>* mice. Together with the juxtaposition to the Kit-positive ICC, these cells may represent a subset of the Pdgfra-positive and Kit-negative fibroblast-like cells as reported by others<sup>61</sup>. Alternatively, they could represent a subset of the reported Pdgfra-expressing ICC precursors, in which Kit expression is downregulated<sup>64</sup>. This



is in agreement with the evidence suggesting that KIT and PDGFRA activity can replace each other during GIST progression in humans<sup>161</sup>. Thus, the *Ptch<sup>flxflx</sup>LysMcre<sup>+/-</sup>* mouse model is not only the first murine model in which endogenous GIST develop independently of Kit mutations, but also gives insights into the nature of the cell of origin of GIST different from ICC.

#### 6.1.5 GIST-like tumors of *Ptch<sup>flxflx</sup>LysMcre<sup>+/-</sup>* mice may occur due to cooperation of active Hh and *Pdgfra* signaling in LysM<sup>+</sup> cells

In addition to high *Pdgfra* expression and *Pdgfra* activity, the GIST-like tumors of *Ptch<sup>flxflx</sup>LysMcre<sup>+/-</sup>* mice express increased levels of Hh target genes. Strikingly, the positive correlation between HH pathway genes and PDGFRA expression and mutational status is also observed in human GIST and thus seems to be a common phenomenon in this tumor.

Our data provide evidence that activated *Pdgfra* cooperates with Hh in tumor formation. This is suggested by the cooperative effect of activated PDGFRA signaling and of the HH target GLI1 on cellular transformation. To this end, we have analyzed the activation of PDGFRA, ERK and JUN in control and PDGFB-treated HaCaT cells. The data revealed a strong phosphorylation/activation of all 3 proteins after PDGFB-treatment. Since JUN phosphorylation is crucial for the cooperative transformation effect of active HH and receptor-tyrosine kinase signaling such as EGFR signaling<sup>116</sup>, a similar mechanism can be assumed for active HH and PDGFRA signaling. Furthermore, the PDGFRA-mediated induction of JUN in our experimental setting may be similar to the situation in PDGFRA-associated human GIST that show high expression of JUN<sup>128</sup>. Admittedly, the aberrant activity of the Hh pathway in mouse GIST-like tumors results from the intended deletion of the Hh receptor and tumor suppressor *Ptch*. Notwithstanding the artificial nature of this manipulation, deletions of the *PTCH* locus or aberrant activity of the HH signaling pathway have been reported in up to 50% or 80% of GIST cases, respectively<sup>45, 46</sup>. It follows that the mutational or otherwise activation of the HH pathway may be a driving and early event in the formation of human GIST. Alternatively, active PDGFRA signaling (e.g. due to a PDGFRA mutation) may stimulate GLI activity, as recently shown for signaling by EGFR<sup>112</sup>.

Taken together, we present a new model of GIST formation, which does not involve Kit activation, but probably an interaction between Hh- and *Pdgfra*-signaling.

These findings add to the accumulating lines of experimental evidence, revealing that an aberrant activation of HH signaling and RTK signaling, such as the EGFR signaling cascade, frequently cooperate during cancer initiation and progression. RTK signaling has been shown to cooperate with HH signaling through multiple cross-talks which results in the malignant transformation of cells and also can cause treatment resistance and disease relapse. For example, activity of GLI proteins can be modified by integration of distinct signals, such as the MEK/ERK and PI3K/AKT pathway in BCC by integration of the HH/GLI and EGFR pathway. It has been shown that both pathways synergistically induced oncogenic transformation, which was dependent on EGFR-mediated activation of the RAS/RAF/MEK/ERK but not of the PI3K/AKT pathway. Furthermore, EGFR/MEK/ERK signaling induced JUN activation, which was essential for oncogenic transformation in combination with the GLI activator forms GLI1 and GLI2. In addition, pharmacologic inhibition of EGFR and HH/GLI efficiently reduced growth of BCC cell lines derived from mice with activated HH/GLI signaling. These results identified the synergistic integration of GLI activator function and EGFR signaling as a critical step in oncogenic transformation<sup>112</sup>. Due to these data, it is possible that oncogenic transformation due to the activation of both PDGFRA and HH signaling follows a similar mechanism.

However, future studies are required to more precisely establish the molecular mechanisms and specific downstream signaling elements that may contribute to the cooperative or synergistic interactions of HH and PDGFRA signaling. It would also be of great therapeutic interest to define the potential interaction between PDGFRA and HH signaling in human GIST.

#### **6.1.6 Implications for GIST therapy**

GIST is the most common mesenchymal tumor affecting the GI tract and occurs with an annual frequency of 10 to 14.5 per million of the population<sup>165</sup>. Surgery is the standard of care for primary disease, whereas imatinib is recommended for first-line treatment of unresectable and/or metastatic GIST. Although imatinib and other tyrosine kinase inhibitors have improved survival of patients with advanced GIST, complete responses are rare. Primary resistance to imatinib occurs in 12–14% of patients and the majority of patients who initially benefit from tyrosine kinase inhibitors eventually become resistant, with a median time to progression of 2 years<sup>166</sup>.

Our data now implicate a role of HH signaling in GIST. Thus, GIST patients with HH pathway activation may benefit from combination treatment protocols that besides imatinib include an HH antagonist e.g. GDC-0449, which has recently been shown to exhibit antitumor activity in clinical studies<sup>167, 168</sup>.

## 6.2 Functional role of *Ptch* in the innate immune system

In another line of this study, the role of *Ptch*-deficient macrophages and other myeloid cells such as granulocytes in inflammatory responses and tumor progression was examined. For this purpose, BMDM derived from *Ptch*<sup>flx/flx</sup>*LysMcre*<sup>+/-</sup> and *Ptch*<sup>flx/flx</sup> control mice were stimulated with the TLR agonists LPS and BLP, and the influence of the *Ptch* deletion on viability, cytokine expression and secretion, and proliferation was investigated. Then, in order to analyze the function of *Ptch* in myeloid cells during tumor surveillance, two different tumor cell lines were transplanted in *Ptch*<sup>flx/flx</sup>*LysMcre*<sup>+/-</sup> and *Ptch*<sup>flx/flx</sup> mice. In addition, tumors were chemically induced in the skin of the animals, and the growth of the tumors was monitored. Furthermore, the infiltration of the tumor microenvironment with macrophages and granulocytes was investigated. Due to lack of time, some of the experiments were only done once, which hampers an explicit interpretation of the data.

### 6.2.1 Role of *Ptch* in inflammatory responses after stimulation with TLR agonists

Macrophages and granulocytes are important players in innate immunity. In addition to acting as a first line resistance against pathogens, these cells undergo reprogramming of their functional properties in response to signals derived from different stress or pathogen such as microbes or microbial moieties like LPS from gram-negative bacteria and BLP from gram-positive bacteria<sup>169</sup>. Since LPS and BLP are potent activators of monocytes and macrophages via stimulation of TLR4 and TLR1/2, respectively, these two compounds were used to analyze whether *Ptch* plays a role in regulating inflammatory responses. LPS and BLP have been shown to polarize the macrophages towards the M1 phenotype, which normally includes secretion of cytokines such as IL-6 and TNF $\alpha$ . and low expression of IL-12<sup>170, 171, 172</sup>.

The data showed that *Ptch* has generally no effect on the cytokine production after stimulation with LPS. Thus, LPS stimulation of macrophages resulted in an increased secretion of pro-inflammatory cytokines TNF $\alpha$ , IL-6 and RANTES in a time-dependent manner. Likewise, LPS also stimulated the production of other cytokines such as IL-10, IL-

12p40, and of the chemokines KC, MCP-1, MIP-1 $\alpha$ . However, *Ptch* did not influence the secreted amount of these chemokines and cytokines, because no differences were detected when comparing the values derived from *Ptch* mutant or control BMDM. These data indicate that *Ptch* is probably dispensable for TLR4-mediated activation and production of macrophage-derived cytokines and chemokines.

In contrast to LPS, the preliminary data suggest that BLP-stimulation may result in a stronger activation of the *Ptch* mutant BMDM when compared to the controls. This was revealed by qRT-PCR of the pro-inflammatory cytokine *IL-6*, which appeared upregulated in *Ptch* mutant BMDM after the BLP stimulus. However, the expression levels of *RANTES* and *TNF $\alpha$*  in *Ptch* mutant and control BMDM were not different. Since this experiment was only performed once, and since *IL-6* secretion by ELISA was not examined, these results have to be regarded with reservation. If *IL-6* is indeed upregulated in BLP-stimulated *Ptch* mutant BMDM, it is possible that *Ptch* modulates TLR1/2-mediated signaling. The modulation would be specific for the TLR1/2 pathway, because *Ptch* did not influence TLR4-mediated signaling i.e. *IL-6* expression after stimulation with LPS.

Furthermore, the viability and proliferation of *Ptch* mutant and control BMDM after exposure to BLP and/or LPS was examined. Cell viability was not affected when the cells were incubated with LPS for 6, 12, and 24 hours. Unfortunately, the results for a longer exposure (i.e. 48 h and 72 h) and for the exposure to BLP are not available yet. However, the BrdU-incorporation assay revealed that the amount of incorporated BrdU decreased in both *Ptch* mutant and control BMDM after a 72 h and a 48 h exposure to LPS and BLP, respectively. Most interestingly, the decrease in BrdU incorporation was more pronounced in *Ptch* control macrophages when compared to the *Ptch* mutant BMDM. These data indicate that *Ptch* mutant BMDM are more resistant to LPS- and BLP-treatment. Whether this is due to an increased proliferation rate or to a decreased apoptosis rate or to a resistance to general toxicity of the mutant cells is hard to say. For this purpose, cell viability at these time points (i.e. after 72 h or 48 h of stimulation with LPS or BLP, respectively) as well as the apoptosis rate must be analysed.

Although these data are preliminary, it is tempting to speculate that the observed protection from apoptosis and or toxicity due to BLP stimulation may contribute to the increased *IL-6* expression of the *Ptch*-deficient macrophages. It is known that *IL-6* operates to control the magnitude of inflammatory responses<sup>173</sup>. If these results turn out to be true, it would be

interesting to investigate how *Ptch* regulates the BLP-mediated modulation of *IL-6* expression, and whether this regulation involves TLR1/2 signaling and is specific for said signaling.

Finally, and importantly, the comparison between unstimulated BMDM derived from *Ptch<sup>flox/flox</sup>LysMcre<sup>+/-</sup>* and *Ptch<sup>flox/flox</sup>* mice suggests that *Ptch*-deficiency did not result in activation of the Hh signaling pathway (i.e. *Gli1* and *Ptch* expression) in these cells. This suggests that the differences between *Ptch* mutant and *Ptch* wt BMDM after LPS and BLP stimulation are independent of Hh signaling activity. However, more experiments are needed to confirm this suggestion, e.g. it would be important to investigate Hh signaling activity in cells after stimulation with LPS or BLP.

### 6.2.2 The role of *Ptch* in tumor immune surveillance

Tumors consist of neoplastic cells and non-malignant stromal cells. The development of tumors is regulated by interactions between the neoplastic cells and their microenvironment. The interactions between tumor cells and cells of the immune system are extremely complex. The outcome of such interactions can span all scenarios from suppression of tumor growth by to enhancement of tumor progression by the immune system<sup>174</sup>.

Residential macrophages have early contact with the arising tumor. Tumor-associated macrophages can have different functions according to their physiological or pathophysiological context and can be associated with poor prognosis and tumor progression<sup>72</sup>. As already stated in the introduction, macrophages are able to secrete growth factors, cytokines and chemokines. The secretion of the respective cytokines is dependent on local stimuli such as cytokines, the engagement of adhesion molecules, or interaction with pathogens. According to their activation state, receptor expression, cytokine production, and functions, macrophages have been broadly classified in the M1 or M2 type. "Classically activated" M1 macrophages, which are activated by microbial products or IFN- $\gamma$ , produce large amounts of proinflammatory cytokines and are implicated in the killing of tumor cells. M1 macrophages usually express the Th1 cell-attracting chemokines such as CXCL9 and CXCL10 and release large amounts of proinflammatory cytokines such as IL-12, IL-23 and TNF $\alpha$ . They usually produce reactive nitrogen and reactive oxygen intermediates and show a higher expression of major histocompatibility complex (MHC) class II molecules<sup>171</sup>. In contrast, "alternatively activated" M2 macrophages exert immune regulation by inducing

anti-inflammatory responses. They also promote angiogenesis and generally have a tumor-promoting effect <sup>72</sup>. The M2 phenotype is shared by tumor-associated macrophages and is characterized by the expression of e.g. Arg1 and Trem2. The phenotype of a macrophage population can change over time, like in tumor progression where the macrophage phenotype can change from M1 to M2 <sup>72</sup>. We have started to analyze the involvement of *Ptch* in determining a) the fate of macrophages and b) the numbers of macrophages and other cells from the immune system during tumor development.

For this purpose *Ptch*<sup>flx/flx</sup>*LysMcre*<sup>+/-</sup> and *Ptch*<sup>flx/flx</sup> control mice on a C57BL/6 background were transplanted with the syngeneic melanoma cell line B16F10, both by subcutaneous and intravenous injection, to obtain locally growing and “metastatic” tumors, respectively. Transplanted mice were all younger than 10 weeks to avoid a potential modulation of the immune system by the endogenously developing GIST-like tumors in *Ptch*<sup>flx/flx</sup>*LysMcre*<sup>+/-</sup> mice (although the exact time point of GIST initiation in *Ptch*<sup>flx/flx</sup>*LysMcre*<sup>+/-</sup> mice is not known, most of the GIST-like tumors became phenotypically conspicuous at around 25 to 26 weeks of age). As demonstrated by the experiments, *Ptch*-deficient macrophages and other *Ptch*-deficient myeloid cells did neither influence growth nor metastasis in this model. However, because the B16F10 cell line is fast-growing, it may be possible that subtle differences in tumor growth and progression were overlooked. Therefore, we repeated this experiment with the slow-growing ovarian carcinoma cell line ID8-LUC, which is derived from a transformed late-passage mouse ovarian surface epithelium from adult C57BL6 mice and which was stably transfected with luciferase by lentiviral infection. These cells were injected i.p.. The *in vivo* tumor growth was monitored by injecting D-luciferin, and the bioluminescence was monitored by a CCD camera. As previously reported, all the injected animals displayed multiple tumors throughout the peritoneum, which covers the peritoneal cavity, the diaphragm, and all other intraperitoneal organs <sup>119</sup>. Nevertheless, as already seen in the B16F10 melanoma model, there was no significant difference in ID8-LUC growth in *Ptch*<sup>flx/flx</sup>*LysMcre*<sup>+/-</sup> when compared to *Ptch*<sup>flx/flx</sup> control mice. However, as already stated in the results section, the growth of ID8-LUC cells seemed to cease in *Ptch*<sup>flx/flx</sup> mice at week 7 after transplantation. Because implantation of ID8-LUC cells causes progressive disease state in wt mice, this effect is rather due to the variability of ID8-LUC growth in individual mice <sup>143</sup>.

In addition, transplantation of ID8-LUC cells can result in ascites. Indeed, ascites developed after 14 to 16 weeks in both *Ptch*<sup>flox/flox</sup>*LysMcre*<sup>+/-</sup> and *Ptch*<sup>flox/flox</sup> control mice. The occurrence of ascites is associated with late-stage ovarian cancer and is due to an abnormal collection of fluid with a cellular fraction consisting mainly of cancer cells, lymphocytes, and mesothelial cells in the peritoneal cavity<sup>175, 176</sup>. The cell composition of the ascites can give some clues about the status of the “tumor microenvironment”. For example, it was shown that a subset of tumor-associated macrophages expressing B7-H4 was significantly increased in the ascites of human ovarian carcinoma. These tumor-associated macrophages were furthermore shown to inhibit the proliferation and activity of T cells<sup>177</sup>. Thus, the phenotype and the number of cells present in the tumor microenvironment are crucial in their contribution to the tumor immune response.

Our preliminary data showed that the *Ptch*-deficiency probably does not influence the cellular composition of the ascites, meaning that there is no gross difference between the genotypes. This was revealed by the analysis of the expression of the M2 macrophage markers, *Arg1* and *Trem2*. Increased expression of these two genes would indicate not only the M2-phenotype, but would also indicate an increased number of macrophages and MDSC expressing these genes. Unfortunately, due to the high number of erythrocytes, the analysis of the cellular composition of the ascites by flow cytometry was not possible. These experiments would be crucial to learn more about the recruitment of different cell types in the tumor environment and will be performed in the future.

Nevertheless, splenic MDSC, macrophages and granulocytes were analyzed. The rationale for the analysis was the fact that the spleen acts as a reservoir of myeloid cells, which can be mobilized to amplify the tumor-associated neutrophils (granulocytes), tumor-associated macrophages, and MDSC responses on tumor recruitment. Also, HSC and GMP accumulate in large numbers within the splenic red pulp of tumor-bearing mice. These cells establish niches of proliferation, produce new MDSC locally, and participate in the continuous replenishment of the myeloid cell reservoir<sup>147</sup>. Therefore, and as previously shown<sup>147</sup>, we expected that the counts of these splenic cells will mirror the number of these cells in the ascites of the ID8-LUC transplanted animals. The analysis revealed that the *Ptch*-deficiency did not impact the number of splenic MDSC, macrophages or granulocytes.

MDSC are a heterogeneous population of cells that consist of myeloid progenitors and immature macrophages, immature granulocytes, and immature DC present in both the tumor



and the spleen of tumor-bearing animals. These cells have been reported to regulate innate immune responses by modulating the cytokine production of mature macrophages. In addition, they play a role in tumor angiogenesis, tumor cell invasion, and metastasis<sup>178</sup>. MDSC also express high levels of Arg1 and act as immunosuppressors during tumor growth. Arg1 produced by MDSC can impair T cell function in tumor-bearing animals by decreasing the expression of the TCR zeta chain. Thus, MDSC apparently interfere with the T cell antigen receptor, so that there is no signal to activate the T cells<sup>178</sup>. Due to the fact that CD11b<sup>+</sup> Gr-1<sup>+</sup> IL-4R $\alpha$ <sup>+</sup> F4/80<sup>+</sup> splenic cells were not elevated in tumor-bearing *Ptch*<sup>flx/flx</sup>*LysMcre*<sup>+/-</sup> mice when compared to tumor-bearing control mice, and since *Arg1* expression levels were not increased in the “tumor microenvironment” (as judged by qRT-PCR analysis of mRNA derived from ascites), *Ptch* apparently is not necessary for stimulation of MDSC. *Ptch* is also not necessary for the elevation of numbers of MDSC, granulocytes or macrophages, at least in the spleen. Furthermore, these results also indicate that potentially developing GIST-like tumors in *Ptch*<sup>flx/flx</sup>*LysMcre*<sup>+/-</sup> mice did not alter the number of splenic cells derived from the myeloid lineage.

Another approach to study the role of *Ptch* in tumor immune surveillance was the chemical induction of skin tumors in *Ptch*<sup>flx/flx</sup>*LysMcre*<sup>+/-</sup> mice. With respect to the following data it should be mentioned that these results are considered reliable.

The mouse skin chemical carcinogenesis model has been widely used to study initiation, promotion, and progression (malignant conversion) of mouse skin tumors. The initiation of the tumors is achieved through a single topical application of DMBA. This causes a genetic mutation in the stem cell or progenitor cell compartment, which is either an activating mutation in a proto-oncogene such as *H-ras* or an inactivating mutation in a tumor suppressor gene such as *p53*. Repeated exposure of the skin to chemical tumor promoters like TPA (or other irritants) promotes the expansion of the initiated cell and a generalized epidermal hyperplasia. The initiated cells can further outgrow the normal epidermal cells to form premalignant papillomas. Due to further genetic changes, some of the papillomas convert to malignant carcinomas capable of invading through the basement membrane and finally metastasizing to the lymph nodes and lungs<sup>179</sup>. In addition, the two-stage chemical carcinogenesis protocol can result in melanoma-like nevi and BCC-like structures<sup>180</sup>. Furthermore, it is well known that the immune system plays a role in the occurrence of chemically induced tumors. For example it has been demonstrated that CXCR3 promotes

epidermal tumorigenesis likely through a T cell-dependent induction of keratinocyte proliferation<sup>181</sup>. In addition, DMBA/croton-oil-associated melanoma does not occur in mice deficient for TLR4 (information: as TPA, croton-oil is a phorbol-derivative)<sup>182</sup>. Furthermore, and most interestingly, DMBA/TPA-treated mice deficient in Langerhans Cells (LC) develop a high number of papilloma and carcinoma<sup>183</sup>.

We showed here that in DMBA/TPA-treated *Ptch*<sup>fllox/fllox</sup>*LysMcre*<sup>+/-</sup> mice the numbers and the onset of papilloma were comparable with those induced in control animals. However, the epidermis of *Ptch*<sup>fllox/fllox</sup>*LysMcre*<sup>+/-</sup> mice was more hyperplastic, which was accompanied by an increased, although not significant, number of Ki-67<sup>+</sup> cells when compared to the controls. In addition, the nevi developing in *Ptch*<sup>fllox/fllox</sup>*LysMcre*<sup>+/-</sup> mice were larger than those induced in *Ptch*<sup>fllox/fllox</sup> control mice and microscopically resembled melanoma. Furthermore, these “melanoma-like” tumors showed an enhanced infiltration with both MHCII<sup>+</sup> and F4/80<sup>+</sup> cells, but a decrease in CD3<sup>+</sup> cells when compared to the controls.

These data suggest that a *Ptch*-deficiency in macrophages and in other myeloid cells in the tumor microenvironment enhances keratinocyte proliferation in DMBA/TPA treated skin, but does not influence the initiation or progression of tumors derived from the epidermal skin layer such as papilloma. However, the *Ptch*-deficiency in *Ptch*<sup>fllox/fllox</sup>*LysMcre*<sup>+/-</sup> mice seems to increase the size of DMBA/TPA-associated nevi, but not their numbers. This suggests that the *Ptch*-deficiency promotes the progression, but not the initiation, of the latter tumors. Furthermore, in *Ptch*<sup>fllox/fllox</sup>*LysMcre*<sup>+/-</sup> mice, the area of “melanoma-like” tumors was strongly surrounded with F4/80<sup>+</sup> cells. In addition, the tumor surrounding also showed an increased number of MHCII<sup>+</sup> cells. This is of importance because in the mouse skin F4/80<sup>+</sup> and MHCII<sup>+</sup> cells could be either dermal macrophages, DC or LC (for review see<sup>184</sup>).

The main role of DC is to induce specific immunity against invading pathogens while maintaining tolerance to self-antigens. As described previously by Norian and colleagues, DC play a critical role in the outcome of adaptive immune responses against growing tumors. While it is generally assumed that the presence of mature DC should promote protective anti-tumor immunity, evidence to the contrary does exist. Thus, Norian and colleagues showed that tumor-infiltrating DC actively contribute to the suppression of protective CD8<sup>+</sup> T cell-based antitumor immunity. In addition, the DC inhibited the expansion of T cells.

Furthermore, tumor-infiltrating DC were found in every murine tumor type including transplanted fibrosarcoma and breast carcinoma cell lines and spontaneously developing mammary tumors<sup>185</sup>. Based on these data the authors hypothesized that tumors can induce matured tumor-infiltrating DC to act as potent suppressors of T cell-based antitumor immunity.

LC are a myeloid subset of tissue DC located in the epidermis<sup>186</sup> and constitutively express MHCII<sup>187</sup>. Immature LC residing in the epidermis can collect antigen, and upon various stimuli, they mature and migrate to draining LN<sup>188</sup>, where they can directly present antigen secreted from keratinocytes<sup>189</sup>. Thus, they are presumed to play a key role in promoting immune responses.

LC have traditionally been thought to stimulate adaptive immunity. Indeed, LC have been shown to present antigens to activate the CD4 helper T cell and CD8 cytotoxic T cell compartments, including potent antitumor effector cells. However, emerging data have also revealed that LC might suppress T cell function, and that LC might contribute to cutaneous responses that facilitate keratinocyte transformation and growth of papilloma and SCC (reviewed in<sup>190</sup>). Indeed, mice deficient in LC are almost completely resistant to papilloma and carcinoma formation by this two-stage carcinogenesis protocol<sup>183</sup>. It is thought that LC might have the capacity to internalize and metabolize and increase mutagenicity of polyaromatic hydrocarbons such as DMBA. Moreover, it is speculated that LC might influence the growth of mutated epidermal cells, for example via the local production of growth factors or anti-apoptotic factors (reviewed in<sup>190</sup>). In contrast, and to our best knowledge, a role of LC in DMBA/TPA-induced nevi/melanoma-formation has not been reported so far. However, LC seem to play a very important role in human melanoma. Thus, it has been reported that LC were significantly increased around in situ and early-invasive stages of melanoma<sup>191</sup>.

The aspects described above may allow an interpretation of the data derived from DMBA/TPA-treated *Ptch*<sup>flox/flox</sup>*LysMcre*<sup>+/-</sup> mice:

The *Ptch* mutation in *Ptch*<sup>flox/flox</sup>*LysMcre*<sup>+/-</sup> mice did not result in promotion of papilloma growth. This indicates that the *Ptch*-deficiency in myeloid cells apparently did not promote the growth of “initiated” keratinocytes, i.e. those keratinocytes that could give rise to papilloma. However, since the epidermis of *Ptch*<sup>flox/flox</sup>*LysMcre*<sup>+/-</sup> mice was very hyperplastic,

the *Ptch*-deficiency apparently promoted the proliferation of the “normal” keratinocytes. Thus, one could speculate that the role of *Ptch* in skin macrophages such as dermal macrophages, DC and LC, is to prevent hyperproliferation of “normal” keratinocytes. Why the growth of “initiated” keratinocytes was not prevented is hard to explain. In addition, *Ptch* in skin macrophages may be a necessary factor to prevent proliferation of melanocytic cells. Due to i) the higher numbers of F4/80<sup>+</sup> and MHCII<sup>+</sup> cells in and around the nevi, ii) the decrease in CD3<sup>+</sup> cells in and around the nevi, and iii) due to the larger size of the nevi in *Ptch*<sup>flox/flox</sup>*LysMcre*<sup>+/-</sup> mice, one can speculate that DC and LC in the melanoma-like areas in mutant mice contribute to a tumor escape mechanism. This would fit very nicely to the above-mentioned observations that tumor-infiltrating DC inhibit T cell migration and proliferation and thus act as potent suppressors of T cell-based antitumor immunity<sup>185</sup>. It also fits the observation that LC seem necessary for the promotion of in situ and early-stage melanoma in humans<sup>191</sup>. Together one could speculate that role of *Ptch* in skin macrophages such as DC and LC are to prevent proliferation of “normal” keratinocytes and of preneoplastic melanocytes.

The mechanism how the *Ptch*-deficiency in *Ptch*<sup>flox/flox</sup>*LysMcre*<sup>+/-</sup> mice resulted in an increase of the DC and LC in the tumor area is hard to explain. However, it is possible that *Ptch* is a factor necessary for migration of skin macrophages including DC and LC to the tumor area. In other words, it is possible that *Ptch* mutant macrophages showed a higher migratory capacity than *Ptch*-wt macrophages because they were either hypo- or hyper-responsive to chemokine that could be produced by the preneoplastic melanocytes. Indeed, melanoma cells can produce the macrophage migration inhibitory factor MIF<sup>192</sup>. Therefore it is possible that *Ptch*-deficient macrophages just do not respond to this factor. On the other hand, melanoma also produces factors that result in macrophage-recruitment to the tumors. One example is Thrombospondin-1, which is produced by melanoma cells and is a very potent attractant for macrophages<sup>193, 194</sup>. Therefore, it is possible that *Ptch*-deficient macrophages are hyperreactive to those factors and migrate to the melanoma-like lesions. Whether this is true or not remains to be established in the future.

In summary, our data strongly suggest that *Ptch* in myeloid cells such as skin macrophages is an important factor in the immune surveillance of melanoma. However, more experiments are needed to confirm this hypothesis.

### 6.3 Outlook on the future studies on the role *Ptch* in macrophages and other cells derived from the myeloid lineage

Many data presented in the second part of this study are preliminary results. The only results considered solid are those derived from the DMBA/TPA treatment of the *Ptch<sup>fllox/fllox</sup>LysMcre<sup>+/-</sup>* mice and *Ptch<sup>fllox/fllox</sup>* control mice.

It will be important to repeat the experiments to show that the increase of IL-6 after TLR1/2-mediated (i.e. BLP-mediated) stimulation as well as the higher BrdU incorporation rate after BLP- and LPS-stimulation are “real” characteristics of *Ptch* mutant BMDM. With respect to BrdU incorporation it will be interesting to see whether this indeed reflects a higher proliferation rate or rather a resistance to apoptosis. Furthermore, the effects of BLP and LPS should be studied *in vivo* in *Ptch<sup>fllox/fllox</sup>LysMcre<sup>+/-</sup>* mice. If BLP indeed modulates IL-6 expression/secretion as well as the proliferation/apoptosis rate of *Ptch* mutant macrophages, it is possible that this could also induce a different inflammatory response in *Ptch<sup>fllox/fllox</sup>LysMcre<sup>+/-</sup>* mice treated with the substance. Indeed, mice heterozygous for a *Ptch* mutation have been reported to be more responsive to systemic LPS treatment.<sup>195</sup>, which could be related to cells derived of the myeloid lineage.

In addition, the observation that DMBA/TPA-treated *Ptch<sup>fllox/fllox</sup>LysMcre<sup>+/-</sup>* mice develop melanoma-like structures, which are surrounded by increased numbers of MHC<sup>+</sup> and F4/80<sup>+</sup> cells but decreased numbers of CD3<sup>+</sup> cells, must be followed up. Furthermore, there are still several questions that need to be answered. While we have high recombination efficiency at the *Ptch* locus of BMDM, PM and splenic macrophages, we have not looked at the recombination efficiency in tissue macrophages of the skin. The first question is whether skin macrophages of *Ptch<sup>fllox/fllox</sup>LysMcre<sup>+/-</sup>* mice are indeed *Ptch* knock-out and whether these knock-out cells show active Hh signaling. This question can be answered by *Ptch* recombination assay and *in situ* hybridization assay using *Ptch* and/or *Gli1* probes.

The second question is whether *Ptch* mutant macrophages have increased migratory capacity towards melanoma cells. This could be answered by macrophage/melanoma cell co-culture in a Boyden chamber or Transwell migration assay. If there is an increase in the migratory capacity of *Ptch* mutant macrophages, this could explain the increased presence of F4/80<sup>+</sup> cells in and around the melanoma-like nevi of *Ptch<sup>fllox/fllox</sup>LysMcre<sup>+/-</sup>* mice.

Another interesting question is whether the “melanoma”-infiltrating macrophages in *Ptch<sup>fllox/fllox</sup>LysMcre<sup>+/-</sup>* mice are of the M1 or M2 phenotype. Since the melanoma-like nevi in

these mice are larger, one would certainly expect that they are rather M2- than M1-like. If so, then it would also be important to know by which mechanism the *Ptch* mutation is influencing the macrophage phenotype and the tumor immune response.

Unraveling the exact function of *Ptch* in macrophages during the tumor immune response may provide a basis for the better understanding of melanoma pathogenesis and the role of *Ptch*, and probably also its signaling pathway, in the tumor microenvironment.

## 7 References

1. Nusslein-Volhard C, Wieschaus E. Mutations affecting segment number and polarity in *Drosophila*. *Nature* 1980;287:795-801.
2. van den Brink GR. Hedgehog signaling in development and homeostasis of the gastrointestinal tract. *Physiol Rev* 2007;87:1343-75.
3. Mann JF, Ferro VA, Mullen AB, Tetley L, Mullen M, Carter KC, Alexander J, Stimson WH. Optimisation of a lipid based oral delivery system containing A/Panama influenza haemagglutinin. *Vaccine* 2004;22:2425-9.
4. Marigo V, Scott MP, Johnson RL, Goodrich LV, Tabin CJ. Conservation in hedgehog signaling: induction of a chicken patched homolog by Sonic hedgehog in the developing limb. *Development* 1996;122:1225-33.
5. Marigo V, Tabin CJ. Regulation of patched by sonic hedgehog in the developing neural tube. *Proc Natl Acad Sci U S A* 1996;93:9346-51.
6. Chiang C, Litingtung Y, Lee E, Young KE, Corden JL, Westphal H, Beachy PA. Cyclopia and defective axial patterning in mice lacking Sonic hedgehog gene function. *Nature* 1996;383:407-13.
7. St-Jacques B, Hammerschmidt M, McMahon AP. Indian hedgehog signaling regulates proliferation and differentiation of chondrocytes and is essential for bone formation. *Genes Dev* 1999;13:2072-86.
8. Bitgood MJ, Shen L, McMahon AP. Sertoli cell signaling by Desert hedgehog regulates the male germline. *Curr Biol* 1996;6:298-304.
9. Rohatgi R, Milenkovic L, Scott MP. Patched1 regulates hedgehog signaling at the primary cilium. *Science* 2007;317:372-6.
10. Denef N, Neubuser D, Perez L, Cohen SM. Hedgehog induces opposite changes in turnover and subcellular localization of patched and smoothened. *Cell* 2000;102:521-31.
11. Bijlsma MF, Spek CA, Zivkovic D, van de Water S, Rezaee F, Peppelenbosch MP. Repression of smoothened by patched-dependent (pro-)vitamin D3 secretion. *PLoS Biol* 2006;4:e232.
12. Sasaki H, Nishizaki Y, Hui C, Nakafuku M, Kondoh H. Regulation of Gli2 and Gli3 activities by an amino-terminal repression domain: implication of Gli2 and Gli3 as primary mediators of Shh signaling. *Development* 1999;126:3915-24.
13. Xie J. Hedgehog signaling pathway: development of antagonists for cancer therapy. *Curr Oncol Rep* 2008;10:107-13.
14. Aberger F, Kern D, Greil R, Hartmann TN. Canonical and noncanonical Hedgehog/GLI signaling in hematological malignancies. *Vitam Horm* 2012;88:25-54.
15. Hooper JE, Scott MP. Communicating with Hedgehogs. *Nat Rev Mol Cell Biol* 2005;6:306-17.
16. Irvine DA, Copland M. Targeting hedgehog in hematologic malignancy. *Blood* 2012;119:2196-204.
17. Beachy PA, Karhadkar SS, Berman DM. Tissue repair and stem cell renewal in carcinogenesis. *Nature* 2004;432:324-31.
18. Varjosalo M, Taipale J. Hedgehog: functions and mechanisms. *Genes Dev* 2008;22:2454-72.
19. Shibuya K, Mathers CD, Boschi-Pinto C, Lopez AD, Murray CJ. Global and regional estimates of cancer mortality and incidence by site: II. Results for the global burden of disease 2000. *BMC Cancer* 2002;2:37.
20. Hanahan D, Weinberg RA. Hallmarks of cancer: the next generation. *Cell* 2011;144:646-74.



21. Scales SJ, de Sauvage FJ. Mechanisms of Hedgehog pathway activation in cancer and implications for therapy. *Trends Pharmacol Sci* 2009;30:303-12.
22. Berman DM, Karhadkar SS, Maitra A, Montes De Oca R, Gerstenblith MR, Briggs K, Parker AR, Shimada Y, Eshleman JR, Watkins DN, Beachy PA. Widespread requirement for Hedgehog ligand stimulation in growth of digestive tract tumours. *Nature* 2003;425:846-51.
23. Vestergaard J, Pedersen MW, Pedersen N, Ensinger C, Tumer Z, Tommerup N, Poulsen HS, Larsen LA. Hedgehog signaling in small-cell lung cancer: frequent in vivo but a rare event in vitro. *Lung Cancer* 2006;52:281-90.
24. Mukherjee S, Frolova N, Sadlonova A, Novak Z, Steg A, Page GP, Welch DR, Lobo-Ruppert SM, Ruppert JM, Johnson MR, Frost AR. Hedgehog signaling and response to cyclopamine differ in epithelial and stromal cells in benign breast and breast cancer. *Cancer Biol Ther* 2006;5:674-83.
25. Takezaki T, Hide T, Takanaga H, Nakamura H, Kuratsu J, Kondo T. Essential role of the Hedgehog signaling pathway in human glioma-initiating cells. *Cancer Sci* 2011;102:1306-12.
26. Dierks C, Beigi R, Guo GR, Zirlik K, Stegert MR, Manley P, Trussell C, Schmitt-Graeff A, Landwerlin K, Veelken H, Warmuth M. Expansion of Bcr-Abl-positive leukemic stem cells is dependent on Hedgehog pathway activation. *Cancer Cell* 2008;14:238-49.
27. Peacock CD, Wang Q, Gesell GS, Corcoran-Schwartz IM, Jones E, Kim J, Devereux WL, Rhodes JT, Huff CA, Beachy PA, Watkins DN, Matsui W. Hedgehog signaling maintains a tumor stem cell compartment in multiple myeloma. *Proc Natl Acad Sci U S A* 2007;104:4048-53.
28. Lin TL, Wang QH, Brown P, Peacock C, Merchant AA, Brennan S, Jones E, McGovern K, Watkins DN, Sakamoto KM, Matsui W. Self-renewal of acute lymphocytic leukemia cells is limited by the Hedgehog pathway inhibitors cyclopamine and IPI-926. *PLoS One* 2010;5:e15262.
29. Greaves WO, Kim JE, Singh RR, Drakos E, Kunkalla K, Sanchez-Espiridion B, Garcia JF, Medeiros LJ, Vega F. Glioma-associated oncogene homologue 3, a hedgehog transcription factor, is highly expressed in Hodgkin and Reed-Sternberg cells of classical Hodgkin lymphoma. *Hum Pathol* 2011;42:1643-52.
30. Hahn H, Wicking C, Zaphiropoulos PG, Gailani MR, Shanley S, Chidambaram A, Vorechovsky I, Holmberg E, Uden AB, Gillies S, Negus K, Smyth I, Pressman C, Leffell DJ, Gerrard B, Goldstein AM, Dean M, Toftgard R, Chenevix-Trench G, Wainwright B, Bale AE. Mutations of the human homolog of *Drosophila* patched in the nevoid basal cell carcinoma syndrome. *Cell* 1996;85:841-51.
31. Gorlin RJ. Nevoid basal cell carcinoma syndrome. *Dermatol Clin* 1995;13:113-25.
32. Raffel C, Jenkins RB, Frederick L, Hebrink D, Alderete B, Fults DW, James CD. Sporadic medulloblastomas contain PTCH mutations. *Cancer Res* 1997;57:842-5.
33. Taylor MD, Liu L, Raffel C, Hui CC, Mainprize TG, Zhang X, Agatep R, Chiappa S, Gao L, Lowrance A, Hao A, Goldstein AM, Stavrou T, Scherer SW, Dura WT, Wainwright B, Squire JA, Rutka JT, Hogg D. Mutations in *SUFU* predispose to medulloblastoma. *Nat Genet* 2002;31:306-10.
34. Tostar U, Malm CJ, Meis-Kindblom JM, Kindblom LG, Toftgard R, Uden AB. Deregulation of the hedgehog signalling pathway: a possible role for the PTCH and *SUFU* genes in human rhabdomyoma and rhabdomyosarcoma development. *J Pathol* 2006;208:17-25.
35. Athar M, Li C, Tang X, Chi S, Zhang X, Kim AL, Tying SK, Kopelovich L, Hebert J, Epstein EH, Jr., Bickers DR, Xie J. Inhibition of smoothened signaling prevents



- ultraviolet B-induced basal cell carcinomas through regulation of Fas expression and apoptosis. *Cancer Res* 2004;64:7545-52.
36. Berman DM, Karhadkar SS, Hallahan AR, Pritchard JI, Eberhart CG, Watkins DN, Chen JK, Cooper MK, Taipale J, Olson JM, Beachy PA. Medulloblastoma growth inhibition by hedgehog pathway blockade. *Science* 2002;297:1559-61.
37. Romer JT, Kimura H, Magdaleno S, Sasai K, Fuller C, Baines H, Connelly M, Stewart CF, Gould S, Rubin LL, Curran T. Suppression of the Shh pathway using a small molecule inhibitor eliminates medulloblastoma in *Ptc1(+/-)p53(-/-)* mice. *Cancer Cell* 2004;6:229-40.
38. Sanchez P, Hernandez AM, Stecca B, Kahler AJ, DeGueme AM, Barrett A, Beyna M, Datta MW, Datta S, Ruiz i Altaba A. Inhibition of prostate cancer proliferation by interference with SONIC HEDGEHOG-GLI1 signaling. *Proc Natl Acad Sci U S A* 2004;101:12561-6.
39. Thayer SP, di Magliano MP, Heiser PW, Nielsen CM, Roberts DJ, Lauwers GY, Qi YP, Gysin S, Fernandez-del Castillo C, Yajnik V, Antoniu B, McMahon M, Warshaw AL, Hebrok M. Hedgehog is an early and late mediator of pancreatic cancer tumorigenesis. *Nature* 2003;425:851-6.
40. Feldmann G, Dhara S, Fendrich V, Bedja D, Beaty R, Mullendore M, Karikari C, Alvarez H, Iacobuzio-Donahue C, Jimeno A, Gabrielson KL, Matsui W, Maitra A. Blockade of hedgehog signaling inhibits pancreatic cancer invasion and metastases: a new paradigm for combination therapy in solid cancers. *Cancer Res* 2007;67:2187-96.
41. Sanchez P, Ruiz i Altaba A. In vivo inhibition of endogenous brain tumors through systemic interference of Hedgehog signaling in mice. *Mech Dev* 2005;122:223-30.
42. Rudin CM. Vismodegib. *Clin Cancer Res* 2012;18:3218-22.
43. Graadt van Roggen JF, van Velthuysen ML, Hogendoorn PC. The histopathological differential diagnosis of gastrointestinal stromal tumours. *J Clin Pathol* 2001;54:96-102.
44. Goettsch WG, Bos SD, Breekveldt-Postma N, Casparie M, Herings RM, Hogendoorn PC. Incidence of gastrointestinal stromal tumours is underestimated: results of a nation-wide study. *Eur J Cancer* 2005;41:2868-72.
45. Meza-Zepeda LA, Kresse SH, Barragan-Polania AH, Bjerkehagen B, Ohnstad HO, Namlos HM, Wang J, Kristiansen BE, Myklebost O. Array comparative genomic hybridization reveals distinct DNA copy number differences between gastrointestinal stromal tumors and leiomyosarcomas. *Cancer Res* 2006;66:8984-93.
46. Yoshizaki A, Nakayama T, Naito S, Wen CY, Sekine I. Expressions of sonic hedgehog, patched, smoothened and Gli-1 in human intestinal stromal tumors and their correlation with prognosis. *World J Gastroenterol* 2006;12:5687-91.
47. Belinsky MG, Skorobogatko YV, Rink L, Pei J, Cai KQ, Vanderveer LA, Riddell D, Merkel E, Tarn C, Eisenberg BL, von Mehren M, Testa JR, Godwin AK. High density DNA array analysis reveals distinct genomic profiles in a subset of gastrointestinal stromal tumors. *Genes Chromosomes Cancer* 2009;48:886-96.
48. Liegl-Atzwanger B, Fletcher JA, Fletcher CD. Gastrointestinal stromal tumors. *Virchows Arch* 2010;456:111-27.
49. Hirota S, Isozaki K, Moriyama Y, Hashimoto K, Nishida T, Ishiguro S, Kawano K, Hanada M, Kurata A, Takeda M, Muhammad Tunio G, Matsuzawa Y, Kanakura Y, Shinomura Y, Kitamura Y. Gain-of-function mutations of c-kit in human gastrointestinal stromal tumors. *Science* 1998;279:577-80.
50. Heinrich MC, Corless CL, Duensing A, McGreevey L, Chen CJ, Joseph N, Singer S, Griffith DJ, Haley A, Town A, Demetri GD, Fletcher CD, Fletcher JA. PDGFRA activating mutations in gastrointestinal stromal tumors. *Science* 2003;299:708-10.

51. Andrae J, Gallini R, Betsholtz C. Role of platelet-derived growth factors in physiology and medicine. *Genes Dev* 2008;22:1276-312.
52. Antonescu CR. Targeted therapy of cancer: new roles for pathologists in identifying GISTs and other sarcomas. *Mod Pathol* 2008;21 Suppl 2:S31-6.
53. Huizinga JD, Thuneberg L, Kluppel M, Malysz J, Mikkelsen HB, Bernstein A. W/kit gene required for interstitial cells of Cajal and for intestinal pacemaker activity. *Nature* 1995;373:347-9.
54. Sanders KM, Ward SM. Kit mutants and gastrointestinal physiology. *J Physiol* 2007;578:33-42.
55. Robinson TL, Sircar K, Hewlett BR, Chorneyko K, Riddell RH, Huizinga JD. Gastrointestinal stromal tumors may originate from a subset of CD34-positive interstitial cells of Cajal. *Am J Pathol* 2000;156:1157-63.
56. Antonescu CR, Sommer G, Sarraf L, Tschernyavsky SJ, Riedel E, Woodruff JM, Robson M, Maki R, Brennan MF, Ladanyi M, DeMatteo RP, Besmer P. Association of KIT exon 9 mutations with nongastric primary site and aggressive behavior: KIT mutation analysis and clinical correlates of 120 gastrointestinal stromal tumors. *Clin Cancer Res* 2003;9:3329-37.
57. Lasota J, Wozniak A, Sarlomo-Rikala M, Rys J, Kordek R, Nassar A, Sobin LH, Miettinen M. Mutations in exons 9 and 13 of KIT gene are rare events in gastrointestinal stromal tumors. A study of 200 cases. *Am J Pathol* 2000;157:1091-5.
58. Lasota J, Dansonka-Mieszkowska A, Sobin LH, Miettinen M. A great majority of GISTs with PDGFRA mutations represent gastric tumors of low or no malignant potential. *Lab Invest* 2004;84:874-83.
59. Corless CL, Schroeder A, Griffith D, Town A, McGreevey L, Harrell P, Shiraga S, Bainbridge T, Morich J, Heinrich MC. PDGFRA mutations in gastrointestinal stromal tumors: frequency, spectrum and in vitro sensitivity to imatinib. *J Clin Oncol* 2005;23:5357-64.
60. Miettinen M, Lasota J, Sobin LH. Gastrointestinal stromal tumors of the stomach in children and young adults: a clinicopathologic, immunohistochemical, and molecular genetic study of 44 cases with long-term follow-up and review of the literature. *Am J Surg Pathol* 2005;29:1373-81.
61. Chan F, Liu Y, Sun H, Li X, Shang H, Fan D, An J, Zhou D. Distribution and possible role of PDGF-AA and PDGFR-alpha in the gastrointestinal tract of adult guinea pigs. *Virchows Arch* 2010;457:381-8.
62. Iino S, Horiguchi K, Horiguchi S, Nojyo Y. c-Kit-negative fibroblast-like cells express platelet-derived growth factor receptor alpha in the murine gastrointestinal musculature. *Histochem Cell Biol* 2009;131:691-702.
63. Iino S, Nojyo Y. Immunohistochemical demonstration of c-Kit-negative fibroblast-like cells in murine gastrointestinal musculature. *Arch Histol Cytol* 2009;72:107-15.
64. Bardsley MR, Horvath VJ, Asuzu DT, Lorincz A, Redelman D, Hayashi Y, Popko LN, Young DL, Lomberg GA, Urrutia RA, Farrugia G, Rubin BP, Ordog T. Kitlow stem cells cause resistance to Kit/platelet-derived growth factor alpha inhibitors in murine gastrointestinal stromal tumors. *Gastroenterology* 2010;139:942-52.
65. Pardanani A, Tefferi A. Imatinib targets other than bcr/abl and their clinical relevance in myeloid disorders. *Blood* 2004;104:1931-9.
66. Metcalf D. On hematopoietic stem cell fate. *Immunity* 2007;26:669-73.
67. Miyamoto T, Iwasaki H, Reizis B, Ye M, Graf T, Weissman IL, Akashi K. Myeloid or lymphoid promiscuity as a critical step in hematopoietic lineage commitment. *Dev Cell* 2002;3:137-47.

68. Mogensen TH. Pathogen recognition and inflammatory signaling in innate immune defenses. *Clin Microbiol Rev* 2009;22:240-73, Table of Contents.
69. Basset C, Holton J, O'Mahony R, Roitt I. Innate immunity and pathogen-host interaction. *Vaccine* 2003;21 Suppl 2:S12-23.
70. Allavena P, Sica A, Solinas G, Porta C, Mantovani A. The inflammatory micro-environment in tumor progression: the role of tumor-associated macrophages. *Crit Rev Oncol Hematol* 2008;66:1-9.
71. Balkwill F, Charles KA, Mantovani A. Smoldering and polarized inflammation in the initiation and promotion of malignant disease. *Cancer Cell* 2005;7:211-7.
72. Hao NB, Lu MH, Fan YH, Cao YL, Zhang ZR, Yang SM. Macrophages in tumor microenvironments and the progression of tumors. *Clin Dev Immunol* 2012;2012:948098.
73. Ydens E, Cauwels A, Asselbergh B, Goethals S, Peeraer L, Lornet G, Almeida-Souza L, Van Ginderachter JA, Timmerman V, Janssens S. Acute injury in the peripheral nervous system triggers an alternative macrophage response. *J Neuroinflammation* 2012;9:176.
74. Raes G, De Baetselier P, Noel W, Beschin A, Brombacher F, Hassanzadeh Gh G. Differential expression of FIZZ1 and Ym1 in alternatively versus classically activated macrophages. *J Leukoc Biol* 2002;71:597-602.
75. Ho VW, Sly LM. Derivation and characterization of murine alternatively activated (M2) macrophages. *Methods Mol Biol* 2009;531:173-85.
76. Bhardwaj G, Murdoch B, Wu D, Baker DP, Williams KP, Chadwick K, Ling LE, Karanu FN, Bhatia M. Sonic hedgehog induces the proliferation of primitive human hematopoietic cells via BMP regulation. *Nat Immunol* 2001;2:172-80.
77. Stewart GA, Lowrey JA, Wakelin SJ, Fitch PM, Lindey S, Dallman MJ, Lamb JR, Howie SE. Sonic hedgehog signaling modulates activation of and cytokine production by human peripheral CD4+ T cells. *J Immunol* 2002;169:5451-7.
78. Chan VS, Chau SY, Tian L, Chen Y, Kwong SK, Quackenbush J, Dallman M, Lamb J, Tam PK. Sonic hedgehog promotes CD4+ T lymphocyte proliferation and modulates the expression of a subset of CD28-targeted genes. *Int Immunol* 2006;18:1627-36.
79. Lowrey JA, Stewart GA, Lindey S, Hoyne GF, Dallman MJ, Howie SE, Lamb JR. Sonic hedgehog promotes cell cycle progression in activated peripheral CD4(+) T lymphocytes. *J Immunol* 2002;169:1869-75.
80. Sacedon R, Diez B, Nunez V, Hernandez-Lopez C, Gutierrez-Frias C, Cejalvo T, Outram SV, Crompton T, Zapata AG, Vicente A, Varas A. Sonic hedgehog is produced by follicular dendritic cells and protects germinal center B cells from apoptosis. *J Immunol* 2005;174:1456-61.
81. Dierks C, Grbic J, Zirlik K, Beigi R, Englund NP, Guo GR, Veelken H, Engelhardt M, Mertelsmann R, Kelleher JF, Schultz P, Warmuth M. Essential role of stromally induced hedgehog signaling in B-cell malignancies. *Nat Med* 2007;13:944-51.
82. El Andaloussi A, Graves S, Meng F, Mandal M, Mashayekhi M, Aifantis I. Hedgehog signaling controls thymocyte progenitor homeostasis and differentiation in the thymus. *Nat Immunol* 2006;7:418-26.
83. Uhmman A, Dittmann K, Nitzki F, Dressel R, Koleva M, Frommhold A, Zibat A, Binder C, Adham I, Nitsche M, Heller T, Armstrong V, Schulz-Schaeffer W, Wienands J, Hahn H. The Hedgehog receptor Patched controls lymphoid lineage commitment. *Blood* 2007;110:1814-23.

84. Detmer K, Walker AN, Jenkins TM, Steele TA, Dannawi H. Erythroid differentiation in vitro is blocked by cyclopamine, an inhibitor of hedgehog signaling. *Blood Cells Mol Dis* 2000;26:360-72.
85. Detmer K, Thompson AJ, Garner RE, Walker AN, Gaffield W, Dannawi H. Hedgehog signaling and cell cycle control in differentiating erythroid progenitors. *Blood Cells Mol Dis* 2005;34:60-70.
86. Zhao C, Chen A, Jamieson CH, Fereshteh M, Abrahamsson A, Blum J, Kwon HY, Kim J, Chute JP, Rizzieri D, Munchhof M, VanArsdale T, Beachy PA, Reya T. Hedgehog signalling is essential for maintenance of cancer stem cells in myeloid leukaemia. *Nature* 2009;458:776-9.
87. Queiroz KC, Ruela-de-Sousa RR, Fuhler GM, Aberson HL, Ferreira CV, Peppelenbosch MP, Spek CA. Hedgehog signaling maintains chemoresistance in myeloid leukemic cells. *Oncogene* 2010;29:6314-22.
88. Dunaeva M, Voo S, van Oosterhoud C, Waltenberger J. Sonic hedgehog is a potent chemoattractant for human monocytes: diabetes mellitus inhibits Sonic hedgehog-induced monocyte chemotaxis. *Basic Res Cardiol* 2010;105:61-71.
89. Pereira TA, Xie G, Choi SS, Syn WK, Voietta I, Lu J, Chan IS, Swiderska M, Amaral KB, Antunes CM, Secor WE, Witek RP, Lambertucci JR, Pereira FL, Diehl AM. Macrophage-derived hedgehog ligands promotes fibrogenic and angiogenic responses in human schistosomiasis mansoni. *Liver Int* 2013;33:149-61.
90. de Zwaan SE, Haass NK. Genetics of basal cell carcinoma. *Australas J Dermatol* 2010;51:81-92; quiz 93-4.
91. Nitzki F, Zibat A, Konig S, Wijgerde M, Rosenberger A, Brembeck FH, Carstens PO, Frommhold A, Uhmman A, Klingler S, Reifenberger J, Pukrop T, Aberger F, Schulz-Schaeffer W, Hahn H. Tumor stroma-derived Wnt5a induces differentiation of basal cell carcinoma of Ptch-mutant mice via CaMKII. *Cancer Res* 2010;70:2739-48.
92. Zibat A, Uhmman A, Nitzki F, Wijgerde M, Frommhold A, Heller T, Armstrong V, Wojnowski L, Quintanilla-Martinez L, Reifenberger J, Schulz-Schaeffer W, Hahn H. Time-point and dosage of gene inactivation determine the tumor spectrum in conditional Ptch knockouts. *Carcinogenesis* 2009;30:918-26.
93. Uhmman A, van den Brandt J, Dittmann K, Hess I, Dressel R, Binder C, Luhder F, Christiansen H, Fassnacht M, Bhandoola A, Wienands J, Reichardt HM, Hahn H. T cell development critically depends on prethymic stromal patched expression. *J Immunol* 2011;186:3383-91.
94. Nitzki F, Zibat A, Frommhold A, Schneider A, Schulz-Schaeffer W, Braun T, Hahn H. Uncommitted precursor cells might contribute to increased incidence of embryonal rhabdomyosarcoma in heterozygous Patched1-mutant mice. *Oncogene* 2011;30:4428-36.
95. Gordon S, Todd J, Cohn ZA. In vitro synthesis and secretion of lysozyme by mononuclear phagocytes. *J Exp Med* 1974;139:1228-48.
96. Klockars M, Reitamo S. Tissue distribution of lysozyme in man. *J Histochem Cytochem* 1975;23:932-40.
97. Peters CW, Kruse U, Pollwein R, Grzeschik KH, Sippel AE. The human lysozyme gene. Sequence organization and chromosomal localization. *Eur J Biochem* 1989;182:507-16.
98. Cross M, Renkawitz R. Repetitive sequence involvement in the duplication and divergence of mouse lysozyme genes. *EMBO J* 1990;9:1283-8.
99. Cortopassi GA, Wilson AC. Recent origin of the P lysozyme gene in mice. *Nucleic Acids Res* 1990;18:1911.

100. Cross M, Mangelsdorf I, Wedel A, Renkawitz R. Mouse lysozyme M gene: isolation, characterization, and expression studies. *Proc Natl Acad Sci U S A* 1988;85:6232-6.
101. Keshav S, Chung P, Milon G, Gordon S. Lysozyme is an inducible marker of macrophage activation in murine tissues as demonstrated by in situ hybridization. *J Exp Med* 1991;174:1049-58.
102. Ganz T, Gabayan V, Liao HI, Liu L, Oren A, Graf T, Cole AM. Increased inflammation in lysozyme M-deficient mice in response to *Micrococcus luteus* and its peptidoglycan. *Blood* 2003;101:2388-92.
103. Ye M, Iwasaki H, Laiosa CV, Stadtfeld M, Xie H, Heck S, Clausen B, Akashi K, Graf T. Hematopoietic stem cells expressing the myeloid lysozyme gene retain long-term, multilineage repopulation potential. *Immunity* 2003;19:689-99.
104. Clausen BE, Burkhardt C, Reith W, Renkawitz R, Forster I. Conditional gene targeting in macrophages and granulocytes using LysMcre mice. *Transgenic Res* 1999;8:265-77.
105. Soriano P. Generalized lacZ expression with the ROSA26 Cre reporter strain. *Nat Genet* 1999;21:70-1.
106. Sommer G, Agosti V, Ehlers I, Rossi F, Corbacioglu S, Farkas J, Moore M, Manova K, Antonescu CR, Besmer P. Gastrointestinal stromal tumors in a mouse model by targeted mutation of the Kit receptor tyrosine kinase. *Proc Natl Acad Sci U S A* 2003;100:6706-11.
107. Shinkai Y, Rathbun G, Lam KP, Oltz EM, Stewart V, Mendelsohn M, Charron J, Datta M, Young F, Stall AM, et al. RAG-2-deficient mice lack mature lymphocytes owing to inability to initiate V(D)J rearrangement. *Cell* 1992;68:855-67.
108. Nitzki F, Zibat A, Frommhold A, Schneider A, Schulz-Schaeffer W, Braun T, Hahn H. Uncommitted precursor cells might contribute to increased incidence of embryonal rhabdomyosarcoma in heterozygous *Patched1*-mutant mice. *Oncogene* 2011.
109. Marim FM, Silveira TN, Lima DS, Jr., Zamboni DS. A method for generation of bone marrow-derived macrophages from cryopreserved mouse bone marrow cells. *PLoS One* 2010;5:e15263.
110. Regl G, Neill GW, Eichberger T, Kasper M, Ikram MS, Koller J, Hintner H, Quinn AG, Frischauf AM, Aberger F. Human *GLI2* and *GLI1* are part of a positive feedback mechanism in Basal Cell Carcinoma. *Oncogene* 2002;21:5529-39.
111. Pedersen M, Ronnstrand L, Sun J. The c-Kit/D816V mutation eliminates the differences in signal transduction and biological responses between two isoforms of c-Kit. *Cell Signal* 2009;21:413-8.
112. Schnidar H, Eberl M, Klingler S, Mangelberger D, Kasper M, Hauser-Kronberger C, Regl G, Kroismayr R, Moriggl R, Sibilio M, Aberger F. Epidermal growth factor receptor signaling synergizes with Hedgehog/GLI in oncogenic transformation via activation of the MEK/ERK/JUN pathway. *Cancer Res* 2009;69:1284-92.
113. Wijgerde M, Ooms M, Hoogerbrugge JW, Grootegoed JA. Hedgehog signaling in mouse ovary: Indian hedgehog and desert hedgehog from granulosa cells induce target gene expression in developing theca cells. *Endocrinology* 2005;146:3558-66.
114. van Dop WA, Uhmman A, Wijgerde M, Sleddens-Linkels E, Heijmans J, Offerhaus GJ, van den Bergh Weerman MA, Boeckxstaens GE, Hommes DW, Hardwick JC, Hahn H, van den Brink GR. Depletion of the colonic epithelial precursor cell compartment upon conditional activation of the hedgehog pathway. *Gastroenterology* 2009;136:2195-2203 e1-7.
115. Li Y, Wheeler DL, Alters W, Chaiswing L, Verma AK, Oberley TD. Early epidermal destruction with subsequent epidermal hyperplasia is a unique feature of the



- papilloma-independent squamous cell carcinoma phenotype in PKCepsilon overexpressing transgenic mice. *Toxicol Pathol* 2005;33:684-94.
116. Eberl M, Klingler S, Mangelberger D, Loipetzberger A, Damhofer H, Zoidl K, Schnidar H, Hache H, Bauer HC, Solca F, Hauser-Kronberger C, Ermilov AN, Verhaegen ME, Bichakjian CK, Dlugosz AA, Nietfeld W, Sibilia M, Lehrach H, Wierling C, Aberger F. Hedgehog-EGFR cooperation response genes determine the oncogenic phenotype of basal cell carcinoma and tumour-initiating pancreatic cancer cells. *EMBO Mol Med* 2012;4:218-33.
117. Ishikawa T, Nakai N, Liu NN, Shiba K, Isozaki K, Matsuda I, Ito T, Fujimoto J, Hatakeyama K, Kanda T, Hirota S. In vivo effect of imatinib on progression of cecal GIST-like tumors in exon 17-type c-kit knock-in mice. *Lab Invest* 2009;89:1161-8.
118. Hwang PH, Yi HK, Kim DS, Nam SY, Kim JS, Lee DY. Suppression of tumorigenicity and metastasis in B16F10 cells by PTEN/MMAC1/TEP1 gene. *Cancer Lett* 2001;172:83-91.
119. Roby KF, Taylor CC, Sweetwood JP, Cheng Y, Pace JL, Tawfik O, Persons DL, Smith PG, Terranova PF. Development of a syngeneic mouse model for events related to ovarian cancer. *Carcinogenesis* 2000;21:585-91.
120. Kulbe H, Thompson R, Wilson JL, Robinson S, Hagemann T, Fatah R, Gould D, Ayhan A, Balkwill F. The inflammatory cytokine tumor necrosis factor-alpha generates an autocrine tumor-promoting network in epithelial ovarian cancer cells. *Cancer Res* 2007;67:585-92.
121. Moz U, Pignatelli U, Forner P, Candiago E, D'Addazio G, Casirati C, Gamba P. Follicular dendritic cell tumour of the cervical lymph node: case report and brief review of literature. *Acta Otorhinolaryngol Ital* 2004;24:223-5.
122. Chu P, Wu E, Weiss LM. Cytokeratin 7 and cytokeratin 20 expression in epithelial neoplasms: a survey of 435 cases. *Mod Pathol* 2000;13:962-72.
123. Terada T. Gastrointestinal stromal tumor of the digestive organs: a histopathologic study of 31 cases in a single Japanese institute. *Int J Clin Exp Pathol* 2009;3:162-8.
124. Mills AM, Beck AH, Montgomery KD, Zhu SX, Espinosa I, Lee CH, Subramanian S, Fletcher CD, van de Rijn M, West RB. Expression of subtype-specific group 1 leiomyosarcoma markers in a wide variety of sarcomas by gene expression analysis and immunohistochemistry. *Am J Surg Pathol* 2011;35:583-9.
125. Taguchi T, Sonobe H, Toyonaga S, Yamasaki I, Shuin T, Takano A, Araki K, Akimaru K, Yuri K. Conventional and molecular cytogenetic characterization of a new human cell line, GIST-T1, established from gastrointestinal stromal tumor. *Lab Invest* 2002;82:663-5.
126. Hernando E, Charytonowicz E, Dudas ME, Menendez S, Matushansky I, Mills J, Socci ND, Behrendt N, Ma L, Maki RG, Pandolfi PP, Cordon-Cardo C. The AKT-mTOR pathway plays a critical role in the development of leiomyosarcomas. *Nat Med* 2007;13:748-53.
127. Yamaguchi U, Nakayama R, Honda K, Ichikawa H, Hasegawa T, Shitashige M, Ono M, Shoji A, Sakuma T, Kuwabara H, Shimada Y, Sasako M, Shimoda T, Kawai A, Hirohashi S, Yamada T. Distinct gene expression-defined classes of gastrointestinal stromal tumor. *J Clin Oncol* 2008;26:4100-8.
128. Subramanian S, West RB, Corless CL, Ou W, Rubin BP, Chu KM, Leung SY, Yuen ST, Zhu S, Hernandez-Boussard T, Montgomery K, Nielsen TO, Patel RM, Goldblum JR, Heinrich MC, Fletcher JA, van de Rijn M. Gastrointestinal stromal tumors (GISTs) with KIT and PDGFRA mutations have distinct gene expression profiles. *Oncogene* 2004;23:7780-90.

129. Ostrowski J, Polkowski M, Paziewska A, Skrzypczak M, Goryca K, Rubel T, Kokoszynska K, Rutkowski P, Nowecki ZI, Vel Dobosz AJ, Jarosz D, Ruka W, Wyrwicz LS. Functional features of gene expression profiles differentiating gastrointestinal stromal tumours according to KIT mutations and expression. *BMC Cancer* 2009;9:413.
130. Verweij J, Casali PG, Zalcberg J, LeCesne A, Reichardt P, Blay JY, Issels R, van Oosterom A, Hogendoorn PC, Van Glabbeke M, Bertulli R, Judson I. Progression-free survival in gastrointestinal stromal tumours with high-dose imatinib: randomised trial. *Lancet* 2004;364:1127-34.
131. Rubin BP, Antonescu CR, Scott-Browne JP, Comstock ML, Gu Y, Tanas MR, Ware CB, Woodell J. A knock-in mouse model of gastrointestinal stromal tumor harboring kit K641E. *Cancer Res* 2005;65:6631-9.
132. Mazurier F, Fontanellas A, Salesse S, Taine L, Landriau S, Moreau-Gaudry F, Reiffers J, Peault B, Di Santo JP, de Verneuil H. A novel immunodeficient mouse model--RAG2 x common cytokine receptor gamma chain double mutants--requiring exogenous cytokine administration for human hematopoietic stem cell engraftment. *J Interferon Cytokine Res* 1999;19:533-41.
133. Regl G, Kasper M, Schnidar H, Eichberger T, Neill GW, Philpott MP, Esterbauer H, Hauser-Kronberger C, Frischauf AM, Aberger F. Activation of the BCL2 promoter in response to Hedgehog/GLI signal transduction is predominantly mediated by GLI2. *Cancer Res* 2004;64:7724-31.
134. Zhao L, Melenhorst JJ, Alemu L, Kirby M, Anderson S, Kench M, Hoogstraten-Miller S, Brinster L, Kamikubo Y, Gilliland DG, Liu PP. KIT with D816 mutations cooperates with CBFB-MYH11 for leukemogenesis in mice. *Blood* 2012;119:1511-21.
135. Elling C, Erben P, Walz C, Frickenhaus M, Schemionek M, Stehling M, Serve H, Cross NC, Hochhaus A, Hofmann WK, Berdel WE, Muller-Tidow C, Reiter A, Koschmieder S. Novel imatinib-sensitive PDGFRA-activating point mutations in hypereosinophilic syndrome induce growth factor independence and leukemia-like disease. *Blood* 2011;117:2935-43.
136. Crompton T, Outram SV, Hager-Theodorides AL. Sonic hedgehog signalling in T-cell development and activation. *Nat Rev Immunol* 2007;7:726-35.
137. Cooper CL, Hardy RR, Reth M, Desiderio S. Non-cell-autonomous hedgehog signaling promotes murine B lymphopoiesis from hematopoietic progenitors. *Blood* 2012;119:5438-48.
138. Carpenter S, O'Neill LA. Recent insights into the structure of Toll-like receptors and post-translational modifications of their associated signalling proteins. *Biochem J* 2009;422:1-10.
139. Takeda K, Kaisho T, Akira S. Toll-like receptors. *Annu Rev Immunol* 2003;21:335-76.
140. Schreiber G, Tel J, Sliepen KH, Benitez-Ribas D, Figdor CG, Adema GJ, de Vries IJ. Toll-like receptor expression and function in human dendritic cell subsets: implications for dendritic cell-based anti-cancer immunotherapy. *Cancer Immunol Immunother* 2010;59:1573-82.
141. Papadopoulos G, Weinberg EO, Massari P, Gibson FC, 3rd, Wetzler LM, Morgan EF, Genco CA. Macrophage-Specific TLR2 Signaling Mediates Pathogen-Induced TNF-Dependent Inflammatory Oral Bone Loss. *J Immunol* 2012.
142. Poste G, Doll J, Hart IR, Fidler IJ. In vitro selection of murine B16 melanoma variants with enhanced tissue-invasive properties. *Cancer Res* 1980;40:1636-44.



143. Hung CF, Tsai YC, He L, Wu TC. Control of mesothelin-expressing ovarian cancer using adoptive transfer of mesothelin peptide-specific CD8<sup>+</sup> T cells. *Gene Ther* 2007;14:921-9.
144. Hagemann T, Lawrence T, McNeish I, Charles KA, Kulbe H, Thompson RG, Robinson SC, Balkwill FR. "Re-educating" tumor-associated macrophages by targeting NF-kappaB. *J Exp Med* 2008;205:1261-8.
145. Solinas G, Germano G, Mantovani A, Allavena P. Tumor-associated macrophages (TAM) as major players of the cancer-related inflammation. *J Leukoc Biol* 2009;86:1065-73.
146. Corzo CA, Condamine T, Lu L, Cotter MJ, Youn JI, Cheng P, Cho HI, Celis E, Quiceno DG, Padhya T, McCaffrey TV, McCaffrey JC, Gabrilovich DI. HIF-1alpha regulates function and differentiation of myeloid-derived suppressor cells in the tumor microenvironment. *J Exp Med* 2010;207:2439-53.
147. Cortez-Retamozo V, Etzrodt M, Newton A, Rauch PJ, Chudnovskiy A, Berger C, Ryan RJ, Iwamoto Y, Marinelli B, Gorbato R, Forghani R, Novobrantseva TI, Kotliansky V, Figueiredo JL, Chen JW, Anderson DG, Nahrendorf M, Swirski FK, Weissleder R, Pittet MJ. Origins of tumor-associated macrophages and neutrophils. *Proc Natl Acad Sci U S A* 2012;109:2491-6.
148. Indra AK, Castaneda E, Antal MC, Jiang M, Messaddeq N, Meng X, Loehr CV, Gariglio P, Kato S, Wahli W, Desvergne B, Metzger D, Chambon P. Malignant transformation of DMBA/TPA-induced papillomas and nevi in the skin of mice selectively lacking retinoid-X-receptor alpha in epidermal keratinocytes. *J Invest Dermatol* 2007;127:1250-60.
149. Takeda K, Clausen BE, Kaisho T, Tsujimura T, Terada N, Forster I, Akira S. Enhanced Th1 activity and development of chronic enterocolitis in mice devoid of Stat3 in macrophages and neutrophils. *Immunity* 1999;10:39-49.
150. Rossi G, Valli R, Bertolini F, Marchioni A, Cavazza A, Mucciarini C, Migaldi M, Federico M, Trentini GP, Sgambato A. PDGFR expression in differential diagnosis between KIT-negative gastrointestinal stromal tumours and other primary soft-tissue tumours of the gastrointestinal tract. *Histopathology* 2005;46:522-31.
151. Fletcher CD, Berman JJ, Corless C, Gorstein F, Lasota J, Longley BJ, Miettinen M, O'Leary TJ, Remotti H, Rubin BP, Shmookler B, Sobin LH, Weiss SW. Diagnosis of gastrointestinal stromal tumors: A consensus approach. *Hum Pathol* 2002;33:459-65.
152. Handra-Luca A, Flejou JF, Molas G, Sauvanet A, Belghiti J, Degott C, Terris B. Familial multiple gastrointestinal stromal tumours with associated abnormalities of the myenteric plexus layer and skeinoid fibres. *Histopathology* 2001;39:359-63.
153. Plaat BE, Hollema H, Molenaar WM, Torn Broers GH, Pijpe J, Mastik MF, Hoekstra HJ, van den Berg E, Scheper RJ, van der Graaf WT. Soft tissue leiomyosarcomas and malignant gastrointestinal stromal tumors: differences in clinical outcome and expression of multidrug resistance proteins. *J Clin Oncol* 2000;18:3211-20.
154. West RB, Corless CL, Chen X, Rubin BP, Subramanian S, Montgomery K, Zhu S, Ball CA, Nielsen TO, Patel R, Goldblum JR, Brown PO, Heinrich MC, van de Rijn M. The novel marker, DOG1, is expressed ubiquitously in gastrointestinal stromal tumors irrespective of KIT or PDGFRA mutation status. *Am J Pathol* 2004;165:107-13.
155. Arora A, Scholar EM. Role of tyrosine kinase inhibitors in cancer therapy. *J Pharmacol Exp Ther* 2005;315:971-9.
156. Heinrich MC, Griffith DJ, Druker BJ, Wait CL, Ott KA, Zigler AJ. Inhibition of c-kit receptor tyrosine kinase activity by STI 571, a selective tyrosine kinase inhibitor. *Blood* 2000;96:925-32.

157. Heinrich MC, Corless CL, Demetri GD, Blanke CD, von Mehren M, Joensuu H, McGreevey LS, Chen CJ, Van den Abbeele AD, Druker BJ, Kiese B, Eisenberg B, Roberts PJ, Singer S, Fletcher CD, Silberman S, Dimitrijevic S, Fletcher JA. Kinase mutations and imatinib response in patients with metastatic gastrointestinal stromal tumor. *J Clin Oncol* 2003;21:4342-9.
158. Price ND, Trent J, El-Naggar AK, Cogdell D, Taylor E, Hunt KK, Pollock RE, Hood L, Shmulevich I, Zhang W. Highly accurate two-gene classifier for differentiating gastrointestinal stromal tumors and leiomyosarcomas. *Proc Natl Acad Sci U S A* 2007;104:3414-9.
159. Rubin BP, Heinrich MC, Corless CL. Gastrointestinal stromal tumour. *Lancet* 2007;369:1731-41.
160. Medeiros F, Corless CL, Duensing A, Hornick JL, Oliveira AM, Heinrich MC, Fletcher JA, Fletcher CD. KIT-negative gastrointestinal stromal tumors: proof of concept and therapeutic implications. *Am J Surg Pathol* 2004;28:889-94.
161. Negri T, Bozzi F, Conca E, Brici S, Gronchi A, Bertulli R, Fumagalli E, Pierotti MA, Tamborini E, Pilotti S. Oncogenic and ligand-dependent activation of KIT/PDGFR $\alpha$  in surgical samples of imatinib-treated gastrointestinal stromal tumours (GISTs). *J Pathol* 2009;217:103-12.
162. Xie J, Aszterbaum M, Zhang X, Bonifas JM, Zachary C, Epstein E, McCormick F. A role of PDGFR $\alpha$  in basal cell carcinoma proliferation. *Proc Natl Acad Sci U S A* 2001;98:9255-9.
163. Rizvi AZ, Swain JR, Davies PS, Bailey AS, Decker AD, Willenbring H, Grompe M, Fleming WH, Wong MH. Bone marrow-derived cells fuse with normal and transformed intestinal stem cells. *Proc Natl Acad Sci U S A* 2006;103:6321-5.
164. Sanders KM, Ward SM. Interstitial cells of Cajal: a new perspective on smooth muscle function. *J Physiol* 2006;576:721-6.
165. Nilsson B, Bumming P, Meis-Kindblom JM, Oden A, Dortok A, Gustavsson B, Sablinska K, Kindblom LG. Gastrointestinal stromal tumors: the incidence, prevalence, clinical course, and prognostication in the preimatinib mesylate era--a population-based study in western Sweden. *Cancer* 2005;103:821-9.
166. Agaram NP, Besmer P, Wong GC, Guo T, Socci ND, Maki RG, DeSantis D, Brennan MF, Singer S, DeMatteo RP, Antonescu CR. Pathologic and molecular heterogeneity in imatinib-stable or imatinib-responsive gastrointestinal stromal tumors. *Clin Cancer Res* 2007;13:170-81.
167. Von Hoff DD, LoRusso PM, Rudin CM, Reddy JC, Yauch RL, Tibes R, Weiss GJ, Borad MJ, Hann CL, Brahmer JR, Mackey HM, Lum BL, Darbonne WC, Marsters JC, Jr., de Sauvage FJ, Low JA. Inhibition of the hedgehog pathway in advanced basal-cell carcinoma. *N Engl J Med* 2009;361:1164-72.
168. Rudin CM, Hann CL, Laterra J, Yauch RL, Callahan CA, Fu L, Holcomb T, Stinson J, Gould SE, Coleman B, LoRusso PM, Von Hoff DD, de Sauvage FJ, Low JA. Treatment of medulloblastoma with hedgehog pathway inhibitor GDC-0449. *N Engl J Med* 2009;361:1173-8.
169. Liu J, Buckley JM, Redmond HP, Wang JH. ST2 negatively regulates TLR2 signaling, but is not required for bacterial lipoprotein-induced tolerance. *J Immunol* 2010;184:5802-8.
170. Meng F, Lowell CA. Lipopolysaccharide (LPS)-induced macrophage activation and signal transduction in the absence of Src-family kinases Hck, Fgr, and Lyn. *J Exp Med* 1997;185:1661-70.
171. Biswas SK, Mantovani A. Macrophage plasticity and interaction with lymphocyte subsets: cancer as a paradigm. *Nat Immunol* 2010;11:889-96.

172. Gambhir V, Yildiz C, Mulder R, Siddiqui S, Guzzo C, Szewczuk M, Gee K, Basta S. The TLR2 agonists lipoteichoic acid and Pam3CSK4 induce greater pro-inflammatory responses than inactivated *Mycobacterium butyricum*. *Cell Immunol* 2012;280:101-107.
173. Gabay C. Interleukin-6 and chronic inflammation. *Arthritis Res Ther* 2006;8 Suppl 2:S3.
174. Mantovani A, Sozzani S, Locati M, Allavena P, Sica A. Macrophage polarization: tumor-associated macrophages as a paradigm for polarized M2 mononuclear phagocytes. *Trends Immunol* 2002;23:549-55.
175. Ho CM, Chang SF, Hsiao CC, Chien TY, Shih DT. Isolation and characterization of stromal progenitor cells from ascites of patients with epithelial ovarian adenocarcinoma. *J Biomed Sci* 2012;19:23.
176. Auersperg N, Ota T, Mitchell GW. Early events in ovarian epithelial carcinogenesis: progress and problems in experimental approaches. *Int J Gynecol Cancer* 2002;12:691-703.
177. Kryczek I, Zou L, Rodriguez P, Zhu G, Wei S, Mottram P, Brumlik M, Cheng P, Curiel T, Myers L, Lackner A, Alvarez X, Ochoa A, Chen L, Zou W. B7-H4 expression identifies a novel suppressive macrophage population in human ovarian carcinoma. *J Exp Med* 2006;203:871-81.
178. Gabrilovich DI, Nagaraj S. Myeloid-derived suppressor cells as regulators of the immune system. *Nat Rev Immunol* 2009;9:162-74.
179. Rundhaug JE, Fischer SM. Molecular Mechanisms of Mouse Skin Tumor Promotion. *Cancers (Basel)* 2010;2:436-482.
180. Sotillo R, Garcia JF, Ortega S, Martin J, Dubus P, Barbacid M, Malumbres M. Invasive melanoma in Cdk4-targeted mice. *Proc Natl Acad Sci U S A* 2001;98:13312-7.
181. Winkler AE, Brotman JJ, Pittman ME, Judd NP, Lewis JS, Jr., Schreiber RD, Uppaluri R. CXCR3 enhances a T-cell-dependent epidermal proliferative response and promotes skin tumorigenesis. *Cancer Res* 2011;71:5707-16.
182. Mittal D, Saccheri F, Venereau E, Pusterla T, Bianchi ME, Rescigno M. TLR4-mediated skin carcinogenesis is dependent on immune and radioresistant cells. *EMBO J* 2010;29:2242-52.
183. Strid J, Roberts SJ, Filler RB, Lewis JM, Kwong BY, Schpero W, Kaplan DH, Hayday AC, Girardi M. Acute upregulation of an NKG2D ligand promotes rapid reorganization of a local immune compartment with pleiotropic effects on carcinogenesis. *Nat Immunol* 2008;9:146-54.
184. Ginhoux F, Ng LG, Merad M. Understanding the murine cutaneous dendritic cell network to improve intradermal vaccination strategies. *Curr Top Microbiol Immunol* 2012;351:1-24.
185. Norian LA, Rodriguez PC, O'Mara LA, Zabaleta J, Ochoa AC, Cella M, Allen PM. Tumor-infiltrating regulatory dendritic cells inhibit CD8+ T cell function via L-arginine metabolism. *Cancer Res* 2009;69:3086-94.
186. Romani N, Holzmann S, Tripp CH, Koch F, Stoitzner P. Langerhans cells - dendritic cells of the epidermis. *APMIS* 2003;111:725-40.
187. Kaplan DH, Jenison MC, Saeland S, Shlomchik WD, Shlomchik MJ. Epidermal langerhans cell-deficient mice develop enhanced contact hypersensitivity. *Immunity* 2005;23:611-20.
188. Hemmi H, Yoshino M, Yamazaki H, Naito M, Iyoda T, Omatsu Y, Shimoyama S, Letterio JJ, Nakabayashi T, Tagaya H, Yamane T, Ogawa M, Nishikawa S, Ryoike K, Inaba K, Hayashi S, Kunisada T. Skin antigens in the steady state are trafficked to

- regional lymph nodes by transforming growth factor-beta1-dependent cells. *Int Immunol* 2001;13:695-704.
189. Mayerova D, Parke EA, Bursch LS, Odumade OA, Hogquist KA. Langerhans cells activate naive self-antigen-specific CD8 T cells in the steady state. *Immunity* 2004;21:391-400.
190. Lewis J, Filler R, Smith DA, Golubets K, Girardi M. The contribution of Langerhans cells to cutaneous malignancy. *Trends Immunol* 2010;31:460-6.
191. Stene MA, Babajanian M, Bhuta S, Cochran AJ. Quantitative alterations in cutaneous Langerhans cells during the evolution of malignant melanoma of the skin. *J Invest Dermatol* 1988;91:125-8.
192. Miracco C, De Nisi MC, Arcuri F, Cosci E, Pacenti L, Toscano M, Lalinga AV, Biagioli M, Rubegni P, Vatti R, Maellaro E, Del Bello B, Massi D, Luzi P, Tosi P. Macrophage migration inhibitory factor protein and mRNA expression in cutaneous melanocytic tumours. *Int J Oncol* 2006;28:345-52.
193. Baumgartner JM, Gonzalez R, Lewis KD, Robinson WA, Richter DA, Palmer BE, Wilson CC, McCarter MD. Increased survival from stage IV melanoma associated with fewer regulatory T Cells. *J Surg Res* 2009;154:13-20.
194. Martin-Manso G, Galli S, Ridnour LA, Tsokos M, Wink DA, Roberts DD. Thrombospondin 1 promotes tumor macrophage recruitment and enhances tumor cell cytotoxicity of differentiated U937 cells. *Cancer Res* 2008;68:7090-9.
195. Yang IV, Alper S, Lackford B, Rutledge H, Warg LA, Burch LH, Schwartz DA. Novel regulators of the systemic response to lipopolysaccharide. *Am J Respir Cell Mol Biol* 2011;45:393-402.

## 9 Abbreviations

AP	Alkaline phosphatase
BCC	Basal cell carcinoma
BLP	Bacterial lipoprotein
BMDM	Bone marrow-derived macrophages
bp	base pair
BrdU	5-Bromo-2-Deoxyuridine
BSA	bovine serum albumine
CD	cluster of differentiation
CCL	chemokine (C-C motif) ligand
cDNA	copyDNA
<i>Ci</i>	<i>Cubitus interruptus (D. Melanogaster Gli-Homolog)</i>
CM	conditioned media
CML	chronic myeloid leukemia
CXCL	chemokine (C-X-C motif) ligand
ddH <sub>2</sub> O	double distilled water
Cy	Indodicarbocyanin-Derivate
Ct	cycle threshold
d	days
DAB	Diamino-Benzidine
DC	Dendritic cells
DEPC	Diethylpyrocarbonate
Dhh/DHH	Desert Hedgehog
DMBA	7,12-dimethylbenzanthracene
DMEM	Dulbeco's Modified Eagle Medium
DMSO	N.N.-Dimethylsulfoxide
DNA	Deoxyribonucleic acid
dNTPs	Desoxyribonucleotide triphosphate
Dog-1	Discover on GIST-1
Dox	Doxycycline
DTT	Dithiothreitol
<i>E</i>	Extinction
E	Exon
EDTA	Ethylen-diamine-tetraacetate
EGFR	endothelial growth factor receptor
FCS	fetal calf serum
FITC	Fluorescein isothiocyanate
FoxF1/FOXF1	Forkhead box F1

Gapdh	Glycerinaldehyd-3-phosphatase-dehydrogenase
gDNA	genomic DNA
GIST	gastrointestinal tumors
Gli/GLI	Glioma oncogene
GSEA	Gene set enrichment analysis
Gy	Gray (radiation unit)
h	hour(s)
hand2/HAND2	Heart and neural crest derivatives expressed 2
HE	Haematoxylin/Eosin
Hh/ HH	Hedgehog
HRP	horseradish peroxidase
i.p.	intraperitoneal
i.v	intravenous
IHC	Immunohistochemistry
Ihh/IHH	Indian Hedgehog
IL	interleukin
ISH	<i>in situ</i> -Hybridisation
kDa	Kilodalton
LacZ	$\beta$ -Galactosidase
LB-Medium	lysogeny broth Medium
LC	Langerhan cells
LMS	Leiomyosarcoma
<i>loxP</i>	<i>loxP</i> Sequence (DNA-Consensus sequence for binding of cre-recombinase)
LPS	lipopolysaccharide
MB	Medulloblastoma
MBSTL	Maleic acid sodium chloride/Levamisole/Tween-20 buffer
MCP-1	Monocyte chemoattractant protein-1
MDSC	Myeloid-derived suppressor cells
min	minute(s)
MIP-1 $\alpha$	Macrophage inflammatory protein-1 $\alpha$
mRNA	messenger RNA
n	number (sample)
neoR	Neomycin resistance
Nkx3-2/NKX3-2	NK3 homeobox 2
NT	Sodium chloride/Tris-Buffer
N-terminal	aminoterminal
NTMLT	Sodium chloride/ Tris/Magnesium chloride/Levamisole/Tween-20-buffer
OD	optical density
Pam <sub>3</sub> CSK <sub>4</sub>	Pam3CysSerLys4

PBS	Phosphate buffered saline
PCR	Polymerase chain reaction
Pdgf/PDGF	Platelet-derived growth factor
Pdgfr- /PDGFR- $\alpha$ , $\beta$	Platelet-derived growth factor receptor- $\alpha$ , $\beta$
PE	Phycoerythrin
PFA	paraformaldehyde
PS	Penicillin/Streptomycin
Ptch	Patched
<i>Ptch</i> <sup>del</sup>	<i>Ptch</i> allele with cre- mediated deletion of Exon 8 and 9
<i>Ptch</i> <sup>flox</sup>	floxed <i>Ptch</i> allele between Exon 8 and 9
p53	Transformation related protein 53
qRT-PCR	quantitative real time PCR
RLU	relative light units
RMS	Rhabdomyosarcoma
RNA	Ribonucleicacid
rpm	rounds per minute
RT	room temperature
RTK	Receptor tyrosine kinase
SCC	Sqamous cell carcinoma
SDS	Sodiumdodecyl sulfate
Shh/SHH	Sonic hedgehog
SMA	Smooth muscle actin
Smo	Smoothened
SNP	single nucleotide polymorphism
SSC	standard saline citrate
STE	SDS/Tris/EDTA-buffer
Sufu	Suppressor of fused
T	transgenes Allele
Taq	Thermus aquaticus
TBE	Tris-Boric acid-EDTA buffer
TBS	Tris-buffered saline
TCR- $\beta$	T cell receptor- $\beta$
TLR	Toll-like receptor
TNF- $\alpha$	Tumor necrotic factor- $\alpha$
TPA	12-O-tetradecanoyl-phorbol-13-acetate
U	unit (enzyme)
v/v	volume/volume
Vol	Volume
w/v	weight/volume



wt	Wild type
X-Gal	5-Bromo-4-chloro-3-indolyl- $\beta$ -Galaktosid
YYE	Yakima Yellow

---

## **10 Acknowledgement**

It would not have been possible to write this thesis without the help and support of the kind people around me, who in one way or another contributed and extended their valuable assistance in the preparation and completion of this study.

Foremost, I would like to express my deepest gratitude to my supervisor, Prof. Dr. Heidi Hahn, for her guidance and mentorship. I cannot have finished this thesis without your patience, motivation and support. Heidi, you rock as a supervisor!

I would also like to thank Prof. Dr. Holger Reichardt and Prof. Dr. Matthias Dobbelsstein for the valuable inputs and insightful comments during my thesis committee meetings.

My deepest gratitude to Prof. Dr. Gijs van den Brink and Prof. Dr. Fritz Aberger for their collaboration and support that had great impact on the GIST project. Thank you to Prof. Dr. Uwe-Karsten Hanisch whom I turned to for advice for my macrophage work.

A big thank you to Dr. Walter Schulz-Schaeffer for the interpretation of all my stainings.

Special thanks also to Dr. Kai Dittmann for the welcoming atmosphere during FACS analyses, to Dr. Julia Bodde for helping me out in imaging experiments and to Dr. Annalen Bleckmann for all the statistical analyses that she did.

To the animal care givers, especially Mr. Stefan Wolf and Ms. Susan Peters, thank you for the excellent care for the animals.

I have been very privileged to get to know and work with many great people who became more than just colleagues over the last several years. I learned a lot from them about life, research, how to approach new problems, and how to develop techniques to solve them. In particular, I'd like to thank Dr. Frauke Nitzki, Dr. Anja Uhmann, Dr. Simone König and Dr. Diana Marklein. You guys are just amazing to work with. Thank you for the fun and encouraging discussions. I would also like to thank Anke Frommhold for taking the time to cut all the slides that I needed and for the great technical support. Similarly, my gratitude goes to Ina Hess and Tobias Goldak for always being available whenever I needed technical assistance. Thanks to Nicole Cuvelier, Marco Becker, Benedict Albert and Rosalie Ridzewski. It's great to work with you all.

I am forever grateful to my family for their continuous support and encouragement. To my mom and dad and to my sister and brother, who have been my all-time sources of inspiration, thank you with all my heart!

Most importantly, I would like to thank my life partner and best friend, Christopher. No words can express how grateful I am for your love and support. Chris, to you I dedicate this dissertation.

## 11 Curriculum vitae

### EDUCATIONAL BACKGROUND

<b>Aug. 2009- Mar. 2013</b>	<b>PhD in Biology</b> <b>Georg-August University of Göttingen, Germany</b> Göttingen Graduate School for Neurosciences, Biophysics, and Molecular Biosciences Program: Molecular Biology of Cells Dissertation: <i>The role of Hedgehog Receptor Patched in LysM<sup>+</sup> Cells in Mice</i>
<b>Mar. 2004 – Feb. 2006</b>	<b>MSc. in Human Ecology</b> <b>Chungnam National University, South Korea</b> Department of Food and Nutrition Dissertation: <i>The Effect of Red Lettuce on the Antioxidant Activity of Mice Fed with High Fat Diet</i>
<b>Jun. 1996 - Jun 2001</b>	<b>BSc. in Public Health</b> <b>University of the Philippines, Philippines</b> College of Public Health

### WORK EXPERIENCE

<b>Researcher</b> June 2006-Feb. 2009	Korea Atomic Energy Research Institute Radioisotope Research Division
<b>Junior Researcher</b> 2002-2004	National Institutes of Health-Manila Institute of Biotechnology and Molecular Biology

### RESEARCH PUBLICATIONS

**Pelczar P**, Zibat A, van Dop WA, Heijmans J, Bleckmann A, Gruber W, Nitzki F, Uhmman A, Guijarro MV, Hernando E, Dittmann K, Wienands J, Dressel R, Wojnowski L, Binder C, Taguchi T, Beissbarth T, Hogendoorn PC, Antonescu CR, Rubin BP, Schulz-Schaeffer W, Aberger F, van den Brink GR, Hahn H. *Inactivation of Patched1 in Mice Leads to Development of Gastrointestinal Stromal-Like Tumors That Express Pdgfralpha but Not Kit*. Gastroenterology 2013;144(1); 134-144.

Lee SY, Hong YD, **Felipe PM**, Pyun MS, Choi SJ. *Radiolabeling of monoclonal anti-CD105 with (177)Lu for potential use in radioimmunotherapy*. Appl Radiat Isot 2009;67: 1366-1369.

Lee SY, Hong YD, Pyun MS, **Felipe PM**, Choi SJ. *Radiolabeling of monoclonal anti-vascular endothelial growth factor receptor 1 (VEGFR 1) with <sup>177</sup>Lu for potential use in radioimmunotherapy*. Appl Radiat Isot 2009;67: 1185-1189.

Lee JH, **Felipe P**, Yang YH, Kim MY, Kwon OY, Sok DE, Kim HC and Kim MR. *Effects of dietary supplementation with red-pigmented leafy lettuce (Lactuca sativa) on lipid profiles and antioxidant status in C57BL/6J mice fed a high-fat high-cholesterol diet*. Brit J Nutr, 2009; 101(8); 1246-1254.

**Felipe P**, Yang YH, Lee JH, Sok D, Kim HC, Yoon WK, Kim HM, Kim MR. *Combinational Effect of Moist Heating and Gamma Irradiation on the Inactivation of Trypsin Inhibitory Activity in Soybean*. Food Sci. Biotechnol. 2005;14(6); 732-737.

**Felipe P**, Yang YH, Lee JH, Sok D, Kim HC, Yoon WK, Kim HM, Kim MR. *Effect of Cultivars, Cooking and Processing on the Trypsin Inhibitor Activity of soybean*. J Food Sci. Nutri. 2005;10:6-10.